Offshore Structures Exposed to Large Slamming Wave Loads

by

Jithin Jose

Thesis submitted in fulfillment of
the requirements for the degree of
PHILOSOPHIAE DOCTOR
(PhD)

Faculty of Science and Technology
Department of Mechanical and Structural Engineering and Materials Science
2017

University of Stavanger
N-4036 Stavanger
NORWAY
www.uis.no

ISBN: 978-82-7644-746-0
ISSN: 1890-1387
PhD Thesis UiS: 373

This thesis is dedicated to

my daughter Gizel Marie Jose

and

my god-daughter Minna Liz Jerin

"If you desire ease, forsake learning.
If you desire learning, forsake ease.
How can the man at his ease acquire knowledge,
And how can the earnest student enjoy ease?"

-The Tree of Wisdom, Nagarjuna (150BC)

Abstract

In sloping shallow water regions, waves undergo different nonlinear transformations such as wave shoaling and breaking, due to the nonlinear wave interactions with the seabed. The forces from breaking waves are of concern for offshore structures installed in such regions. The wave breaking forces are large impulsive forces acting for short period of time. The substructures of offshore wind turbines are usually monopile, gravity-based, tripod and jacket-type structures. Due to the simplicity in the design and installation, monopile structures are widely used for supporting offshore wind turbines. However, the operating water depths and turbine capacity of monopile substructures are limited. With the increase in the turbine capacity and use in larger water depths, the offshore wind industry has recently focused on rigid types of substructures, such as jacket-type structures.

In order to estimate the slamming forces due to wave breaking on offshore structures, many research studies have been conducted in the past. However, most of these studies were limited to simple structures such as monopiles. The empirical force models by Goda et al. [5] and Wienke and Oumeraci [7] are widely used in the industry to estimate the breaking wave forces on monopile structures. However, in the case of the jacket structures there have not been much research. Due to the complexity of jacket structures, it is more difficult to analyse the wave forces on a jacket compared to a monopile. The empirical force models developed for approximating the slamming forces on monopiles cannot be easily transferred to jacket structures due to the different member sizes and orientations. Moreover, the uncertainties in these empirical models need to be addressed while using them for jacket structures.

In order to study breaking wave interactions with a jacket structure, high quality experimental data is required. Within the WaveSlam experiment

([4, 11]) carried out in a joint collaboration with the University of Stavanger, NTNU and the University of Hannover, a large-scale jacket structure of 1:8 scale was tested for a number of relevant breaking wave conditions. According to the author's knowledge this is the first large-scale experiment conducted to estimate the breaking wave forces on a jacket structure. This experimental dataset forms the basis for the present research.

In order to retrieve relevant data from the measurements, suitable methodologies were proposed. The applicability of these methodologies to the present data was verified. The local and total wave slamming forces on the jacket were analysed for all the relevant wave breaking conditions. The local slamming coefficients for the local members of the jacket structure were obtained from the local slamming forces. In addition, the influence of breaking wave parameters such as breaking wave height, wave breaking position and wave front asymmetry on the wave slamming forces on the structure was investigated.

To simulate wave breaking on a jacket, a 3D Navier Stokes numerical model, based on viscous and incompressible momentum equations was used. The capability of the present numerical model was compared with the other well-known numerical model OpenFOAM and the results were in good agreement. The jacket structure was modelled in same scale as that of the experimental set-up. In order to prepare the numerical model for simulations, a sensitivity study was carried out on the model parameters. The numerical simulations were performed for most of the experimental cases and the results were verified with the experimental measurements. The local slamming forces and coefficients acting on the members of the jacket in the wave impact region are studied based on the numerical results.

The results from comparing the experimental analysis and numerical simulations were useful to gain a better understanding of breaking wave interactions with the jacket. The local slamming forces on the members

were found to be important in the design of jacket structures against breaking waves. Based on the present study, a slamming coefficient of 6.16, similar to the value suggested by Wienke and Oumeraci for monopile structures, was found to be sufficient to estimate the local slamming forces on the jacket members in the wave impact region.

Key words: *wave breaking, slamming forces, jacket, truss structure, monopile, numerical model, Navier-Stokes, slamming coefficient.*

Acknowledgments

This research was carried out at the Department of Mechanical and Structural Engineering and Material Science of the University of Stavanger (UiS) in the period from August 2014 to August 2017. The research was supported by a grant (Project No: PR-10077) from the Norwegian Centre for Offshore Wind Energy (NORCOWE) and the University of Stavanger.

First and foremost I want to thank my supervisor Professor Ove Tobias Gudmestad for his immense support and guidance throughout the period of my doctoral study. It has been an honour to be his PhD student. The Professor's positive attitude and vision helped the author to successfully complete this thesis.

The author would also like to thank my co-supervisor Associate Professor Charlotte Obhrai for her valuable comments and suggestions. She provided the author a detailed understanding of the WaveSlam experimental data, which the author used for his research.

The author is also deeply grateful to Dr. Sung-Jin Choi for collaborating on the numerical studies performed during the research. Dr. Choi shared the numerical model which he used during his doctoral study, for the present research. Dr. Choi's experience with the numerical model greatly helped during the research.

The author would also like to express his deepest thanks to Professor Witold Cieślikiewicz and PhD student Ms. Olga Podrażka, University of Gdansk, Poland, for their contributions on experimental data analysis.

The author also extend his gratitude to his friends and department colleagues for their support during the PhD period. The author would like to mention few a people in particular: Mr. Endashaw Tesfaye, Mr.

Arvind Keprate, Mr. Adekunle Orimolade, Mr. Ashish Aeran, Mr. Aboma Wagari, Dr. Sudath Siriwardane, Ms. Nirosha Adasooriya and Mr. Yaseen A. Ahmad. The author is also grateful to Ms. Elisabeth Stornes Paulsen, Ms. Anna Karin Rafos and Ms. Kathrine Molde for all the administrative supports. The author would like to give a special mention to Ms. Kathrine Molde who helped greatly in managing the parental leave, which the author took during the research period.

Last but not least, the author would like to thank his wife Dhanya Therese Jose, daughter Gizel Marie Jose, his parents Dr. P.L Jose and Dr. N.S Mariya, his parents in law Mr. Joseph Mathew and Ms. Liby Jose, his brothers Jerin and Deepu and sister in law Elizabeth, and his whole family and friends for their unwavering and unselfish love and support given to him at all times.

Above all, thanks to God, the Almighty, for his showers of blessings which enabled me to complete this research successfully.

Jithin Jose
University of Stavanger
Norway

Contents

List of Appended Papers

Paper I — Jose, J., Podrażka, O., Obhrai, C., Gudmestad, O.T., and Cieślikiewicz, W., 2016, "Methods for Analysing Wave Slamming Loads on Truss Structures used in Offshore Wind Applications based on Experimental Data," International Journal of Offshore and Polar Engineering, Vol. 26(2), pp. 100-108.
DOI: dx.doi.org/10.17736/ijope.2016.mkr05

Paper II — Jose, J., Podrażka, O., Gudmestad, O.T., and Cieślikiewicz, W., 2017, "Characteristics of the Wave Slamming Forces on Jacket Structures under Plunging Breaking Waves based on Experimental Data," In the Proceedings of ASME 36th International Conference on Ocean, Offshore and Arctic Engineering (OMAE2017), Trondheim, Norway, June 25-June 30.
DOI:10.1115/OMAE2017-61789

Paper III — Jose, J., Podrażka, O., Gudmestad, O.T., and Cieślikiewicz, W., 2017, "Detailed Study on Breaking Wave Interactions with a Jacket Structure based on Experimental Investigations," Journal of Offshore Mechanics and Arctic Engineering, Vol. 140(2), pp. 021301.1-021301.14.
DOI: dx.doi.org/10.1115/1.4037829

Paper IV — Jose, J., Choi, S.J., Giljarhus, K.E.T., and Gudmestad, O. T., 2017, "A Comparison of Numerical Simulations of Breaking Wave Forces on a Monopile Structure using Two Different Numerical Models based on Finite

Difference and Finite Volume Methods," Ocean Engineering, Vol. 137, 78-88.
DOI: doi.org/10.1016/j.oceaneng.2017.03.045

Paper V — Jose, J., Choi, S.J., and Gudmestad, O.T., 2017, "Sensitivity Study on a 3D Numerical Model for Estimating Breaking Wave Forces on a Jacket Structure," In the Proceedings of 27th International Ocean and Polar Engineering Conference (ISOPE2017), San Francisco, California, June 25- June 30.
ISBN: 978-1-880653-97-5

Paper VI — Jose, J., Choi, S.J., Lee, K.H., and Gudmestad, O.T., 2016, "Breaking Wave Forces on an Offshore Wind Turbine Foundation (Jacket Type) in the Shallow Water," In the Proceedings of 26th International Ocean and Polar Engineering Conference, Rhodes, Greece, June 26-July 2.
ISBN: 978-1-880653-88-3

Paper VII — Jose, J., and Choi, S.J., 2017, "Estimation of Slamming Coefficients on Local Members of Offshore Wind Turbine Foundation (Jacket Type) under Plunging Breaker," International Journal of Naval Architecture and Ocean Engineering, Vol. 9(6), pp. 624-640.
DOI: dx.doi.org/10.1016/j.ijnaoe.2017.03.006

Abbreviations

ADV	Acoustic Doppler Velocity
AMG	Algebraic Multi Grid
CFD	Computational Fluid Dynamics
CSF	Continuum Surface Force
EMD	Empirical Mode Decomposition
EXP	Experimental
FDM	Finite Difference Method
FVM	Finite Volume Method
FRF	Frequency Response Function
LES	Large Eddy Simulation
NWT	Numerical Wave Tank
OWT	Offshore Wind Turbine
VG	Velocity Gauge
VOF	Volume of Fluid
WG	Wave Gauge

Chapter 1
Introduction

1.1 General

Wind energy is one of the fastest growing energy sources in the world. Due to the clean energy concepts and growing energy demands, wind energy is becoming popular these days. Compared with the onshore counterpart, offshore wind turbines have unique advantages due to the availability of high quality wind (low variability) and the large extent of offshore wind farms. Hence the potential of offshore wind energy is huge compared to onshore wind. The major components of an offshore wind turbine are the upper turbine part and the lower supporting structure. The supporting structures for the offshore wind turbines are either fixed-type (monopile, jacket structure, tripod and gravity based structure) or floating-type structures (TLP, semi-sub and spar) (Figure 1.1). As most of the offshore wind farms are located in shallow waters, the substructures for these turbines are mostly fixed type. Among them, monopile structures comprise almost 97% ([1]) of the global offshore wind turbine installations.

Offshore structures installed in shallow waters with a sloping bottom are subjected to nonlinear wave interactions such as shoaling and wave breaking etc. Wave breaking is one of the major concerns in the design of such offshore structures ([2, 3, 4]), as it imposes highly varying hydrodynamic loads on the structures. Many researches have been conducted regarding the wave breaking forces acting on both vertical and inclined piles (monopile), on flat and sloping bottoms ([5, 6, 7]). Based on those studies, there are empirical force models which can estimate the

breaking wave forces on monopile structures. However, most of the studies were confined to monopile structures only.

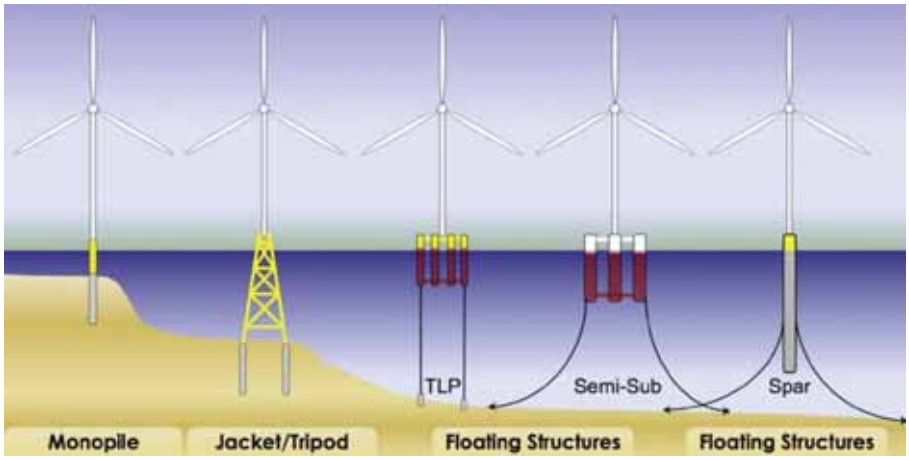

Figure. 1.1 Substructures of offshore wind turbines [8]

With the increase in the turbine capacity and feasibility of installing offshore wind turbines in deeper waters, the wind industry is more focused on the rigid type of offshore wind turbine support structures, like jacket structures. The jackets are 3D lattice structures, which have a larger load bearing capacity compared to monopiles. The Thornton bank offshore wind farm installed on the Belgian coast is an example. Out of the three phases of the wind farm development, the final two phases used steel jacket structures as the support structures for the wind turbines. One of the major hydrodynamic challenges during the design of the Thornton bank wind farm was the large slamming forces from the breaking waves in harsh environmental conditions. The experiences from the specific wind farm highlighted the necessity of investigating the breaking wave forces on jacket structures. However, there are only limited studies ([9, 10]) in the past regarding this and further investigation is needed. This was the motivation for the WaveSlam experiment ([4, 11]), in which a jacket structure of 1:8 scale, designed similar to the one used in the Thornton bank, was tested against breaking waves.

1.2 Background

The non-breaking wave force on a vertical column is typically calculated using the Morison equation as the sum of quasi-static inertia and drag forces (Equation 1.1).

$$dF = dF_D + dF_M = \rho_w C_D R|u|u\,dz + \rho_w C_M \pi R^2 \frac{du}{dt} dz \tag{1.1}$$

where, ρ_w is the water density, R is the radius of the column, u is the water particle velocity, z is the water depth and t is time. C_D and C_M are the drag and inertia coefficients respectively, which depend on the Reynolds and Keulagen-Carpenter numbers, the roughness and interaction parameters, respectively. The total wave force acting on the column can be calculated by integrating Equation 1.1 along the immersed height of the pile. However, the Morison equation is valid only for small diameter members where diffraction effects can be neglected.

As the wave propagates along the sloping bottom, due to the interaction of the wave with the bottom, the wave particle velocities become larger than the phase speed. At a certain critical point, the wave becomes unstable and breaks, dissipating a large amount of wave energy in the form of turbulent kinetic energy. As the breaking wave front possesses large particle velocities and kinetic energy, it imparts a significant impact force on the structure. In order to calculate the total wave force, F, on the structure subjected to breaking waves, this short duration impact force component due to breaking waves must be added to the Morison force (Equation 1.2). This additional force term is called the slamming force (F_s).

$$F = F_D + F_M + F_S \tag{1.2}$$

Von Karman [12], first proposed the theoretical formulation of water impact forces on a rigid body. In his work, he considered a horizontal

cylindrical body with a wedged-shaped surface striking a horizontal surface of water. The force acting between the body and the water was calculated by application of the conservation of momentum. Although Von Karman's theories were based on wedges, the approach can be extended to a cylinder of a circular cross-section.

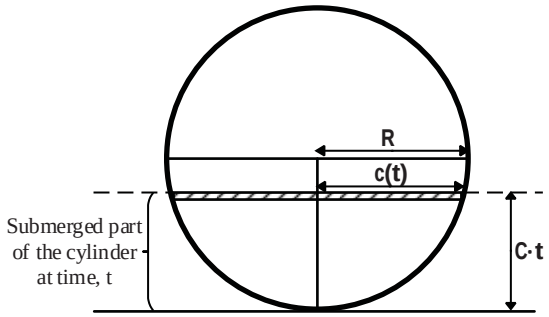

Figure 1.2 Sketch of wave impact on a circular cross section based on Von Karman's model

An infinitely long cylinder with a circular cross section of radius R entering into still water at a fixed speed C can be approximated by a flat plate of width $2c(t)$, where $c(t)$ is the half width of submerged part of the cylinder at each time point of the impact, t (see Figure 1.2). The half width $c(t)$ is given by Equation 1.3.

$$c(t) = \sqrt{2CtR - (Ct)^2} \tag{1.3}$$

The vertical impact force (slamming force) is calculated by integrating the pressure over the wetted surface, using linearised Bernoulli's equation.

The slamming force per unit length can be then expressed by:

$$f(t) = \rho_w C_s R C^2 \tag{1.4}$$

$$C_s = \pi\left(1-\frac{C}{R}t\right) \tag{1.5}$$

where, C_s is the slamming coefficient. The maximum slamming force occurs at the beginning of the impact ($t = 0$) and hence the slamming coefficient becomes equal to π.

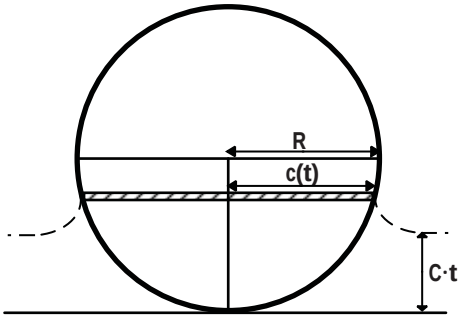

Figure 1.3 Sketch of wave impact on a circular cross section based on Wagner's model for impact force

The Von Karman approach neglects the "pile-up effect", which is the rise of free surface elevation when the impact occurs. However, the Wagner's model [13] (Figure 1.3) not only includes the conservation of momentum during the impact as Von Karman did, but also the flow beside the flat plate which results in the deformation of the water free surface. The inclusion of the pile-up effect, results in the immersion of the cylinder earlier than in the Von Karman's model. This results in the reduction of impact duration and hence increases the maximum slamming force. This maximum slamming force is found to be twice the force calculated based on Von Karman's model. The slamming coefficient is calculated to be 2π and the slamming force per unit length at the initial moment of impact is given as follows:

$$f(t = 0) = 2\pi\rho_w R C^2 \tag{1.6}$$

In the Von Karman's and the Wagner's models, the slamming force was estimated for the unit length of the cylinder. In order to calculate the

slamming force acting on the whole cylinder, the slamming force per unit length should be integrated along the length of impact. Goda et al. [5] adapted the approach by Von Karman and extended the formula for wave impact on a vertical cylinder by introducing a new factor called the curling factor (λ), which indicates the part of the wave front active at the time of the wave impact (see Figure 1.4). The breaking wave was considered as a vertical wall of water hitting the cylinder and progressing with velocity equal to wave celerity C_b. The impact length is characterised as $\lambda\eta_b$, in which η_b is the surface elevation of the breaking wave as shown in Figure 1.4.

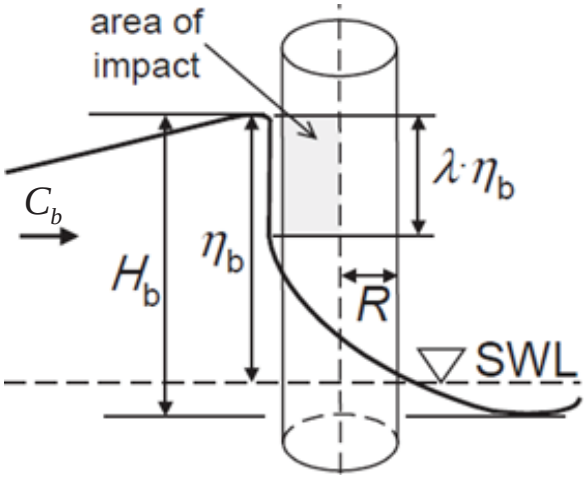

Figure 1.4 Sketch of impact force on a vertical cylinder [5]

The total slamming force acting on the cylinder of radius R due to wave impact is given by,

$$F(t) = C_s \rho_w R C_b^2 \lambda \eta_b \qquad (1.7)$$

The slamming coefficient C_s is one of the most investigated parameters related to slamming forces, as the estimated slamming force is directly proportional to it. According to Von Karman [13], who was followed by

Goda et al. [5] and Tanimoto et al. [13], the C_s value is π. Wagner's theory suggests a slamming coefficient value equal to 2π. Wienke and Oumeraci [7] and Basco and Niedzwiedzki [15], who published the experimental results indicating much higher impact forces than those predicted by Goda et al. [5], suggested a slamming coefficient of 2π and showed that the formulation of the Wagner's theory is more accurate. Further many researchers have suggested different empirical values for the C_s, mostly for the single vertical cylinder, however the discussion is still open. Table 1.1 shows a summary of the slamming coefficients suggested by various researchers and the design guidelines. However, there is no clear agreement on the value of the slamming coefficient to be used. As per the author's knowledge a slamming coefficient equal to 2π is widely acceptable for the design of monopile structures.

Table 1.1 Values of slamming coefficient based on experimental studies and design guidelines [16].

Slamming Load Model / Author	Slamming Coefficient
Goda et al. (1966)	π
Sarpkaya (1978)	π or 5.5
Swaragi & Nochino (1986)	π
Tanimoto et al. (1986)	π
Wienke & Oumeraci (2005)	2π
IEC 61400-3 (2009), ISO 21650 (2007), GL (2005), ABS (2010)	2π
DNV-RP-C205 (2010)	5.15
API RP 2A-WSD (2007), ISO 19902 (2007)	0.5π~1.7π

1.3 Problem Statement

One of the main challenges in the hydrodynamic problem of wave breaking is the higher number of physical parameters involved during the breaking process [17]. The breaking process is highly nonlinear and the physical understanding of breaking wave interactions with a structure is very complicated. However, the degree of complexity depends on the

type of structure. These challenges are evident in the wave force models used for estimating breaking wave forces on cylindrical structures ([5, 7]). In the case of a jacket structure, the structural complexity is much greater compared to monopiles. The jacket structures are designed to have minimum resistance to incoming waves with smaller member sizes, distributed over the space. Alternatively, a jacket can be considered as a combination of a number of monopile members in various orientations. Hence, the breaking wave interactions with a jacket would be more complex than for a monopile. Moreover, there is not many detailed studies on this topic, except some preliminary studies ([3, 10, 18]).

1.4 Research Objectives

Based on the background study and the problem statement, the main objectives of the present research are:

- *To obtain a better understanding of wave breaking on a jacket structure with the help of high quality experimental data. Introduce suitable methodologies to extract relevant data from the experimental measurements.*

- *Based on the experimental data, study the wave slamming forces on the jacket structure under different breaking conditions. Obtain the total slamming forces on the jacket and local slamming forces on jacket members based on the measurements. Investigate the applicability of the monopile force formula to estimate the slamming forces on the jacket structure. Obtain suitable values of the slamming coefficient, which can be used to estimate the total and local slamming forces on the jacket. Further, study the dependency of various breaking wave parameters on the slamming forces on the structure.*

- *Adopt and further develop a 3D numerical model, which can estimate the breaking wave impact forces on the jacket structure*

and validate the numerical model results with the experimental measurements. Perform a detailed study on slamming forces on the jacket based on the numerical simulations.

In order to achieve these goals for the study,

1. The experimental data was obtained from the WaveSlam experiment [4, 11] carried out in Hannover, Germany, in 2013, during a joint collaboration project with the University of Stavanger (UiS), the Norwegian University of Science and Technology (NTNU) and the University of Hannover. This high quality experimental data was used for the present study. During the experiments, a jacket structure of 1:8 scale was tested for a large number of breaking wave conditions. As one of the objectives of the present research is to estimate the wave breaking forces on the structure, the author filtered out the slamming force from the measured force using two different filtering methods. The Empirical Mode Decomposition (EMD) method and the Frequency Response Function (FRF) method were used to filter the total and local slamming forces from the measured force data, respectively. The various breaking wave parameters were calculated based on the wave gauge measurements taken during the experiment.

2. The experimental data analysis was performed for relevant wave cases. The selected wave cases represent different wave breaking positions with respect to the jacket structure, with different wave heights and wave periods. The total and local breaking wave forces on the jacket structure were estimated from the measured force data. The slamming coefficients were obtained based on these estimated total and local slamming forces. A modified form of the force formula by Goda et al. [5] was used to estimate the slamming coefficients valid for the jacket structure. The dependency of various wave parameters such as breaking wave

height and wave front asymmetry on the wave slamming forces on the structure was studied.

3. A 3D numerical model based on a finite difference scheme was adopted for the present research. This numerical model was previously used to estimate the breaking wave forces on a monopile structure ([19]). The capability of the present numerical model was compared with the well-known numerical model, OpenFOAM. The jacket structure was modelled in the same model scale as that of the experimental set-up. Further, a sensitivity study was performed on the various numerical parameters used in the model and appropriate parameters were chosen for the simulations. The numerical model simulated the breaking wave interactions with the jacket structure reasonably well in comparison with the experimental measurements. The local wave forces on the jacket members were calculated along the length of the members. Based on these local force calculations, the distribution of local slamming coefficients on the members was estimated.

1.5 Research Questions

Based on the literature study and discussion with experts in the field, the research questions were formulated. The research questions indicate the key problems which the present research is trying to answer.

1. ***How to make use of the WaveSlam measurement data to investigate the breaking wave interactions with the jacket structure? Is this dataset sufficient to perform a comprehensive study on breaking wave interactions with the jacket structure? What are the methodologies need to be used to interpret the measurement data?***

2. ***How do the total slamming forces on a jacket and local slamming forces on jacket members vary? Are the empirical force models used for estimating slamming forces on monopile structures, suitable for jackets? If so, what are the values of slamming coefficients to be used for estimating these slamming forces? What are the recommendations for the safe design of a jacket structure against breaking waves?***

3. ***With the present experimental data, is it possible to validate a numerical model, which is capable of simulating breaking wave interactions with the jacket structure? If so what are the implications from the numerical simulations? How to make use of the numerical simulation results to gain a better understanding of slamming forces on the jacket structure?***

1.6 Limitations of the Research

In the WaveSlam experiment dataset, there were wave force measurements on the jacket for both regular and irregular waves. However, in the present research, the slamming forces on the jacket were studied only for regular wave cases.

During the experiment, the breaking waves induced dynamic effects on the structure's responses. However, in the present research, the dynamic effects in the response were not studied in detail.

In addition, this research mainly focussed on the impact of breaking waves on the local member design of the jackets.

1.7 Thesis Organisation

The thesis consists of three chapters. Chapter 1 briefly presents an introduction to the present research, background, research objectives and the key research questions answered in the thesis. Chapter 2 presents the research methodologies and approaches used in the present study

including both experimental and numerical studies. A brief summary and discussion on the appended papers is also presented. In Chapter 3, the conclusions and recommendations are presented.

Chapter 2

Research Methodology and Approach

2.1 Research Methodology

As mentioned in the previous chapter, the main objective of the present research is to obtain a better understanding of breaking wave interactions with a jacket structure. In order to achieve this goal, experimental and numerical studies were performed. The various methodologies adopted for these studies are presented in this section.

2.1.1 Experimental Set-up

As there are many physical parameters involved in the wave breaking process, an analytical approach towards this problem is cumbersome. In the case of monopile structures, most of the studies have been based on experimental measurements. The force formulas suggested by many researchers for estimating breaking wave forces on monopile structures have been based on an empirical approach. In the case of jackets, there are not many experiments, except, a small-scale (1:50) model test conducted at the Norwegian University of Science and Technology (NTNU) ([18, 20]). However, there were many limitations in those experiments in terms of scale effects and local slamming force measurements ([18]). The WaveSlam experiment [4, 11], carried out in 2013, was designed as an extension to the tests conducted at NTNU, in which a large-scale (1:8) jacket model was tested for a number of wave breaking conditions. The experimental data for the present research is obtained from the WaveSlam experiment. The experiment was carried

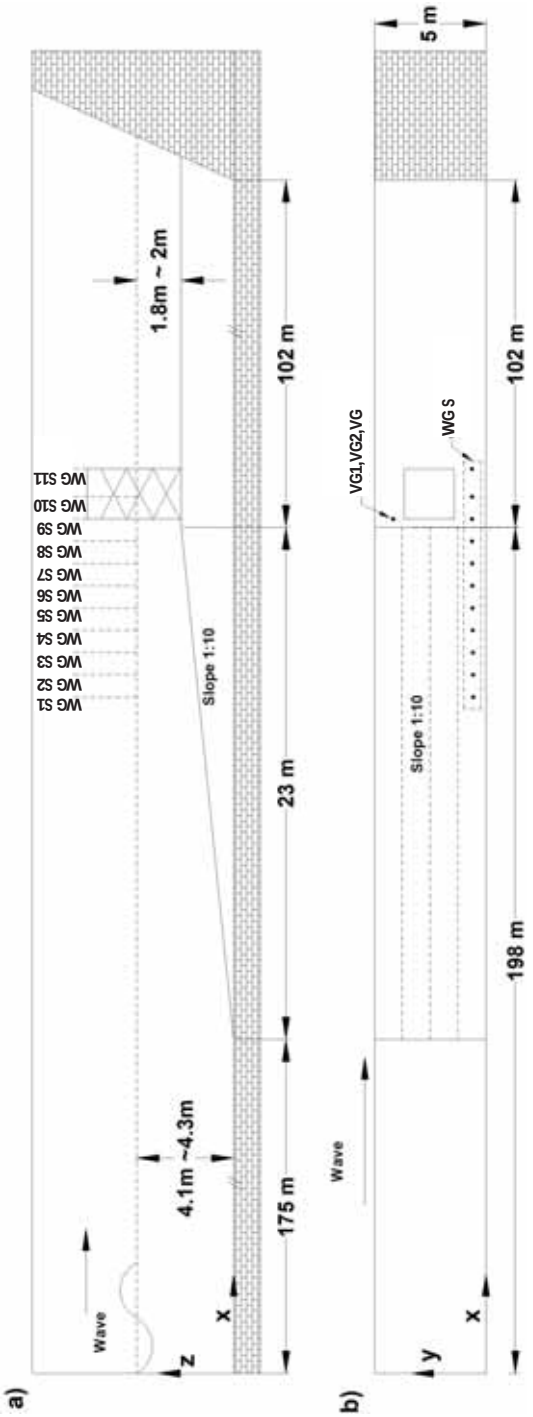

Figure 2.1 Schematic representation of experimental setup: a) side view and b) top view

out during a joint project with the University of Stavanger, NTNU and the University of Hannover. This experiment is considered to be one of the first attempts to study breaking wave forces on a jacket using a large-scale model.

Figure 2.2 Wave Slam experimental set-up

The measurements were carried out in large wave flume at the University of Hannover, Germany. The wave flume is 308 m long; 5 m wide and 7 m deep. The waves were generated by a wave paddle, acting in a horizontal direction and the strokes were superimposed by an upper flap movement in order to simulate water wave kinematics most accurately. The jacket structure at the scale of 1:8 was located approximately 200 m from the wave generator, on a 10% slope as shown in Figures 2.1 and 2.2. The structure was suspended on a bar at the top of the frame. The legs of the truss structure were hanging freely with a bottom clearance of four centimetres. There were eight wave gauges distributed along the wave flume, and additionally one was located at the front member of the structure, one in the middle and one at the back of the structure (WG S1-S11). The wave kinematics were measured by three Acoustic Doppler Velocity meters (ADVs), which were positioned in the line of the front

members (VG1-VG3).

The truss structure was equipped with four total force transducers (Model/Type: HBM/S9M) installed at the top (two transducers: FTTF02 and FTTF04) and the bottom (two transducers: FTTF01 and FTTF03) of the structure (see Figure 2.3). There were ten local force transducers (FTLF01–FTLF10) placed on the vertical front legs and twelve dual axis force transducers (FTBF01–FTBF12) on the bracings, which measured the response of the structure to the impact forces.

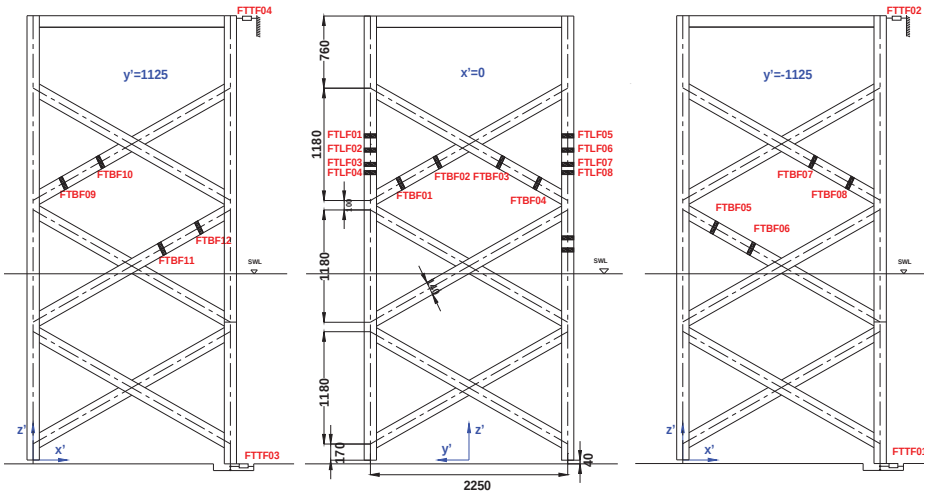

Figure 2.3 Locations of the force transducers and the dimensions of the jacket structure (all dimensions in mm)

The majority of the measurements were carried out for regular waves (H=0.75 m-1.9 m and T=3 s-5.55 s) with specific frequencies and wave heights as well as for the random waves based on the JONSWAP spectrum. The readings from all instruments were logged using the data acquisition system, with a true time recording. In addition, one high-speed and two normal-speed cameras were used to capture the slamming events on the structure. For each wave breaking cases, there were 20 repetitions of the waves in the wave flume. However, for the present study only few wave samples were considered, neglecting waves which

were contaminated by beach reflection effects.

2.1.2 Force Filtration Methods

During the WaveSlam experiment, the wave forces on the jacket structure were measured using total and local force transducers. A typical wave force measured by a force transducer during wave breaking on the structure has three major components: the Morison force, the amplified force component due to the structure's vibration and the slamming force due to wave breaking on the structure. The Morison force is quasi-static in nature, which consists of drag and inertia force components, whose frequency is very close to the wave frequency. The dynamic amplification of the force is due to the structure's vibration at its natural frequency. The slamming force is the force component due to the wave impact on the structure. The slamming force is impulsive in nature with a small impact duration. Separating these force components from the measurements is a challenging task. However, it is necessary to separate these forces in order to study the slamming wave forces acting on the structure. In the present data, there are mainly two types of force measurements; total force on the jacket structure measured by total force transducers and local force on the jacket members measured by local force transducers. The author has introduced two different methods to filter out the slamming force components from these measured forces. The methods are chosen based on some preliminary studies performed on the measurement data ([21]). The Empirical Mode Decomposition (EMD) method was used for filtering the total wave slamming force from the total measured force. In order to filter the local slamming force from the local measured forces, the Frequency Response Function (FRF) method was used. The application of both methods is explained in the following section.

Empirical Mode Decomposition (EMD) Method

The Empirical Mode Decomposition (EMD) method was developed by Huang et al. [22] to decompose the given signal in the time domain. The

EMD decomposes the signal into a number of intrinsic mode functions (IMFs) and a residue. Since the decomposition is based on the local characteristics of the time series data, this method is widely used for nonlinear processes.

The basic steps in the EMD method are:

1. Obtain the local extremes of the measured signal.
2. The extracted local extremes are connected to obtain the upper and lower envelopes.
3. The mean of the upper envelope and the lower envelope is obtained, which is the residue and is subtracted from the measured signal to obtain the IMF.

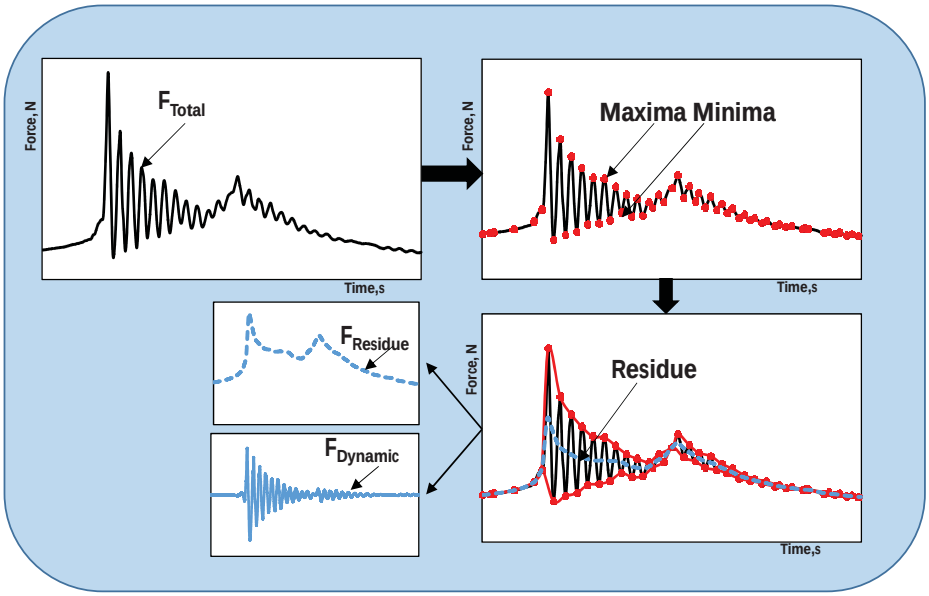

Figure 2.4 Slamming force separation using EMD method

In the present research, the EMD method was used to separate the total slamming forces from the measured total force on the jacket structure. As there are different frequencies in the measured force, the EMD will decompose the measured total force response into an IMF, which

represents the amplified force component due to the structure's vibration and a residue which is the net breaking wave force. The net breaking wave force is the summation of the Morison force component and the wave slamming force component.

Figure 2.4 illustrates the total slamming force filtration using the EMD method. The output of the EMD method is a residue and an intrinsic mode function. In this case, the residue is the net breaking wave force ($F_{Residue}$), and the intrinsic mode function is the dynamic amplification part ($F_{Dynamic}$). The total wave slamming force on the structure is obtained from the net breaking wave force ($F_{Residue}$) by filtering the quasi-static part (Morison force) with a low pass filter. As the frequency of the quasi-static part is similar to the wave frequency, the cut-off frequency of the low pass filter is set very close to the wave frequency, in such a way that it will not remove any actual contribution to the wave breaking force.

Frequency Response Function (FRF) Method

Määtänen [23] used the Frequency Response Function (FRF) method to resolve ice forces from the measured forces, when the structure is impacted by moving ice. The applicability of the same method for analysing the wave slamming forces on structures was verified by Tørum [24]. The preliminary analysis of the WaveSlam data ([21]) showed the effectiveness of this method in obtaining wave slamming forces from the measured forces.

In the case of any forced excitation, the response of the structure $f(t)$ can be expressed in Fourier integral form as,

$$f(t) = \frac{1}{2\pi} \int_{-\infty}^{\infty} H(\omega) Y_F(\omega) e^{i\omega t} d\omega \qquad (2.1)$$

where, $H(\omega)$ is the Frequency Response Function or transfer function and $Y_F(\omega)$ is the linear spectrum of the forcing function $F(t)$.

The Fourier transform of Equation 2.1 gives,

$$H(\omega)Y_F(\omega) = \int_{-\infty}^{\infty} f(t)e^{-i\omega t}d\omega = Y_f(\omega) \tag{2.2}$$

$$Y_F(\omega) = \frac{Y_f(\omega)}{H(\omega)} \tag{2.3}$$

$Y_f(\omega)$ is the linear spectrum of the response function $f(t)$ .The forcing function $F(t)$ can be obtained by taking the inverse Fourier transform of the Equation 2.3.

$$F(t) = \frac{1}{2\pi}\int_{-\infty}^{\infty} \frac{Y_f(\omega)}{H(\omega)}e^{i\omega t}d\omega \tag{2.4}$$

The above equation implies that, if the transfer function and the response spectrum are known, the forcing function can be calculated. The transfer function $H(\omega)$ is the calibration function for finding the forcing function.

In the present study, the frequency response function/transfer function is the quantitative measurement of the response of the structure when it is subjected to any impact. In the experimental set-up, impulse hammer tests were performed to determine these transfer functions. The impulse hammer has an interchangeable impact tip. The impulse hammer excites the test structure with a constant force over the frequency range of interest. The force sensor mounted on the head of the impulse hammer, transforms the force impulse into electrical signals which completely describe the forcing function. The response of the structure was recorded by the force transducers mounted on the jacket.

The transfer function $H(\omega)$ is calculated as,

$$H(\omega) = \frac{S_{ham}(\omega)}{S_{imp}(\omega)} \tag{2.5}$$

where, $S_{ham}(\omega)$ is the linear spectrum of the response force and $S_{imp}(\omega)$ is the spectrum of the hammer impulse force.

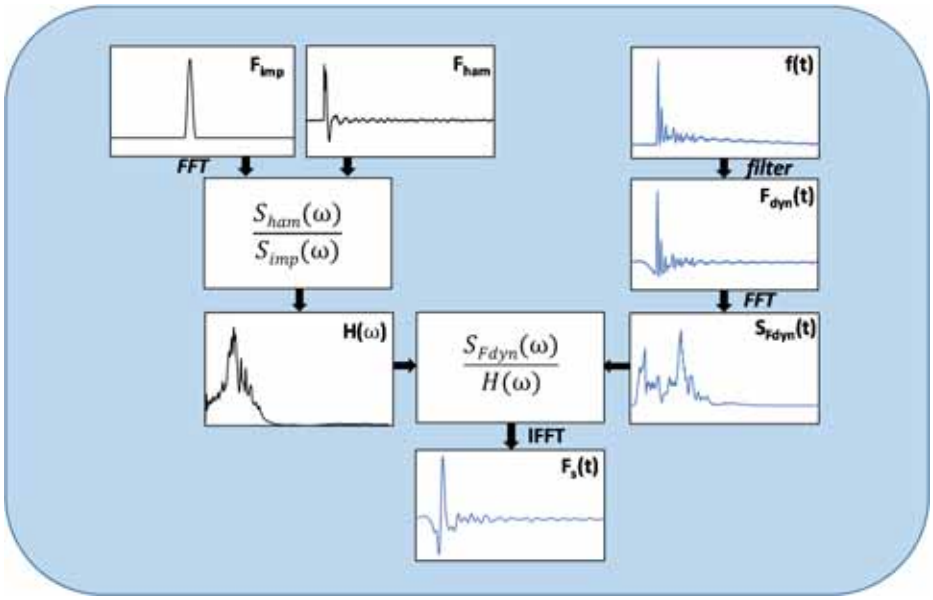

Figure 2.5 Frequency Response Function (FRF) method

Figure 2.5 illustrates the local slamming force filtration using the FRF method. The transfer function was calculated for each of the local force transducers from the hammer test measurements. In order to analyse the force measured by a local force transducer ($f(t)$), firstly the quasi-static part of the measured force is filtered out, using a low pass filter, before applying the FFT method. The remaining force is the dynamic force (F_{dyn}), which contains the dynamic amplification due to the structure's vibration and the wave slamming force. The dynamic force spectrum (S_{Fdyn}) is operated with the transfer function ($H(\omega)$) in order to obtain the slamming force. The final slamming force ($F_s(t)$) is obtained after filtering any high frequency noise in the estimated slamming force using a low pass filter. The cut-off frequency of this filter is kept in such a way that only the high frequency noise is filtered from the final force.

2.1.3 Estimation of Slamming Coefficient

The empirical force model proposed by Goda et al. [5] (see Equation. 2.6), is widely used to estimate the breaking wave force on a monopile structure. This formula is suggested to be a good approximation of the actual physical parameters involved in the wave breaking process. However, there is no exact agreement on the empirical coefficient, the slamming coefficient (C_s), to be used in this formula. In many cases, the value of the slamming coefficient is chosen in the range of π to 2π.

$$F_s = \frac{1}{2}\rho_w C_s D C_b{}^2 \lambda \eta_b \tag{2.6}$$

In Equation 2.6, D is the diameter of the cylinder, λ is the curling factor which indicates how much of the wave crest is active at the time of the wave impact, η_b is the breaking wave height and ρ_w is the water density.

In the case of jackets there are no guidelines on the estimation of slamming forces on the structure. However, a jacket can be considered as a combination of monopile members at different orientations. The basic form of empirical models for approximating slamming forces on monopiles can be applied on jacket members. In the present research, an extended form of the monopile formula is used to estimate the slamming coefficients on the jacket structure. The slamming forces are obtained from the measured forces from the experiment or from numerical simulations. The impact area denoted by $D\lambda\eta_b$ in Equation 2.6 is considered as the projected area of the local member (A_P), where the local wave force is measured. The wave celerity at the time of breaking (C_b) is equal to the horizontal water particle velocity for plunging waves ([7]). Due to the limitations in the velocity gauge measurements in the experiment, the wave celerity at the time of breaking is calculated using the wave gauge measurements. The time taken by the wave crest to cross the adjacent wave gauge is used to calculate the wave celerity at the time

of wave breaking. The slamming coefficient on the local member is estimated using the Equation 2.7.

$$C_s = \frac{2f_l}{\rho_w C_b{}^2 A_P} \tag{2.7}$$

where A_P is the projected area of the local force transducer, f_l is the maximum slamming force measured by the force transducers and C_b is the breaking wave celerity.

The present approach (Equation 2.7) is applicable for the jacket members in the wave impact region. In order to obtain the total slamming coefficient for the jacket structure, the summation of the slamming forces on all jacket members in the wave impact zone is considered and a single value of slamming coefficient is obtained to represent the total slamming force on the jacket.

2.1.4 Breaking Wave Parameters

The nature of wave slamming forces on the structure are impulsive. Due to shorter impact durations, these forces are highly sensitive to various wave parameters which govern wave breaking. It is important to identify these wave parameters and study their impact on the wave slamming forces on the structure. For the present research, some of these governing parameters are identified as breaking wave height, wave front asymmetry and wave breaking position relative to the jacket structure. These parameters are estimated from the available experimental measurements as follows:

- ***Breaking Wave Height***

During the experiment, the development of the breaking wave along the wave channel was tracked with the help of eleven wave gauges distributed along the sloping region of the wave flume and in the vicinity of the structure (see Figure 2.1). It is well known that the wave height

reaches its maximum at the wave breaking point and hence the breaking wave height is estimated from the wave gauge measurements.

- ***Wave Front Asymmetry***

The wave front asymmetry is a dimensionless parameter which represents the overall geometry of the wave. It is a more efficient means of tracing breaking wave deformations, especially in the case of plunging breakers ([25, 26, 27]).

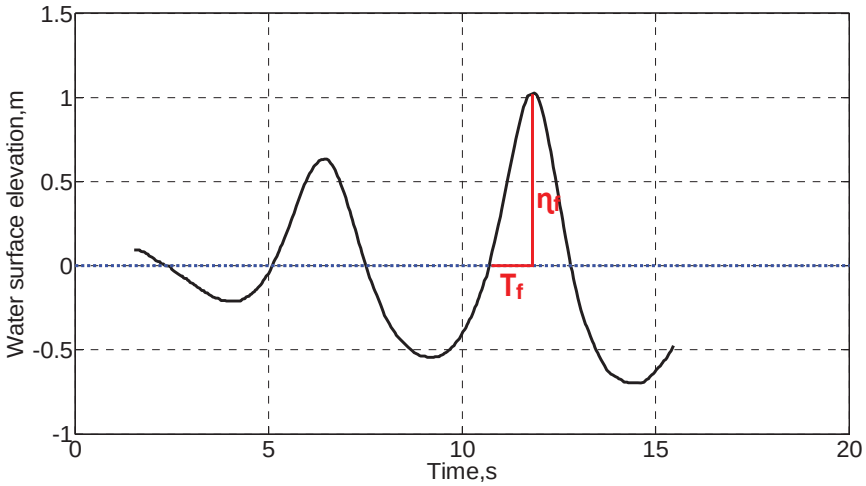

Figure 2.6 Definition sketch of wave front asymmetry [27, 28]

The wave front asymmetry (A_f) is defined as,

$$A_f = \eta_f / \lambda_f \tag{2.8}$$

where η_f is the crest height of the wave front. The length of the wave front (λ_f) is estimated from the wave front period T_f (Figure 2.6). The phase velocity C, obtained from the shallow water approximation of the dispersion relation as $C = \sqrt{gh}$, is used to estimate λ_f , as shown in Equation 2.9. The period of the wave front (T_f) is calculated based on the measurements from the wave gauges.

$$\lambda_f = C \times T_f = T_f \sqrt{gh} \tag{2.9}$$

where, h is the water depth.

- ***Wave Breaking Position***

Most of the wave energy is dissipated in the early stage of wave breaking. The amount of wave energy imparted on the structure depends on the relative positions of the wave breaking with respect to the structure. If the structure is located at a far distance from the breaking position of the wave, most of the wave energy will be dissipated before it reaches the structure. Therefore the wave breaking position is an important factor which governs the wave slamming forces on the structure. There are many empirical relations ([29]) which can be used to estimate the approximate breaking position of the wave. However, for the present study, instead of using any empirical formulas, the breaking position of the wave is estimated directly from the measurements. It is known that when the wave propagates in shallow waters with a sloping bottom, both the wave front asymmetry and the wave height increase until they reach the critical point, which is the start of wave breaking. Afterwards, a sudden decrease in these two parameters is observed. Based on this knowledge and with the aid of high definition video recording of the wave train propagation, the breaking positions of each individual wave are estimated.

2.1.5 3D Numerical Model

The numerical wave tank (NWT) method used for the present research was developed by Lee [30]. The waves are generated in the computational domain by an internal wave source. In order to absorb the reflected waves at the lateral boundaries, artificial damping zones are provided.

- ***Governing equations***

As the fluid is modelled as viscous and incompressible with constant density, the fluid motion can be described by the continuity equation (Equation. 2.10) and the modified Navier-Stokes equation (Equation 2.11).

$$\frac{\partial(m v_j)}{\partial x_j} = q^* \tag{2.10}$$

$$m\frac{\partial v_i}{\partial t} + m v_j \frac{\partial v_i}{\partial x_j} = \frac{-m}{\tilde{\rho}}\frac{\partial p}{\partial x_i} + \frac{\partial}{\partial x_j}(2\tilde{\nu} D_{ij} - \tau_{ij}) - Q_i - \beta_{ij} v_j + f_i \tag{2.11}$$

where, t is the time; $v_i = [u, v, w]^T$ is the velocity vector; p is pressure; $x_i = [x, y, z]^T$ is the position vector; m is the ratio of the fractional area open to the flow; f_i is the arbitrary body forces due to the effects of gravity and surface tension; $D_{ij} = \left(\partial v_i / \partial x_j + \partial v_j / \partial x_i\right)/2$ is the strain rate tensor; τ_{ij} is the turbulent stress based on the Smagorinsky SGS (sub-grid scale) model; $\beta_{ij} = \beta \delta_{i3}\delta_{j3}$ is the dissipation factor matrix, in which β is the dissipation factor that equals 0, except in the added dissipation zone; $q^* = q(y, z; t)/\Delta x_s$ is the wave generation source, where $q(y, z; t)$ is the source density assigned only at the source position $\left(x = x_s\right)$ and Δx_s is the mesh width at the source position; $\tilde{\rho}$ and $\tilde{\nu}$ are the density and the kinematic viscosity averaged over the computational grid, respectively.

- ***Free surface and fluid properties tracking***

The Volume of Fluid (VOF) method developed by Hirt and Nichols [31] is used for free surface tracking. In this method, the interface between air and water is modelled according to a VOF function, F.The VOF function

calculates the volume of water in each cell over time, instead of directly tracking the free surface. The value of the VOF function varies between zero and unity, depending on the air and water proportion in each cell. Unity occurs if the cell is completely filled with water and zero occurs if the cell is completely filled with air or an obstacle. The advection of the VOF function is obtained by solving the conservation of fluid mass in each cell (see Equation 2.12).

$$\frac{\partial(mF)}{\partial t}+\frac{\partial(mv_jF)}{\partial x_j}=Fq^* \tag{2.12}$$

If the fluids are assumed to be incompressible and immiscible, the density and kinematic viscosity can be calculated using the VOF function F,

$$\hat{\rho}=F\rho_w+(1-F)\rho_a \tag{2.13}$$

$$\hat{\nu}=F\nu_w+(1-F)\nu_a \tag{2.14}$$

where ρ_w and ρ_a are the density of water and air, respectively; ν_w and ν_a are the kinematic molecular viscosity of water and air, respectively.

- ***Cutcell method***

The numerical model uses a Cartesian grid system to discretise the governing equations. In order to incorporate obstacles (e.g., the structure and bottom slope) in the numerical domain, the cut cell method is used. This method is similar to the fraction area/volume obstacle representation (FAVOR) method, developed by Hirt and Sicilian [32]. The shape of the structure was made up of cut cells, whose details were stored in the input data file. The information stored in the input data file included the following four parameters in each cell: the ratio of fractional volume open to flow, m_v ; the ratio of fractional area open to flow in each direction, m_x, m_y, and m_z; the area of the wetted surface of the

structure; and the unit normal vectors to the obstacle surfaces. The governing equations were formulated in terms of the computed four parameters to block portions of each cell containing the obstacle.

- ***Turbulence model***

The large-scale turbulences occurring during the fluid flow are resolved by the governing equations. However, in order to resolve the small-scale turbulences, the Smagorinsky SGS model ([33]) is used. The momentum exchange by the sub-grid scale turbulence is transported by means of an eddy viscosity term. The eddy viscosity term ν_e, is determined as shown in Equation 2.15.

$$\nu_e = (C_{sg}\Delta)^2 \left|D_{ij}\right| \tag{2.15}$$

where $D_{ij} = \left(\partial v_i / \partial x_j + \partial v_j / \partial x_i\right)/2$ is the strain rate tensor; C_{sg} is the Smagorinsky constant; Δ is the sub-grid scale characteristic length.

- ***Boundary conditions***

In regard to the boundary conditions, the dynamic boundary condition is automatically satisfied due to the two-phase flow model (i.e., the water and the air phases are modelled as fluid), while the kinematic boundary condition is achieved by tracking the VOF function. An impermeable (normal velocities) and a non-slip condition (tangential velocities) are imposed to treat the bottom boundary condition and obstacle boundary condition. In order to prevent reflected waves in the computational domain, there are numerical dissipation zones, which are added to the inlet and outlet open boundaries. This dissipation method is similar to that proposed by Hinatsu [34], in which the dissipation zones are gradually coarsened towards the open boundary.

- ***Solution method***

A staggered grid system is used for discretization of the governing

equations using the finite difference technique. For the discretisation of the Navier-Stokes equations, the forward difference method is used for the time derivative terms, while a combination of the central difference method and the upwind method called the hybrid method is used for the advection terms, and the central difference method is employed for the non-advection terms. In the hybrid method, the relative contribution of the central difference method and the upwind method in the solution can be adjusted by changing a parameter alpha in the solution method. The Simplified Maker and Cell (SMAC) method ([35]) is incorporated to iteratively adjust the velocities and pressure in each cell until the continuity equation is reasonably satisfied. In order to solve the Poisson pressure equation, an algebraic multi grid (AP-AMG) solver developed by the Allied Engineering Corporation [36], Japan, is used.

2.2 Research Approach

The overall research approach used in the thesis is as follows:

Based on the literature review, it is found that there are not many guidelines available for the estimation of breaking wave forces on a jacket structure. There is a clear research gap in understanding the breaking wave interactions with jacket structures. The aim of the present research is to fill this research gap based on experimental and numerical investigations. The overall research approach is illustrated in Figure 2.7.

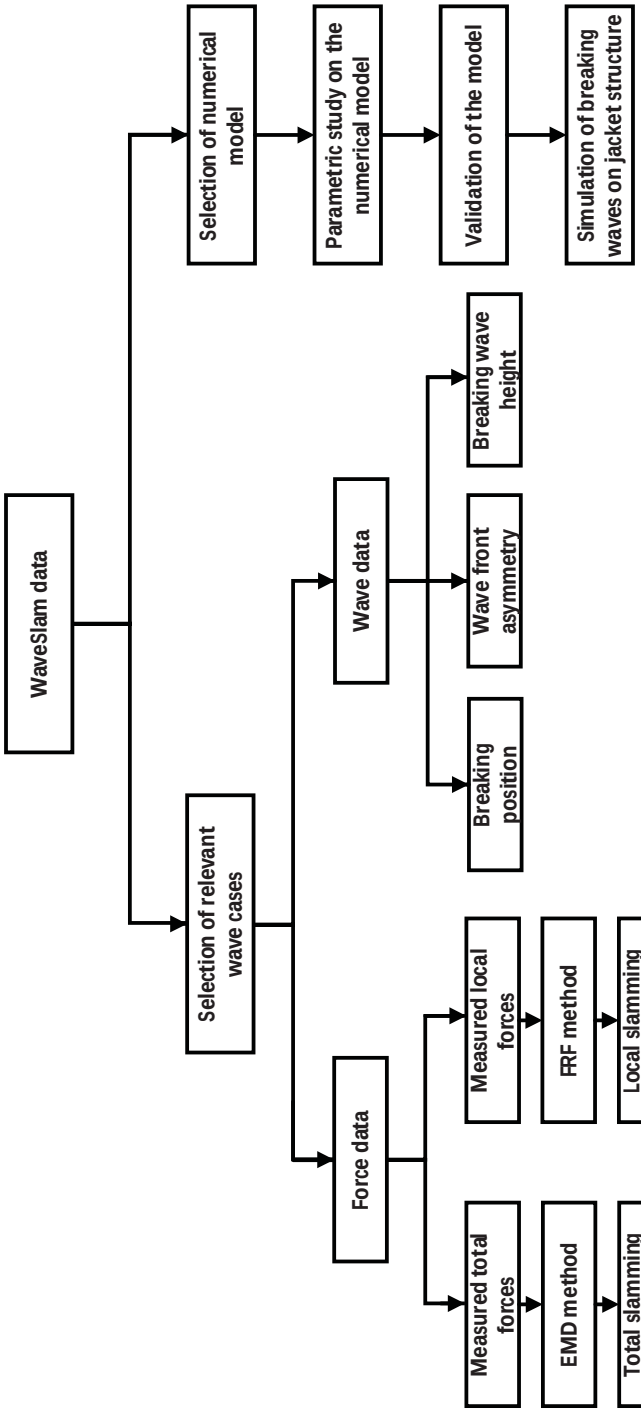

Figure 2.7 Overall research approach used in this thesis

In each stage of the research, the results were published in various international journals and conference papers. The present thesis is based on these published papers, which are appended in the thesis. The link between these appended papers is shown in Figure 2.8.

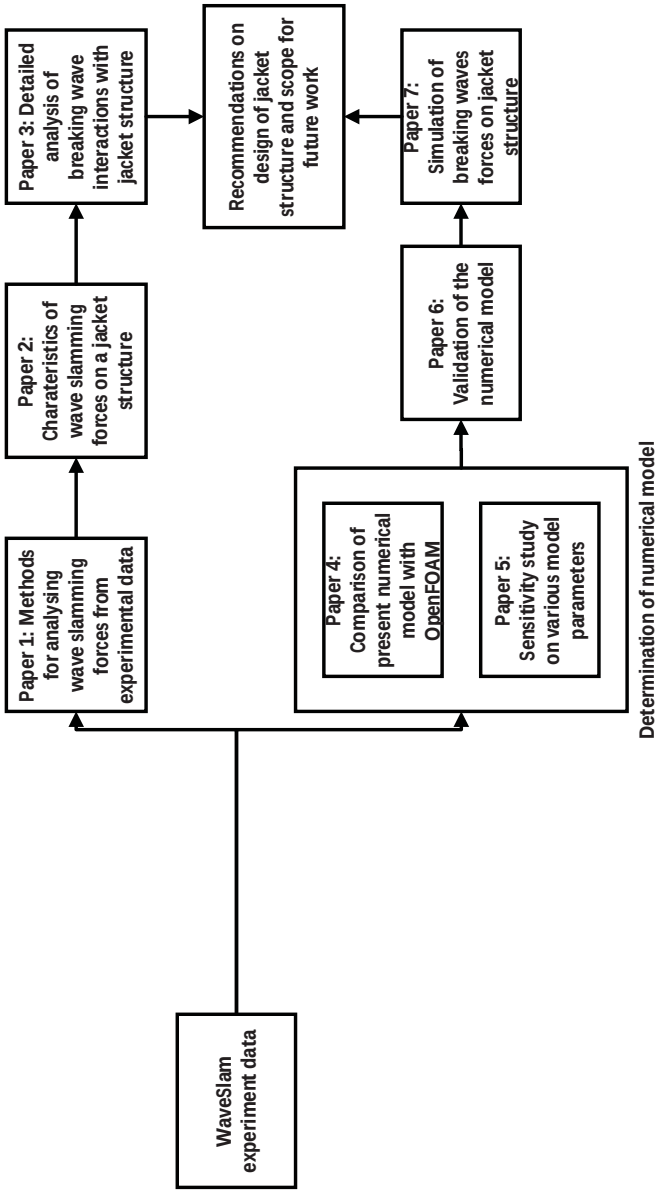

Figure 2.8. Link between appended papers

2.2.1 Experimental Data Analysis

In the experimental data, there are measurements of the wave deformations and kinematics in addition to the wave forces on the jacket structure. In this section a detailed description of the experimental data analysis and an interpretation of the results are presented.

2.2.1.1 Determining breaking wave forces from experimental data

During the WaveSlam experiment, the jacket structure was tested for large number of breaking wave conditions, especially plunging breakers. The wave forces on the jacket were measured by total and local force transducers integrated into the jacket as shown in Figure 2.3. As our main interest is the wave slamming forces, it is important to filter out these forces from the measured forces.

Paper 1: "Methods for Analysing Wave Slamming Loads on Truss Structures used in Offshore Wind Applications based on Experimental Data "*

***** Jose, J., Podrażka, O., Obhrai, C., Gudmestad, O.T., and Cieślikiewicz, W., 2016, "Methods for Analysing Wave Slamming Loads on Truss Structures used in Offshore Wind Applications based on Experimental Data," *International Journal of Offshore and Polar Engineering*, Vol. 26(2), pp. 100-108.

In the case of non-breaking waves, the forces on the jacket structure are due to the drag and inertia effects which are represented by the Morison equation. The complexity of the wave forces increase when there are breaking wave structure interaction. When the wave breaks on the structure, there is a slamming action of the wave front on the structural members. The forces due to these wave slamming are impulsive in nature with an impact duration in the range of milliseconds. In addition to these two forces, there is a dynamic amplification of the forces due to the effect

of the structure's natural frequency. In the present experimental force measurements there existed the presence of these three force components. A typical measured total wave force on the jacket structure is shown in Figure 2.9.

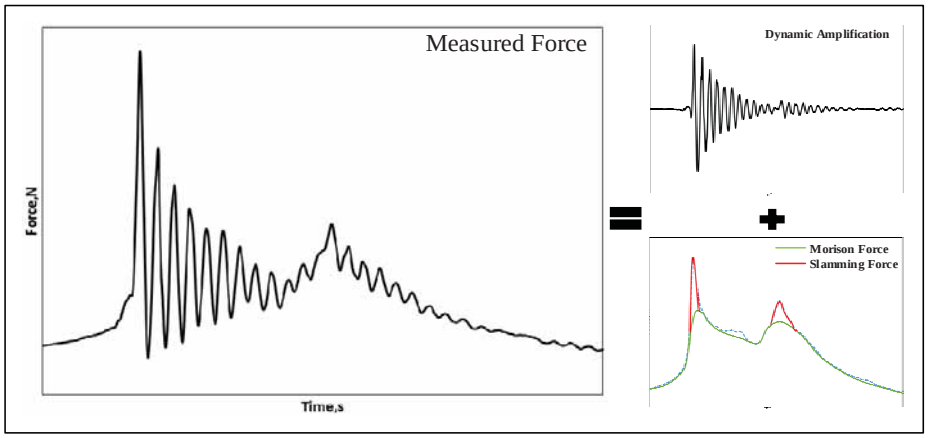

Figure 2.9. Force components in the total measured force

In this paper, two different methodologies to separate the slamming forces from the total and local force measurements were presented. The EMD method was used for filtering the slamming forces from the total measured forces and the FRF method was used to filter out the local slamming forces from the local measured forces. The detailed application of the above mentioned methods on the experimental data was demonstrated in this paper for a certain wave case. The descriptions of both methods were given in section 2.1.2 in this thesis.

- ***Total slamming force filtration***

The EMD method followed by a low pass filtration of the measured force was found to be sufficient to separate the total slamming force from the total force measurements. Figures 2.10 and 2.11 show the separation of the total slamming force from the measured total force for a selected wave case.

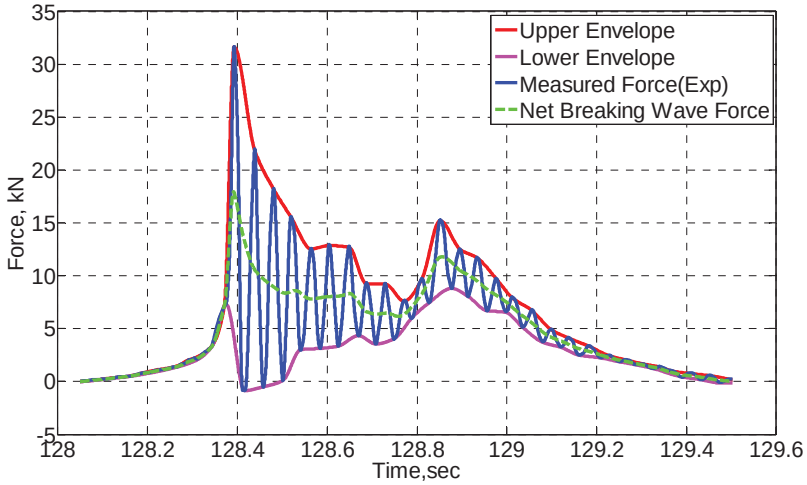

Figure 2.10 Net breaking wave force filtered out by the EMD method

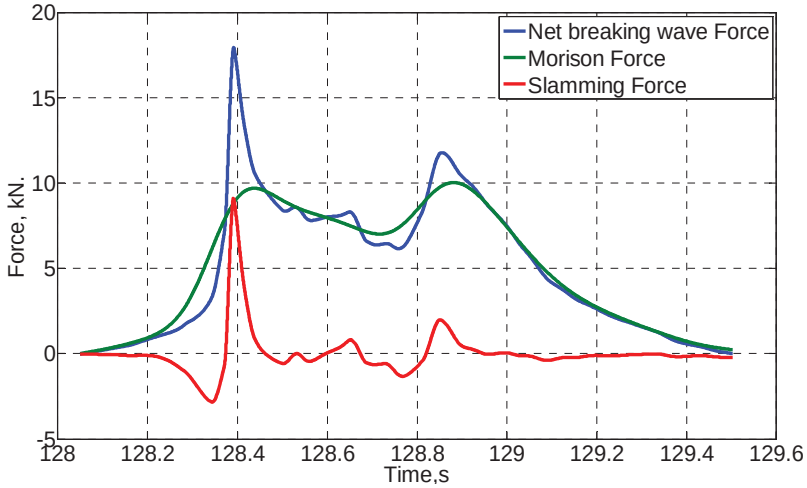

Figure 2.11 Total slamming force obtained after filtering the Morison force from the net breaking wave force

The EMD method eliminates the dynamic amplification component and the resulting force time series is the net breaking wave force, which is a combination of the Morison force and the wave slamming force (see Figure 2.10). In order to remove the Morison force from the net breaking wave force, a low pass filter is used. As the frequency of the Morison force component is similar to the wave frequency, the cut-off frequency

of the low pass filter is set very close to the wave frequency, in such a way that it will not remove any actual contribution to the wave slamming force (Figure 2.11).

- ***Local slamming force filtration***

The nature of the local wave forces on the jacket members is similar to the total forces. It also has three force components. In order to separate the local slamming forces from the local measured forces, the FRF method was used. During the experiment, there were hammer tests performed on the local force transducers and those measurements were used to obtain the transfer functions for these transducers against impulsive loadings. The transfer function calculated for a typical hammer test performed on the local force transducer FTBF01 is shown in Figure 2.12. Similarly, the transfer functions were calculated for all of the local force transducers. In order to obtain the local slamming force, these transfer functions were applied on the measured local forces as described in section 2.1.2. The separation of the local slamming force from the local measured force measured by the bracing transducer FBF01 for the selected wave case is demonstrated in Figures 2.13 and 2.14. The slamming force obtained after the FRF method was filtered in order to get rid of any unwanted noise signals using a low pass filter.

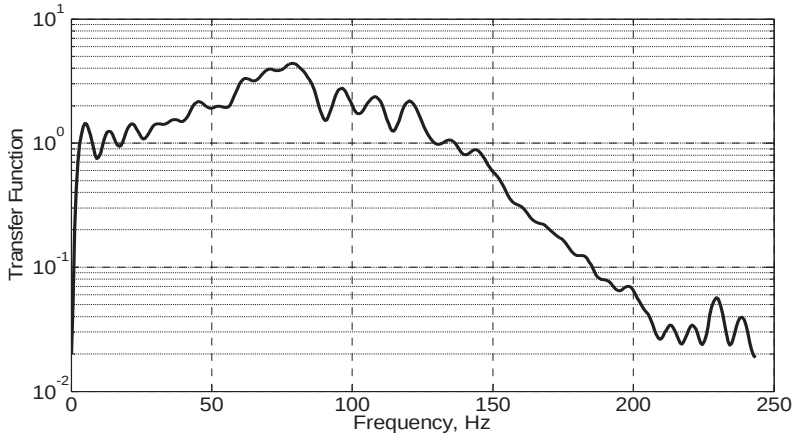

Figure 2.12 Transfer function (semi log scale) calculated for the bracing force transducer FTBF01.

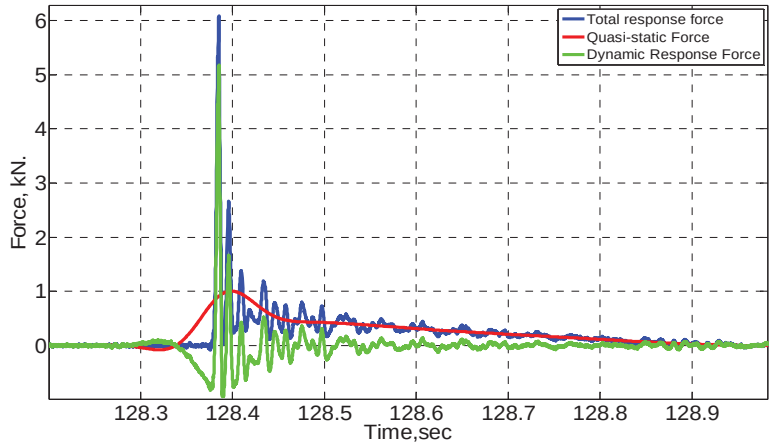

Figure 2.13 Local force recorded by the bracing force transducer FTBF01, quasi- static part and the dynamic response force.

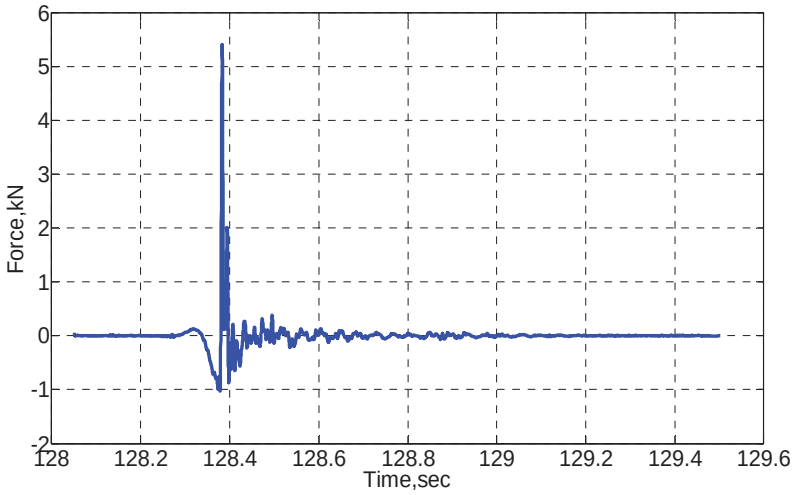

Figure 2.14 Filtered local slamming force

- ***Slamming coefficient***

In the case of the monopile, there is only a single value of the slamming coefficient which is used to estimate the slamming forces on the structure using the empirical force formula. The slamming forces are estimated for the entire monopile, not locally along the member. However, in the case

of jackets, there are many local members running in different orientations in the space. Each member can be represented as a monopile. Hence it is important to consider the total slamming forces on the jacket and local slamming forces on jacket members.

Based on the estimated slamming forces, the local and total slamming coefficients on the jacket structure were obtained. In order to calculate the total slamming coefficient, the total slamming force was assumed to be distributed on the jacket members in the wave impact region (see Figure 2.15). The wave impact region was defined based on the preliminary studies ([3, 11, 18]) and video recordings. For the present wave case the total slamming coefficient was obtained as 1.10, which is much smaller than the values suggested in the literature for monopile structures.

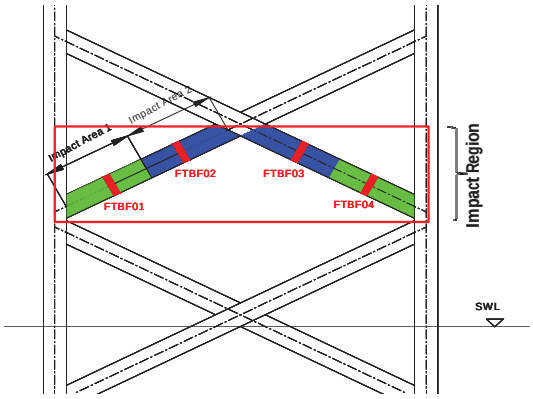

Figure 2.15 Definition of impact region for total and local force measurements

In the case of the local slamming coefficient, the method is more straight forward. The obtained slamming coefficient represents the coefficient for the local area of the member. The slamming coefficient obtained for the present wave case, 3.95, was closer to the value suggested by Wienke and Oumeraci [7]. However, these results are not sufficient to suggest a final value of the slamming coefficient for the jacket structure. However,

the conclusions from this paper are important for the further analysis of the measurement data.

Discussions on the findings in Paper 1

The two methods, the EMD and the FRF methods, performed well for the initial analysis of the force data. These two methods were then used to analyse further wave cases as reported in section 2.2.1.2.

Even though, the total and local measured forces have three force components, the characteristics of these forces were different in both the cases. The relative contribution of the Morison forces in the local measured force was much lower compared to the total measured forces (see Figures 2.10 and 2.13). The local slamming forces were found to be more impulsive compared to the total slamming forces. The reasons for such behaviour of the forces need to be studied further.

All the discussions from this paper were based on a single wave case. Additional wave cases were studied in papers 2 and 3, to provide more robust estimates of the slamming coefficients on a jacket structure

2.2.1.2 Characterisation of breaking wave interactions with the jacket structure based on the experimental data

In paper 1, the methodologies for estimation of the slamming forces and slamming coefficients from the experimental measurements were presented. The study was performed for a selected wave case in order to verify the applicability of the chosen methods. In this section, a detailed study on the experimental data is carried out, analysing the slamming forces for a wide range of wave cases. The characteristics of the breaking wave are governed by different wave parameters. A detailed study on these parameters is carried out based on the experimental measurements. The impact of these parameters on the slamming forces on the jacket is also investigated. This section is organised into two papers; paper 2 and paper 3. Paper 2 is an introduction to these studies and the results for a

limited number of wave cases. Further in paper 3, a detailed study is carried out based on all the available relevant experimental data. Paper 3 concludes the results from all possible wave breaking scenarios (within the WaveSlam project) with respect to the jacket structure.

Paper 2: "Characteristics of the Wave Slamming Forces on Jacket Structures under Plunging Breaking Waves based on Experimental Data"*

* Jose, J., Podrażka, O., Gudmestad, O.T., and Cieślikiewicz, W., 2017, "Characteristics of the Wave Slamming Forces on Jacket Structures under Plunging Breaking Waves based on Experimental Data," *In the Proceedings of ASME 36th International Conference on Ocean, Offshore and Arctic Engineering* (OMAE2017), Trondheim, Norway, June 25-June 30.

In this paper, data analysis was carried out for four different wave cases, which represents four different wave breaking scenarios. The wave cases were chosen in such a way that the wave heights were the same for all the cases and the wave period varies from 4.6 s to 5.55 s, resulting in a shift in the wave breaking position with respect to the jacket structure. For each wave case, five different wave samples were chosen for the study. The wave parameters which influence the overall behaviours of the breaking waves were identified and the methodologies to calculate these parameters were introduced.

- ***Slamming forces***

The total and local wave slamming forces on the structure were obtained for the selected wave cases using the methods already described in paper 1. The wave case in which the wave breaks closer to the front members of the jacket imparted maximum slamming forces on the structure. It was also observed that as the relative distance of the breaking location with respect to the jacket increases, the slamming forces reduces. There were

variability in the local and total slamming forces, even for the same wave conditions, especially for stronger breaking cases.

- ***Slamming Coefficient***

In paper 1, slamming coefficients were obtained for both overall jacket and for the local members of the jacket. However, the total slamming coefficient was found to be much smaller compared to the local slamming coefficient. In the present study the slamming coefficients were only obtained for the local members, not for the overall structure. The reasons for ignoring the calculation of the total slamming coefficients are as follows,

- It was observed that there was a "time delay" in the wave impact on the jacket members when the wave breaks on the structure. This time delay in the wave impact on jacket members was observed for all of the wave cases. The occurrence of this delay was random from wave to wave. This was confirmed from the local force measurements (a typical example is shown in Figure 2.16). It was observed that the peak forces recorded by each of the local force transducers on the jacket front were at slightly different times during the wave impact. If the wave front hits the jacket simultaneously, these transducers would have peak forces at the same time. As the total slamming force is the sum of the slamming forces on the jacket members, this impact delay significantly affects the total slamming forces due to shorter impact duration of these forces. Due to this reason the total slamming forces were found to be less impulsive compared to the local slamming forces.

- In most of the wave cases considered in the study, the local slamming forces were found to be much higher than the local Morison forces. Moreover, the total slamming forces were comparable or lower than the total Morison forces. The main reason for such a difference in the slamming forces were due to the "impact delay" as mentioned before. As the Morison force is

a slow varying force, there is no impact of these "time delays" on these forces. The total Morison force will be a sum of the drag and inertia forces on the members of the jacket.

- The jacket structure is more transparent to the incoming waves than a monopile. The size of jacket members are much smaller compared to the monopiles. Considering the impulsive nature of the breaking wave forces, there would be a higher risk of local impacts on the members than on the global structure.

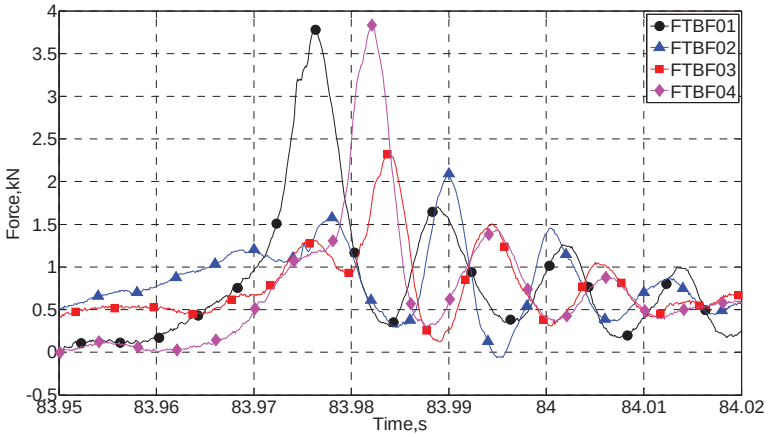

Figure 2.16 Local force measured by the local force transducers on the front bracing members

Considering all the above mentioned points, it was regarded that the local design of the jacket members needs to be focused further in the study. The slamming coefficients for the bracing members were calculated as explained in section 2.1.3. The wave celerity at the time of breaking was obtained from the wave gauge measurement taken during the experiments.

- ***Wave Parameters***

The wave parameters chosen for the present study were breaking wave height, wave breaking location relative to the structure and wave front asymmetry. All of these parameters were estimated from the

measurements by the wave gauges distributed along the wave flume. The variations of these parameters were studied based on the spatial variation in the wave surface elevation along the wave flume. It was noticed that there was a clear dependency of these wave parameters on the breaking wave forces on the structure. Figures 2.17 and 2.18 show the variation in total slamming force against breaking wave height and wave front asymmetry. It was observed that steeper waves imparted maximum slamming forces on the jacket structure.

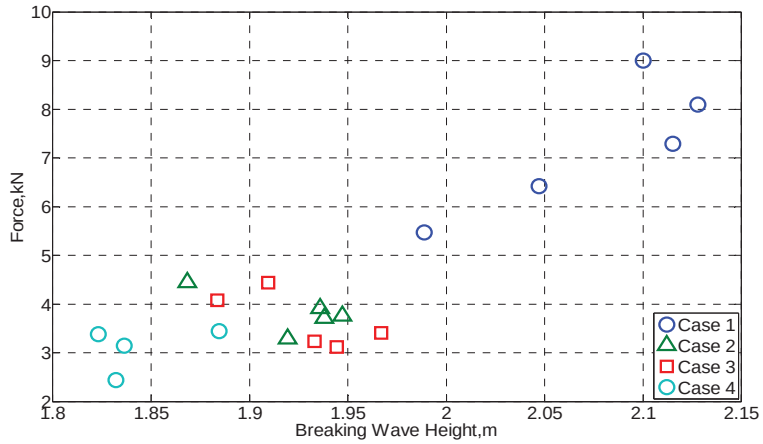

Figure 2.17 Dependency between breaking wave height and total slamming force

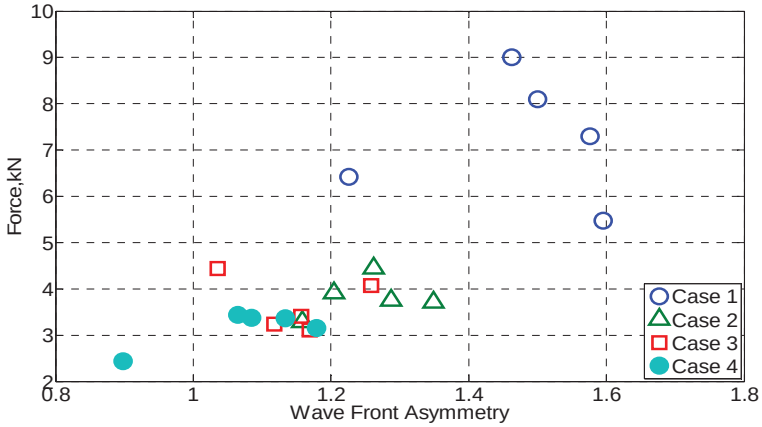

Figure 2.18 Dependency between wave front asymmetry and total slamming force

Paper 3: "Detailed Study on Breaking Wave Interactions with a Jacket Structure based on Experimental Investigations"*

*Jose, J., Podrażka, O., Gudmestad, O.T., and Cieślikiewicz, W., 2017, "Detailed Study on Breaking Wave Interactions with a Jacket Structure based on Experimental Investigations," *Journal of Offshore Mechanics and Arctic Engineering*, Vol. 140(2), pp. 021301.1-021301.14.

It is clear that the wave slamming forces on the structure are very sensitive to the breaking position of the wave and the shape of the wave front. In the experimental set-up, since the position of the structure and the slope of the wave flume are the same, these parameters are governed primarily by the wave height and the wave period of the incoming wave. For the wave cases considered in paper 2, these parameters were varied by changing the incoming wave period only. The wave heights were kept the same for all of the wave cases. However, it was observed (Figure 2.17) that even a slight variation in the breaking wave height had a significant impact on the slamming forces acting on the structure. Hence it was necessary to further extend the study carried out in the paper 2 for various wave breaking conditions. In this paper, most of the relevant wave conditions with respect to the jacket structure were considered taking into account different wave height and wave period combinations.

- ***Breaking Location and Breaking Wave Height***

It was noticed that the breaking location relative to the structure and the wave height have a significant impact on the slamming forces on the jacket. As there were slight changes in these parameters for different wave samples within the same wave condition, an average of these parameters was considered. The estimated breaking location and breaking wave height for all of the wave cases are shown in Figure 2.19.

a)

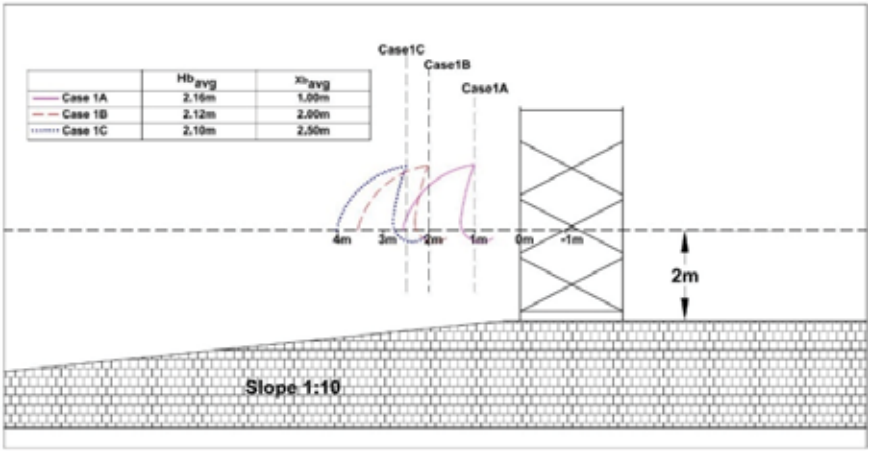
Case1C
Case1B
Case1A
Hb avg
xb avg
Case 1A 2.16m 1.00m
Case 1B 2.12m 2.00m
Case 1C 2.10m 2.50m
4m
3m
2m
1m
0m
-1m
2m
Slope 1:10

b)

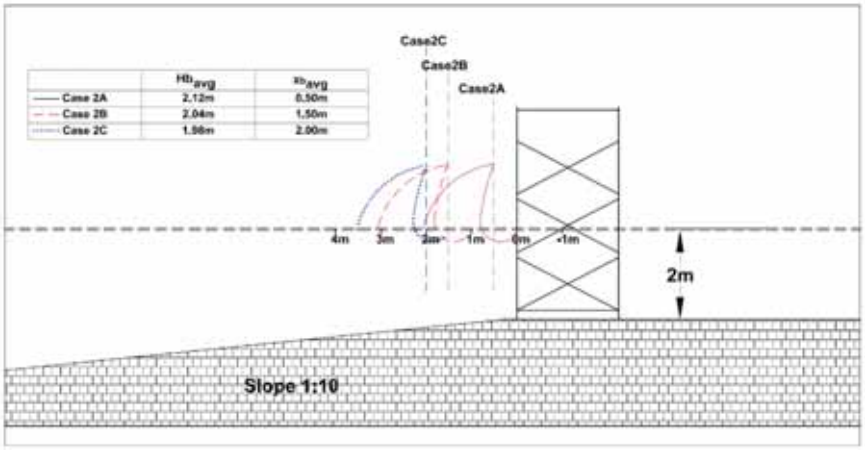
Case2C
Case2B
Case2A
Hb avg
xb avg
Case 2A 2.12m 0.50m
Case 2B 2.04m 1.50m
Case 2C 1.98m 2.00m
4m
3m
2m
1m
0m
-1m
2m
Slope 1:10

c)

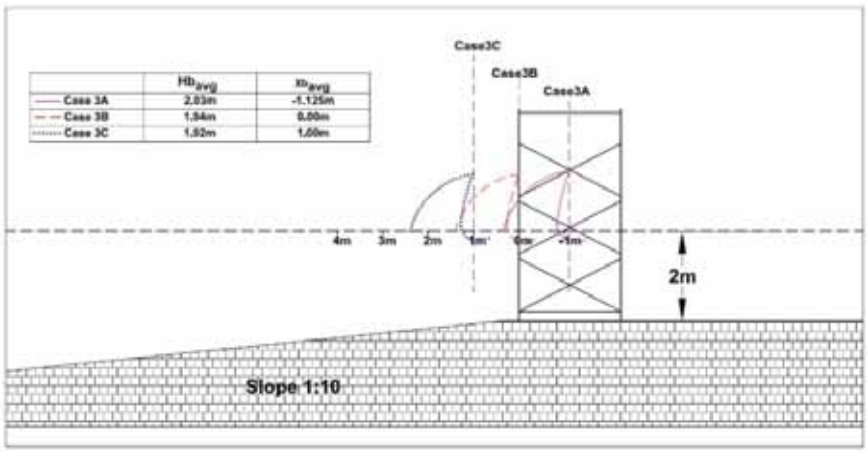

Figure 2.19 Breaking wave height and wave breaking position for different wave cases: a) cases 1A-C, b) cases 2A-C and c) cases 3A-C (Hb_{avg} and Xb_{avg} are average breaking wave height and breaking location with respect to the jacket structure, respectively)

- ***Slamming forces***

The total and local slamming forces on the jacket were estimated for all of the wave cases. There was a significant variation in the slamming forces on the structure for different wave cases. The total slamming forces were found to be maximum when the wave breaks 0.5 m in front of the jacket. In this study wave case 2A represented the scenario with the highest total slamming forces on the jacket structure (see Figure 2.20). There was a noticeable fluctuation in the total slamming force even for the same wave condition, especially for stronger breaking cases.

For the local slamming force study, the force measurements on the bracing members were considered. The local slamming forces were estimated for four different bracing locations (FTBF01-FTBF04). These locations were at symmetric positions on the front of the structure as shown in Figure 2.15. It was observed that the slamming forces on the bracing members were similar at the same elevations. There was a shift in the peak slamming forces from the top of the bracing members to the

bottom as the wave breaking location shifted further ahead of the structure. Similar to the total slamming forces, the maximum local slamming forces on the bracings were obtained for wave case 2A (Figure 2.21). In this wave case, the distribution of local slamming forces on the bracings was more uniform.

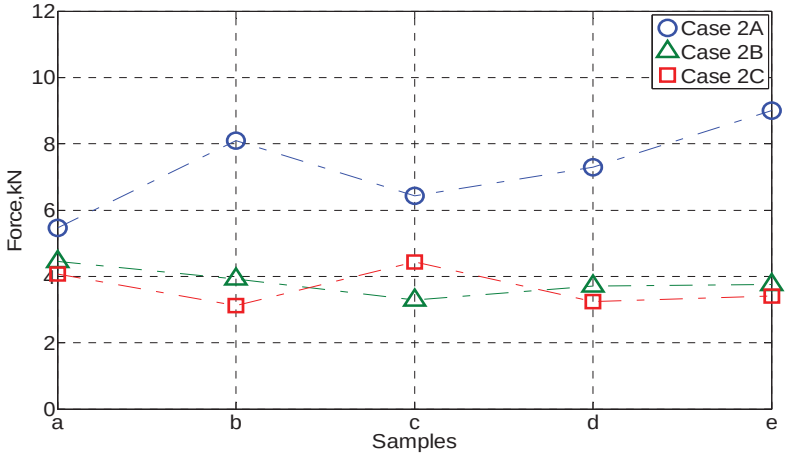

Figure 2.20 Variation in peak total slamming forces on the jacket for five different wave samples for wave cases 2A-2C

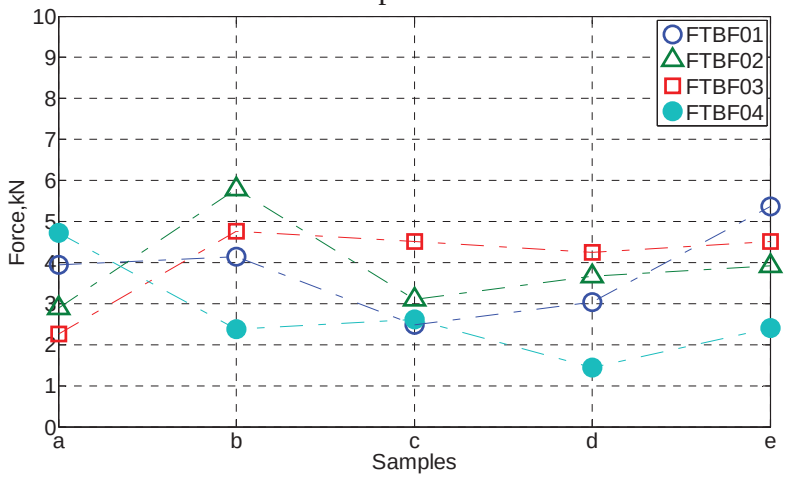

Figure 2.21 Peak local slamming forces on the bracing members FTBF01-04 for wave case 2A

The wave slamming forces were least when the wave breaks in the middle of the structure, as seen in wave case 3A (Figure 2.22). The forces

on the front members of the jacket for this case were merely the quasi-static Morison forces.

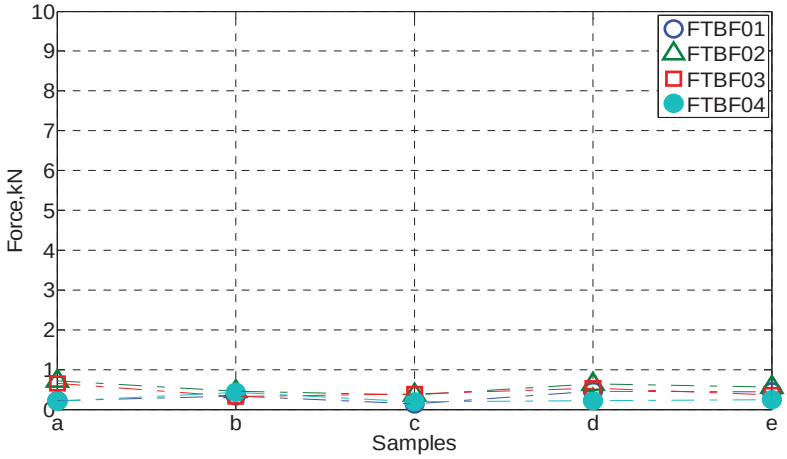

Figure 2.22 Peak local slamming forces on the bracing members FTBF01 to 04 for wave case 3A

- ***Slamming Coefficients***

There were large fluctuations in the slamming coefficients obtained for the bracing members under the different wave cases. The values of the slamming coefficients were mostly affected by the wave breaking position relative to the structure and breaking wave height. The motivation for this study was to find a suitable value of the slamming coefficient which can be used in the design of the jacket members against breaking wave forces. Table 2.1 shows a summary of the slamming coefficients on the bracing members for different wave cases. The maximum value of the slamming coefficient, 6.16, was obtained for wave case 2A.

Table 2.1 Summary of local slamming coefficients

Wave Case No.	Wave Height (m)	Wave Period (s)	Slamming Coefficient, C_s	
			Maximum C_s	Average C_s
1A	1.8	5.55	4.14	2.41

1B	1.8	5.20	4.00	2.45
1C	1.8	4.90	4.96	2.34
2A	1.7	5.55	6.16	3.80
2B	1.7	5.20	4.41	2.86
2C	1.7	4.90	4.64	2.65
3A	1.6	5.55	1.14	0.45
3B	1.6	5.20	3.54	2.38
3C	1.6	4.90	3.05	1.89

- ***Wave Parameters***

A study on the influence of various breaking parameters on the slamming forces showed that the slamming force is also a function of breaking wave height, wave front asymmetry and the breaking location of the wave. However, the impact of the first two parameters was pronounced when the wave breaks near to the structure. In some cases the wave height and wave front asymmetry had little effect on the slamming forces, especially when the wave breaks far from the structure (example, wave case 3A).

Concluding remarks from papers 2 and 3

Based on the results from papers 2 and 3, the major conclusions can be summarised as follows:

- The experimental measurements covered all major breaking wave scenarios with respect to the jacket structure. The slamming forces on the jacket were found to be a function of the wave breaking location and the geometry of the wave front. As the distance of the wave breaking location from the structure increases, the wave slamming forces reduces due to broken waves reaching the structure.

- It can be concluded that the local slamming forces were more impulsive compared to the total slamming forces. Based on the present results, it was concluded that the local slamming forces

on the members are important in the design of jacket structures against breaking waves.

- The wave case in which the breaking occurs at 0.5m ahead of the structure represented the worst wave breaking scenario among all the wave cases considered. In this case, the local slamming forces on the bracing appeared to be symmetrical on the upper and lower parts of the bracings. This is in line with the assumption made by Wienke and Oumeraci [7], that the breaking wave front impacts the vertical cylinder like a vertical wall of water. From the present study, the maximum slamming coefficient obtained for the local members was 6.16, which is similar to the value suggested by Wienke and Oumeraci [7] for the vertical cylinder. It is suggested to use this value of slamming coefficient to obtain the maximum slamming forces on the jacket members in the wave impact region.

2.2.2 Determination and Verification of the 3D Numerical Model

Many complicated engineering problems can be solved with the help of computational fluid dynamics (CFD). There are a number of commercial CFD software packages, such as OpenFOAM, FLOW 3D and Star CCM, which are widely used for such studies. In the present research, a numerical wave tank (NWT) method, 2PM3D, developed by Lee ([30]) was used for solving nonlinear free surface flow. The numerical model was initially developed for performing research on the effect of seepage flow over gravel beaches ([30]). Choi ([19]) further developed the model, incorporating modules to calculate wave forces on obstacles and a sub-model to represent complicated geometries in the computational domain. The numerical model was validated against several experimental measurements ([19]). This numerical model was found to be a useful tool that can predict the nonlinear wave forces on offshore structures. However, compared to previous applications of the numerical model, the simulation of breaking wave forces on the jacket structure is more

complex due to the complexity of the structure and strong nonlinear wave cases considered for the study. The application of the numerical model for the current study is further discussed in this section.

Paper 4: " A comparison of Numerical Simulations of Breaking Wave Forces on a Monopile Structure using Two Different Numerical Models based on Finite Difference and Finite Volume Methods "*

* Jose, J., Choi, S.J., Giljarhus, K.E.T., and Gudmestad, O.T., 2017, "A Comparison of Numerical Simulations of Breaking Wave Forces on a Monopile Structure using Two Different Numerical Models based on Finite Difference and Finite Volume Methods," *Ocean Engineering*, Vol. 137, 78-88.

As mentioned before, there are many commercial and popular CFD software packages, which are widely used for complicated engineering problems like wave breaking. Among them, OpenFOAM is quite popular in the research field as it is open source and technologically equivalent to many commercial software packages. In this paper, the authors compared the present numerical model (2PM3D) with OpenFOAM, being applied to wave breaking studies. The numerical models were used to simulate the breaking wave forces on a monopile structure. The simulation results were compared with theoretical results and available experimental measurements from the hydraulic model tests previously undertaken by Irschik et al. ([37]).

- ***Comparison of both models***

Both of the numerical models were different in many aspects. Table 2.2 summarises a comparison of various parameters used in both of the numerical models. In OpenFOAM, the wave generation and absorption were performed using the waves2Foam toolbox.

Table 2.2 Comparison of 2PM3D and OpenFOAM

Description	**2PM3D**	**OpenFOAM-waves2Foam**
Spatial Discretisation	Finite Difference Method	Finite Volume Method
Mesh	Structured Mesh	Unstructured Mesh
Modelling Method	Cut Cell Method	Body Fitted Mesh
Pressure Velocity Coupling	Simplified Marker Cell (SMAC)	PIMPLE
Turbulence Model	Large Eddy Simulation (LES)	SST k - ω
Surface Tracking Method	VOF Method	VOF Method
Relaxation Method	Artificial Damping Method	Explicit Method

As a first step, a mesh sensitivity study was performed on both the numerical models and suitable grid sizes were chosen in order to make sure the simulation results are independent of grid sizes. The capability of both numerical models to simulate breaking waves was studied by considering two different scenarios.

- ***Scenario 1: without bottom slope and geometry***

In this scenario, the numerical wave tank (NWT) was considered without a bottom slope or any geometry. That means the wave was allowed to flow over a flat bottom without any obstacles. In order to validate the wave generation and the ability of the models to transport the waves without excessive dissipation, the simulated wave surface elevation results were compared with the theoretical waves. In the absence of any bottom slope in the numerical wave tank, there would not be any wave breaking. Hence, it was expected that the same wave would travel along the entire length of the NWT. The non-breaking waves simulated by both the numerical models looked similar to the theoretical results (Figure 2.23).

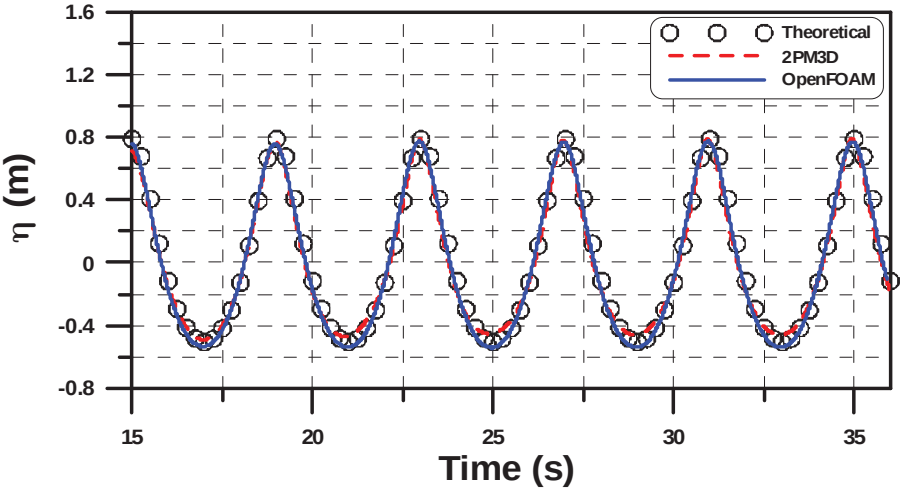

Figure 2.23 Comparison of surface elevation obtained by the numerical models with the theoretical waves at WG2 for non-breaking case

- ***Scenario 2: with bottom slope and cylindrical pile***

In this scenario, the numerical wave tank was made similar to the experimental set-up. The cylindrical pile was modelled near the edge of the slope. There was good agreement of the numerical calculations with the experimental results (Figure 2.24).

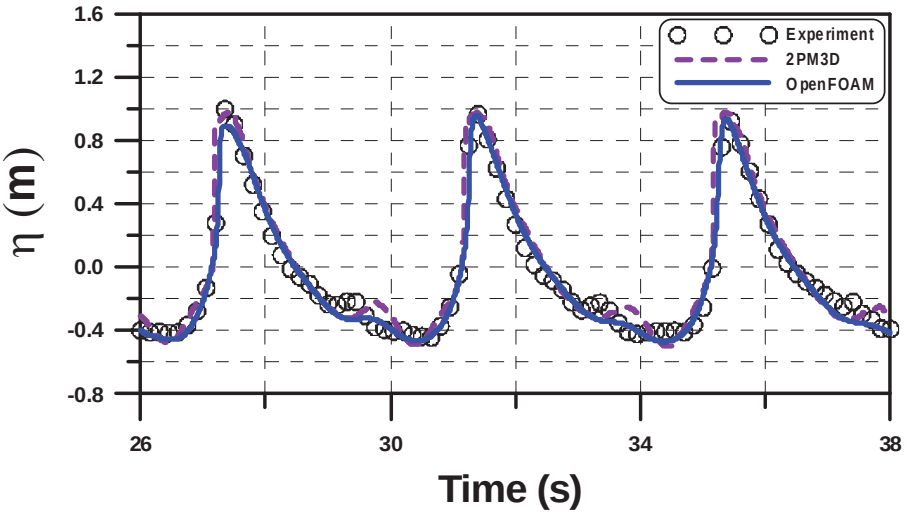

Figure 2.24 Comparison between numerical and experimental results of wave surface elevation measured at WG2 for the breaking case

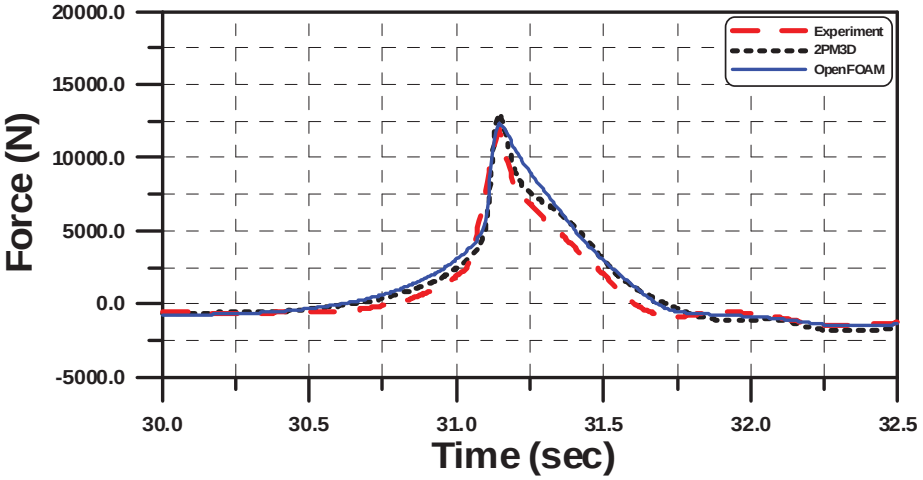

Figure 2.25 Comparison of total breaking wave force obtained by the numerical models with the filtered experimental measurement

The total force on the cylindrical pile under the action of wave breaking was compared for both the numerical models as shown in Figure 2.25. The nature of the wave force calculated by both the numerical models was similar to the experimental measurements. However, the 2PM3D results were slightly higher (5%) compared to the OpenFOAM results.

- ***Secondary Load Cycle***

When the wave flows past the cylinder, the blockage of the flow by the cylinder will result in a downstream gap at the back of the cylinder, which is filled by the diffracted waves. These diffracted waves create local pressure on the back side of the cylinder, which is called a secondary load. The secondary load effects simulated by both the numerical models were reasonably good.

Discussions on the findings in Paper 4

This paper compared the 2PM3D numerical model with the OpenFOAM model. The validation of both numerical models was carried out by

simulating a number of non-breaking and breaking waves in the numerical wave tank and comparing the results with theoretical waves and experimental measurements. Based on the comparisons, it was concluded that the present numerical model is as powerful as popular numerical models in simulating breaking wave forces on structures. However, it is important to further fine-tune the model parameters for the accurate simulation of breaking forces on a jacket structure.

Paper 5: "Sensitivity Study on a 3D Numerical Model for Estimating Breaking Wave Forces on a Jacket Structure"*

*Jose, J., Choi, S.J., and Gudmestad, O.T., 2017, "Sensitivity Study on a 3D Numerical Model for Estimating Breaking Wave Forces on a Jacket Structure," *In the Proceedings of 27th International Ocean and Polar Engineering Conference* (ISOPE2017), San Francisco, California, June 25- June 30.

Within any numerical model, appropriate numerical methods are used to represent various physical phenomena involved in wave breaking. There are many decisions that need to be made in the selection of proper parameters in these numerical methods. The selection of these parameters has a significant impact on the numerical solution. It is important to know the sensitivity of these numerical parameters in the solutions. However, there is not much guidance available on the selection of the correct numerical parameters to be used in these models. In this paper a sensitivity study was performed on various numerical parameters used in the present numerical model, with respect to breaking wave simulations on a jacket structure. The various numerical entities chosen for the sensitivity study were grid sizes, numerical schemes, wall boundary conditions, surface tension, the turbulence model and wave theories. Table 2.3 shows a summary of the parameters used. Simulations were performed for each of these settings in the numerical model and the results were compared with the experimental measurements from the WaveSlam.

Table 2.3 Parameters used in the sensitivity study

Sensitivity Study	Cases	LES Model/C_{sg}	Numerical Schemes	Wave Theory	Wall boundary	Surface Tension
Grid Sensitivity	1	C_{sg}=0.1	Alpha=0.6	Stream	Non Slip	Included
	2	C_{sg} =0.1	Alpha=0.6	Stream	Non Slip	Included
Numerical Schemes	1	C_{sg} =0.1	Alpha=0.6	Stream	Non Slip	Included
	2	C_{sg} =0.1	Alpha=0.8	Stream	Non Slip	Included
	3	C_{sg} =0.1	Alpha=1.0	Stream	Non Slip	Included
Wall Boundary Conditions	1	C_{sg} =0.1	Alpha=0.6	Stream	Non Slip	Included
	2	C_{sg} =0.1	Alpha=0.6	Stream	Slip	Included
Surface Tension Forces	1	C_{sg} =0.1	Alpha=0.6	Stream	Non Slip	Included
	2	C_{sg} =0.1	Alpha=0.6	Stream	Non Slip	Not Included
Turbulence	1	C_{sg} =0.1	Alpha=0.6	Stream	Non Slip	Included
	2	C_{sg} =0.2	Alpha=0.6	Stream	Non Slip	Included
	3	Not included	Alpha=0.6	Stream	Non Slip	Included
Wave Theories	1	C_{sg} =0.1	Alpha=0.6	Stream	Non Slip	Included
	2	C_{sg} =0.1	Alpha=0.6	Airy's	Non Slip	Included

Recommendations from the sensitivity study

Based on the sensitivity study, various recommendations were made on the use of numerical parameters in the present numerical model. The recommended parameters were considered as the optimum values for the simulations.

- ***Grid sizes***

The simulation results showed that a minimum grid size of 0.04 m is sufficient to simulate the breaking waves in the computational domain using the present numerical model. However, considering the complexity of the structure, it was recommended to use a finer grid size (0.03 m) for accurate estimation of breaking wave forces on the jacket

structure.

- ***Numerical Schemes***

A sensitivity study was performed on the hybrid scheme parameter used for the discretisation of the advection term in the Navier Stokes equations. It was concluded that it is important to keep the solution schemes higher order in order to maintain accuracy of the solutions. An alpha factor (refer to section 2.1.5) of 0.6 was recommended for the present simulations.

- ***Wall boundary conditions***

There was no significant impact of slip and non-slip conditions on the numerical solution.

- ***Surface tension***

It was observed that there was no significant impact of the CSF model due to surface tension on the present simulation results as these forces were much smaller compared to wave impact forces. However, it is recommended to use the CSF model for the simulations as the stability of the numerical solution increases due to the use of the interface smoothening method used in this model.

- ***Turbulence model***

For the simulation performed without any turbulence model, there was a significant reduction in the forces on the structure due to the difference in the wave breaking pattern. Based on the sensitivity study on the LES model, a Smagorinsky's constant, C_{sg}, of 0.1 was recommended for the present simulations.

- ***Wave theories***

It was recommended to use a nonlinear wave theory for wave breaking studies in order to account for the nonlinearities during the wave

breaking. For the present simulations, the Stream function wave theory showed good agreement with the experimental measurements.

2.2.3 Simulation of Breaking Wave Forces on the Jacket Structure

The present numerical model (2PM3D) is found to be a good tool for simulating breaking wave forces on the jacket structure. The initial validation of the numerical model was done in papers 4 and 5. In this section, the results from the numerical simulations of breaking wave forces on the jacket are presented. The relevant wave cases identified from the experimental study were used for the simulations. This section is organised into two papers.

Paper 6: "Breaking Wave Forces on an Offshore Wind Turbine Foundation (Jacket Type) in the Shallow Water"*

* Jose, J., Choi, S.J., Lee, K.H., and Gudmestad, O.T., 2016, "Breaking Wave Forces on an Offshore Wind Turbine Foundation (Jacket Type) in the Shallow Water," *In the Proceedings of 26th International Ocean and Polar Engineering Conference*, Rhodes, Greece, June 26-July 2.

In this paper, the numerical simulations were performed for a non-breaking wave and a few breaking wave cases from the experimental study. The numerical simulations were carried out in the same model scale as that of the experimental set-up. The free-surface elevation, horizontal water particle velocities, and breaking wave forces on the jacket calculated by the numerical model were compared with the experimental data to confirm the accuracy of the model. The local slamming forces were calculated for the front and back vertical legs of the jacket. Based on these local slamming forces, the distribution of local slamming coefficients on the members was presented. The incident wave conditions considered for the study are shown in Table 2.4.

Table 2.4 Incident wave conditions

Case	Type	Wave Height	Wave Period	Water Depth
		(m)	(s)	(m)
1	Non-breaking	0.75	4.0	4.3
2	Breaking	1.40	5.2	4.3
3	Breaking	1.50	5.2	4.3
4	Breaking	1.60	5.2	4.3

- ***Non-breaking wave***

In the case of the non-breaking wave, there were no wave slamming forces acting on the jacket. The total wave force on the jacket was due to the Morison force component only (see Figure 2.26). There was no sign of dynamic amplification of the force in the experimental measurements. Consequently, a direct comparison of the experimental data with the CFD results was performed. The wave surface elevation and water particle velocities also showed very good agreement with the experimental measurements.

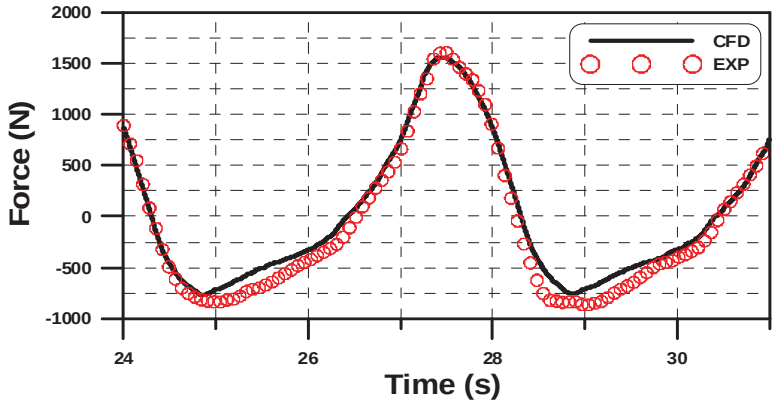

Figure 2.26 Comparison of total wave force on the jacket between the CFD and experimental results for non-breaking wave

- ***Wave Surface Elevation and Water Particle Velocity***

The breaking wave forces are very sensitive to the wave height. Hence it

is important to ensure that the wave generated by the CFD model matches with the experimental measurements. As the wave approaches the sloping bottom, the wave nonlinearities become prominent, with steeper wave crests and flatter troughs. The wave surface elevation and water particle velocities calculated from the simulation agreed reasonably well with the measurements (Figures 2.27 and 2.28).

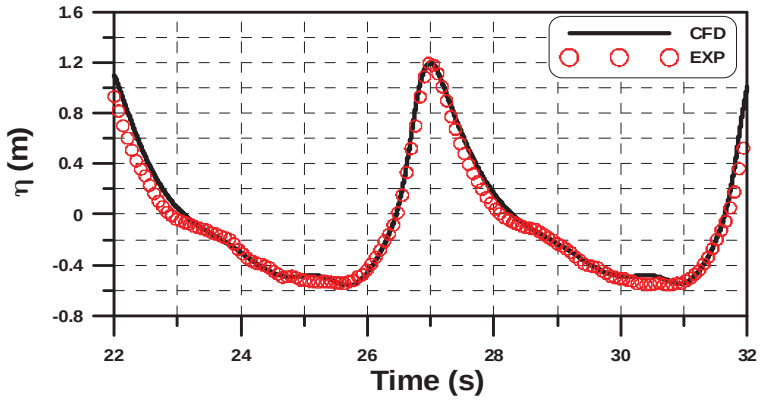

Figure 2.27 Comparison of the free surface elevations between the CFD and experimental results for case 3 at wave gauge WG3

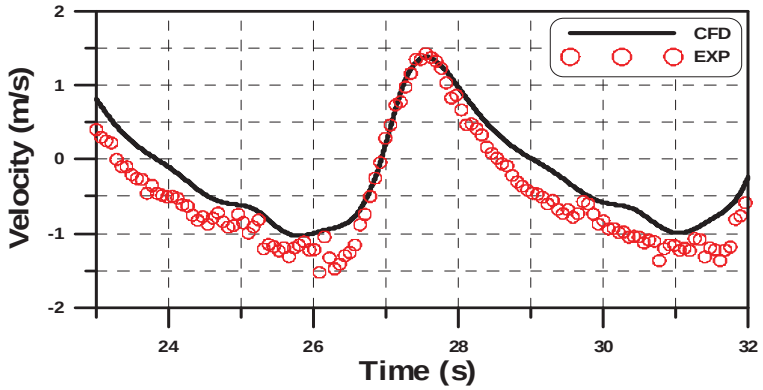

Figure 2.28 Comparison of the water particle velocities between the CFD and experimental results for case 3 at velocity gauge VG1

- ***Total wave force***

In the numerical model, the jacket structure was modelled as a rigid geometry. Unlike the experimental measurements (see Figure 2.9), there

was no dynamic amplification of the forces in the numerical model. Hence a direct comparison of the numerical results with the experimental measurements was not possible. In order to compare the measured force with the CFD calculations, the dynamic amplification component was removed from the measured force with the help of the EMD algorithm. The total forces calculated by the CFD model were compared with the total forces from the measurements after removing the dynamic amplification as shown in Figure 2.29.

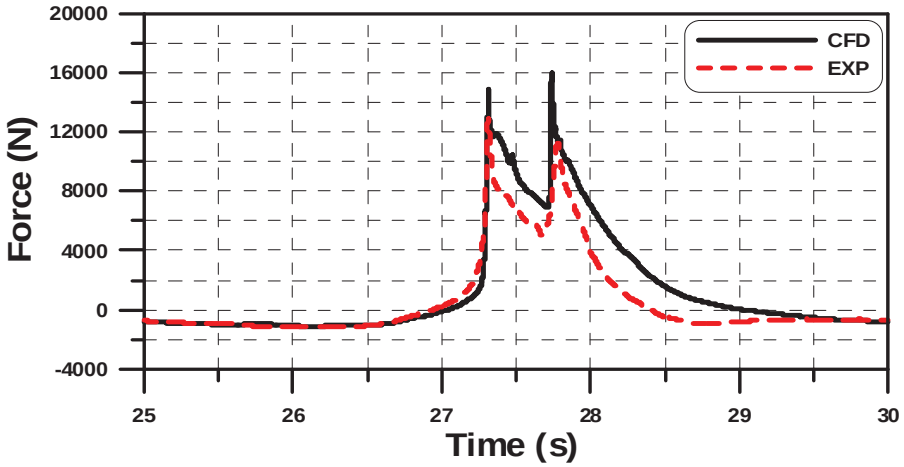

Figure 2.29 Comparison of total wave force on the structure between the CFD and experimental results for breaking wave case 4.

From the simulation results for the breaking wave cases considered, it was observed that the total forces on the jacket structure were slightly overestimated by the numerical model compared to the experimental measurements. These are the three possible reasons for such a behaviour. Firstly, the present numerical model is based on an incompressible flow and hence the effect of entrained air bubbles in the breaking wave were not taken into account in the simulations. The presence of air bubbles in the breaking wave can reduce the effective density of the water and thereby reduces the impact forces. Similar comments were made by many of the previous researchers, who worked with incompressible CFD models on offshore structures (Choi et al. [38], Hu and Kashiwagi [39]).

Secondly, in the numerical model, the structure was modelled taking into account the x axis symmetry. The total forces on the structure were calculated by multiplying the forces on the half structure by a factor of 2. On the other hand, in the experimental measurements, the wave was not hitting the structure simultaneously across the wave tank. The wave impacts the structure's members at slightly different times (impact delay), which may reduce the total measured force. These effects were not considered in the simulation results. Thirdly, the wave breaking process was slightly slower in the numerical model compared with the experiment. This was checked by the videos recorded during the experiments and the spatiotemporal animations of the free surface elevation in the numerical model. Consequently, the distributions of wave forces on the front and back sides of the structure were slightly different.

- ***Calculation of the Slamming Coefficient***

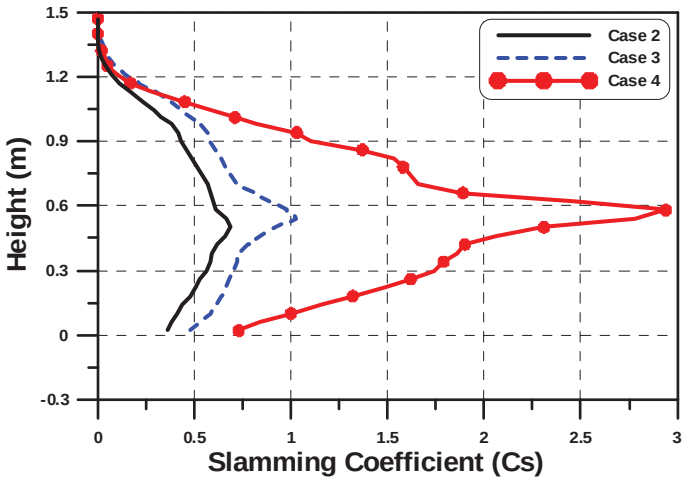

Figure 2.30 Variation in the local slamming coefficients on the front and back vertical members (SWL at 0 m) of the jacket

In the numerical model, the local wave forces on the front and back vertical members (jacket leg) were obtained by incorporating numerical force transducers along the members. The local force transducers, which

are the size of the grid cell in the z direction, were distributed along the length of the vertical members. The slamming coefficients were estimated for the maximum forces calculated by these local force transducers. Using these results, the distribution of the local slamming coefficient along the length of the jacket members were obtained (Figure 2.30).

Discussions on the findings in paper 6

The numerical model simulated the breaking wave interactions with the jacket structure in good agreement with the experimental measurements. However, the numerical model slightly overestimated the total force calculations compared with the experimental results. The distribution of the slamming coefficients on the front and back vertical members of the structure was calculated for the selected wave cases. The maximum slamming coefficient was found to be 2.94, which is smaller than the value suggested by Goda et al. [5] and Wienke and Oumeraci [7]. The numerical results showed a triangular distribution of the slamming coefficients along the vertical members. However the cases presented in the paper were not the extreme cases. Moreover, there was no information on the slamming coefficients on the cross members (inclined members) of the jacket structure.

Paper 7: "Estimation of Slamming Coefficients on Local Members of Offshore Wind Turbine Foundation (Jacket Type) under Plunging Breaker"*

* Jose, J., and Choi, S.J., 2017, "Estimation of Slamming Coefficients on Local Members of Offshore Wind Turbine Foundation (Jacket Type) under Plunging Breaker," *International Journal of Naval Architecture and Ocean Engineering*, Vol. 9(6), pp.624-640.

In this paper a detailed simulation of breaking wave interactions with the jacket structure was performed. The simulations were carried out for 13 incident wave conditions (see Table 2.5), making the wave break in front

of, in the middle of, and at the rear of the structure. The accuracy of each simulations was verified by comparing the wave kinematics and total force on the jacket structure calculated by the numerical model with the experimental measurements. The local wave forces on the jacket members (front and back vertical members, front and back inclined members, and side inclined members) in the wave impact region were calculated with the help of numerical force transducers distributed along the members as shown in Figure 2.31. The distribution of slamming coefficients on the members was obtained based on these local force calculations. The slamming coefficient distributions on jacket members under different breaking scenarios were also investigated.

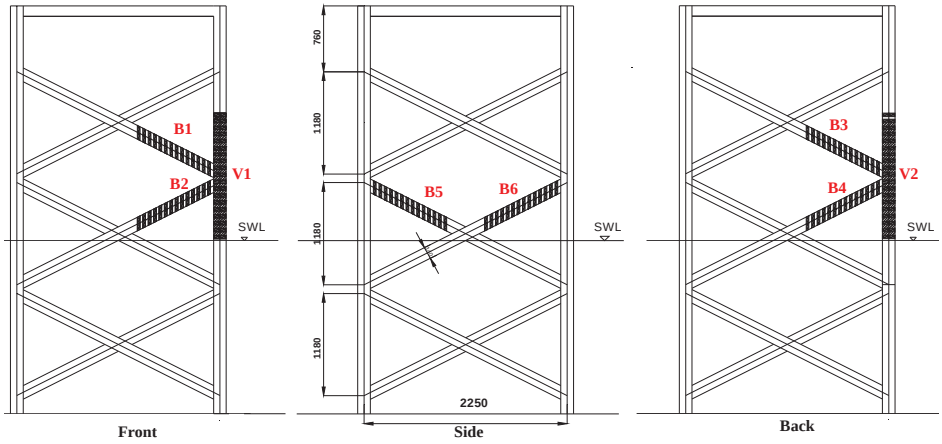

Figure 2.31 Locations of the local force transducers on the jacket structure in the CFD model

Table 2.5 Incident wave conditions

Case	Type	Wave Height	Wave Period	Water Depth
		(m)	(s)	(m)
a1	Non-breaking	0.75	4.00	4.3
b1		1.50		
b2	Breaking	1.60	5.55	4.3
b3		1.70		
c1		1.50		
c2	Breaking	1.60	5.20	4.3
c3		1.70		
d1		1.50		

d2	Breaking	1.60	4.90	4.3
d3		1.70		
e1		1.50		
e2	Breaking	1.60	4.60	4.3
e3		1.70		

- ***Wave surface elevation and water particle velocities***

The wave surface elevations and water particle velocities calculated by the numerical model were validated against the experimental data for all of the wave cases. The comparison of the simulation results and measurements showed reasonable agreement for all of the cases (Figures 2.32 and 2.33).

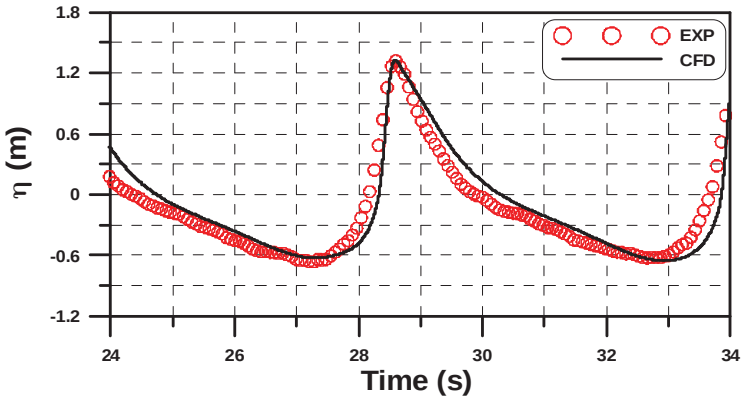

Figure 2.32 Comparison of the free surface elevations between the CFD and experimental results for case b3 at wave gauge WG5

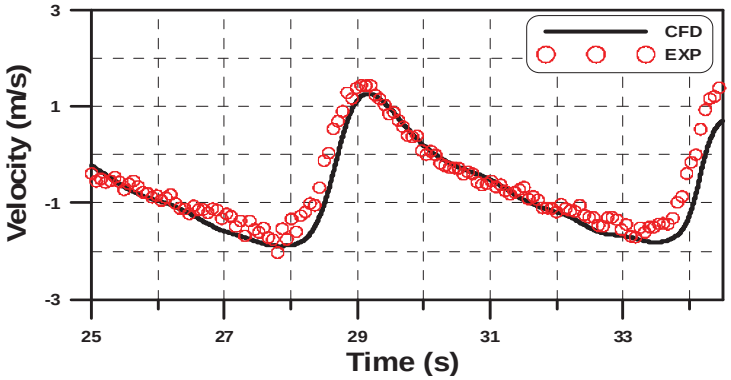

Figure 2.33 Comparison of the water particle velocities between the CFD and experimental results for case b3 at velocity gauge VG1

- ***Total wave force on the structure***

As discussed in paper 6, in order to compare the total wave forces on the structure estimated by the numerical model, the EMD method was used to filter out the dynamic amplification component in the measured force. There was reasonable agreement in the numerical results and experimental measurements for all the wave cases (one of the case is shown in Figure 2.34). However, certain discrepancies were also noticed in the results, especially for the second force peak in the force time series.

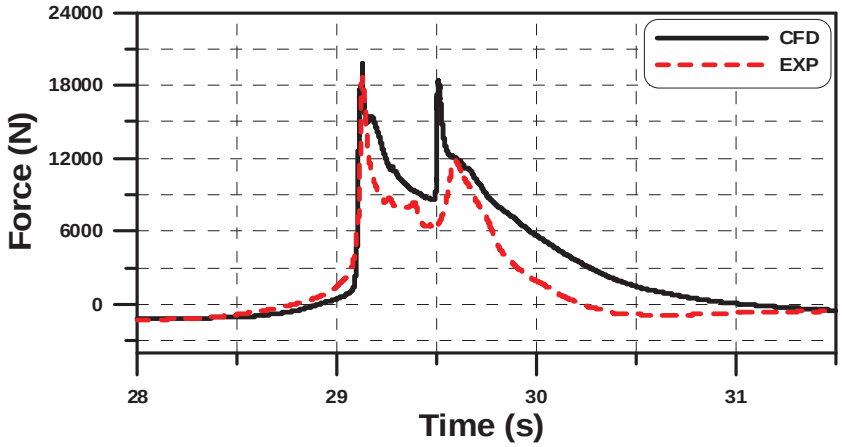

Figure 2.34 Comparison of total wave force on the structure between the CFD and experimental results for breaking wave, case b3

- ***Distribution of slamming coefficients on jacket members***

The slamming coefficients were estimated based on the local forces measured by the numerical force transducers on the members. Based on the study it was noticed that the distributions of slamming coefficient on the members was highly dependent on the breaking wave conditions and breaking position of the wave. The local slamming coefficients were obtained at close positions on the members (Figure 2.35). Table 2.6 shows the summary of the maximum local slamming coefficients estimated for the jacket members in the wave impact zone.

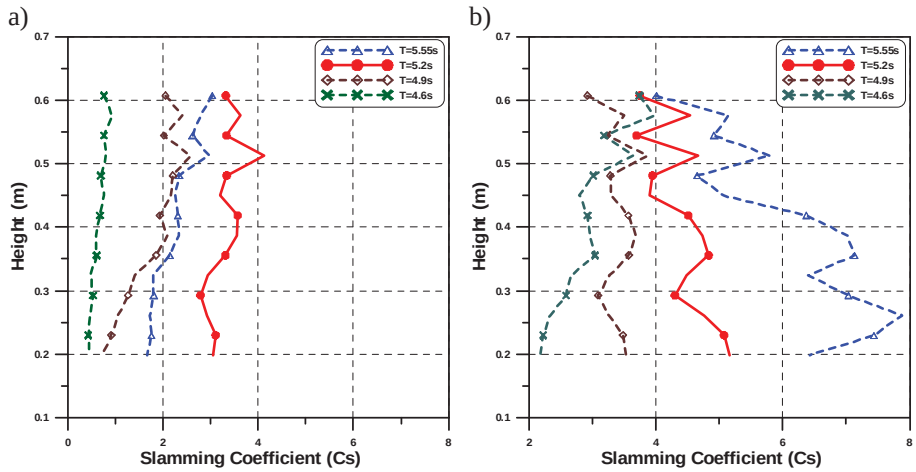

Figure 2.35 Comparison of maximum slamming coefficient along the length of the bracing member of the jacket structure for a) H=1.6m (b2, c2, d2 and e2), b) H=1.7m (b3, c3, d3 and e3)

Table 2.6 Summary of maximum slamming coefficient on members

Members	**Maximum Slamming Coefficient, C_s**
Front bracing members (B1 and B2)	7.87
Back bracing members (B3 and B4)	5.90
Side bracing members (B5 and B6)	1.45
Front vertical member (V1)	2.94
Back vertical members (V2)	2.63

Discussions on the findings in paper 7

A comprehensive study on breaking wave interaction on a jacket structure was performed by simulating a wide range of breaking wave conditions in the NWT. The numerical model results showed reasonable agreement with the experimental measurements. It was observed that the numerical force results were slightly overestimated compared to the

experimental measurements. This was due to the use of the incompressible flow model for the simulations and other modelling considerations. The local slamming coefficients were estimated for the jacket members in the wave impact region. The maximum slamming coefficients were estimated for the front bracing members of the jacket structure. Based on the present simulations, the maximum slamming coefficient for the bracing members of the jacket structure in the wave impact zone was estimated as 7.87, which is 25% higher than the value suggested by Wienke and Oumeraci [7]. This higher value of the slamming coefficient is due to the incompressible flow model used for the present study, which overestimated the forces on the structure. On the other hand, in the case of vertical members, the maximum slamming coefficient was obtained to be 2.96, which is slightly smaller than the values suggested by Goda et al. [5]. For stronger wave breaking cases, the slamming coefficients along the bracing members tend to be uniformly distributed along the members, which is similar to the experimental observations.

Chapter 3
Conclusions

3.1 Summary

In the present thesis, a detailed study on breaking wave interactions with a jacket structure was carried out based on experimental and numerical investigations. The high quality experimental dataset from the WaveSlam experiment was used as the base for the present research. Due to the lack of any related studies in the past, the author has introduced new approaches to handle this complicated wave-structure interaction problem. Based on the understanding of the nature of the measured forces, suitable methods to filter out the slamming forces from the measurements were introduced. The wave forces measured during the wave breaking events on the structure consist of three major force components, including the wave slamming force. In order to separate the total slamming forces from the total measured force, the Empirical Mode Decomposition method was implemented. This time series separation approach worked well with the present data. To separate the local slamming forces from the local force measurements, the Frequency Response Function method was used. This method made use of the hammer test data which were taken during the experiments. The total and local slamming forces on the structure were obtained for all of the relevant wave cases. Based on these forces, the total and local slamming coefficients on the jacket were obtained by fitting the forces with a modified form of Goda's monopile empirical formula [5].

The total slamming force represents the overall slamming force on the jacket, when the wave breaks on the structure. The total slamming force

is important in the overall design of the jacket, especially in the design of foundation system. From the present research it was observed that the total slamming force on the jacket is not the sum of peak slamming force on the local members in the wave impact region. From the experimental data analysis it was confirmed that there was a “time delay” in wave impact on the jacket members in the wave impact region, which resulted in lower value of total slamming forces on the jacket structure. Moreover, the total slamming coefficient obtained for the worst breaking case was 1.1., which is much smaller than the values obtained for monopile structures. From this study, it was concluded that the total slamming forces on the jacket were not as impulsive compared to the local slamming forces on the jacket members.

The local slamming forces were found to be critical in the design of jacket structures against breaking waves. From this study, the maximum slamming force on the jacket was observed when the wave breaks at a distance half meter close to the front members of the jacket. In those breaking events, the wave slamming forces were uniformly distributed on the front members of the jacket in the wave impact region. The local slamming coefficients valid for local members were obtained from the local slamming forces. The maximum slamming coefficient on the bracing members was obtained as 6.16, which is closer to the value 2π suggested by Wienke and Oumeraci [7] for monopile structures. Based on this study, a slamming coefficient of 6.16 is recommended to be used in the modified Goda’s force formula to estimate the local slamming forces on the members in the wave impact region.

The dependency of various wave parameters on the slamming forces was investigated based on the wave measurements taken during the experiment. It was observed that the slamming forces on the structure mainly depends on the geometry of the wave front (breaking wave height and wave front asymmetry) and the breaking location of the wave with respect to the structure. From the results it was concluded that when the wave breaks in front of the jacket, steeper waves imparts maximum

slamming forces on the jacket. However, as the breaking location moves further away from the structure, the impact of these parameters on the slamming forces diminishes.

In the present research, a 3D numerical model based on viscous incompressible momentum equations was used to simulate breaking wave forces on the jacket. The capability of the numerical model was compared with the popular CFD model, OpenFOAM for a dataset provided by Irschik et al. ([37]). The simulation results from both the numerical models were quite similar. Due to the complexity of the present study, the numerical parameters used in the model were decided based on a detailed sensitivity study performed on the numerical model. The numerical simulations were performed for most of the relevant experimental measurement cases. The free surface elevation, water particle velocities and nonlinear wave forces on the structure were calculated, and the calculated results were compared with the experimental measurements. In the simulations, numerical force transducers were used to calculate local wave forces on the jacket members (front, side and back- bracing and vertical members) in the wave impact region. The simulated wave forces by the numerical model were found to be slightly overestimated. The reasons for the overestimation of the wave forces were due to the use of the incompressible flow numerical model and certain attributes in the experiments which the numerical model could not simulate. The local forces were calculated at close locations along the members and these local force measurements were used to calculate the local slamming coefficients. The distribution of local slamming coefficients on the members was obtained for different wave breaking conditions. In the case of strong breaking cases, the distribution of slamming coefficient on the members were uniform, similar to the experimental studies. From the simulations a maximum slamming coefficient of 7.87 was obtained for the bracing members. The obtained value of slamming coefficient is higher than the one obtained from the experimental studies. The

difference in the maximum slamming coefficient was attributed to the incompressible flow model used in the study.

Based on the present experimental and numerical investigations, it was concluded that the wave slamming forces are important and need to be considered in the design of jacket structures against breaking waves. As the local slamming forces on the jacket members are much higher (around 4-5 times) than the local Morison forces, excluding these forces in the design may possibly result in the local failure of the members in the wave breaking zone. The local slamming forces on the jacket members in the wave impact region can be estimated using the modified Goda's formula considering a slamming coefficient of 6.16, which is similar to the values suggested by Wienke and Oumeraci [7] for the design of monopile structures.

All the research questions formulated in this thesis (see section 1.5) were answered in the present thesis as follows:

1. A comprehensive study on breaking wave interactions on the jacket structure was carried out based on the WaveSlam experimental dataset. Different methodologies were introduced to estimate the slamming forces and breaking wave parameters from the measurement data.

2. The total and local slamming forces on the jacket were obtained for all the relevant wave cases. A detailed study was carried out for the local slamming forces on the jacket members as these forces were more impulsive compared to total slamming forces on the jacket. Based on the local slamming forces, the slamming coefficients valid for the jacket members were obtained. Based on the study, it is recommended to use a slamming coefficient of 6.16, to estimate the local slamming forces on the jacket members using the modified Goda's formula.

3. A numerical model was used to simulate breaking wave forces

on the jacket structure and the results were compared with the WaveSlam experimental data. The present numerical model is found to be a useful tool to study the nonlinear wave forces on the structures. The simulation results provided an overall understanding on the local slamming forces on the jacket members.

3.2 Suggestions for Future Work

In the experimental analysis, the focus was on the slamming forces acting on the jacket. It was noticed that there is a significant contribution of dynamic amplification in the measured response force. However, this dynamic amplification effect in the structure response was removed from the measurements while performing the study. In the real case, this dynamic amplification effect is significant. There is a need to further investigate this by using different structural models.

In the present work, the breaking wave forces were studied for a single orientation of the jacket. However, there are other possible orientations of the jacket, which may be more critical for the structure. For example, the jacket is impacted by the breaking waves in an angled position. This was not addressed in the present experimental measurements.

In the present work, the same model scale of 1:8 was used for experimental and numerical studies. The effect of model scale on the slamming forces on the structure was not studied. However, it is known that for breaking wave studies, the scale effects have significant impact on the evolution of entrained air bubbles. As the size of air bubbles remains same at all scales, small-scale models may have more cushion effect due to entrained air bubbles than large-scale models. The effect of model on the slamming forces on a jacket need to be further studied.

In this thesis, the focus was on the local impact of wave slamming forces on the jacket structure. The local slamming coefficients on the jacket members were obtained for various breaking wave cases. However, there

is a need to further extend the study on the total slamming forces on the structure, in order to study the impact of total slamming forces on the overall design of the jacket.

In the WaveSlam dataset, there were measurements for both regular irregular waves. However, for the present research, the measurements for regular waves were only considered. The study need to be further extended to irregular wave cases.

In order to simulate breaking waves, an incompressible Navier Stokes solver was used for the present research. The effect of aeration and air compressibility between the water and structure were not considered in the simulations. This resulted in some discrepancies in the simulations. The jacket structure was modelled in the numerical wave tank as a rigid geometry. Hence the dynamic amplification effects were not captured in the simulations. It is important to simulate these effects for accurate estimation of wave forces on the structure. The use of a compressible flow model with a structural module which can model the jacket as a dynamically equivalent object, will fix this problem.

References

[1] Ho, A., Mbistrova, A., and Corbetta, G., 2016, “The European offshore wind industry-key trends and statistics 2015,” A report by the European Wind Energy Association. Retrieved from: https://www.ewea.org/fileadmin/files/library/publications/statistics/EWEA-European-Offshore-Statistics-2015.pdf

[2] Chella, M.A., Tørum, A., and Myrhaug, D., 2012, “An overview of wave impact forces on offshore wind turbine structures,” Energy Procedia, Vol. 20, pp. 217–226.

[3] Navaratnam, C.U., Tørum, A., and Arntsen, Ø.A., 2013, “Preliminary analysis of wave slamming force response data from tests on a truss structure in large wave flume,” Technical Report, Norwegian University of Science and Technology, Trondheim, Norway.

[4] Arntsen, Ø.A., and Gudmestad, O.T., 2014, “Wave slamming forces on truss structures in shallow water,” Proceedings of the HYDRALAB IV Joint User Meeting, Lisbon, Portugal.

[5] Goda, Y., Haranaka, S., and Kitahata, M., 1966, “Study of Impulsive Breaking Wave Forces on Piles,” Report of Port and Harbor Research Institute, Ministry of Transport, Japan, Vol. 5 (6), pp. 1-30.

[6] Sawaragi, T., and Nochino, M., 1984, “Impact forces of nearly breaking waves on a vertical circular cylinder,” Coastal Engineering in Japan, Vol. 27, pp. 249–263.

[7] Wienke, J., and Oumeraci, H., 2005, “Breaking Wave Impact Force on a Vertical and Inclined Slender Pile-Theoretical and Large-

Scale Model Investigations," Coastal Engineering, Vol. 52, pp. 435-462.

[8] European Wind Energy Association., 2013, "Deep Water: The Next Step for Offshore Wind Energy," Brussels, Belgium, A report by the European Wind Energy Association. Retrieved from: http://www.ewea.org/fileadmin/files/library/publications/reports/Deep_Water.pdf

[9] Aune, L., 2011, "Forces from plunging breaking waves on a truss structure," Master thesis submitted June 2011, Norwegian University of Science and Technology, Department of Civil and Transport Engineering, Trondheim, Norway.

[10] Tørum, A., 2012, "Wave slamming force on truss structures," Preliminary note, NTNU, IBAT, Marine Group.

[11] Arntsen, Ø. A., Obhrai, C., and Gudmestad, O. T., 2013, "Data Storage Report: Wave Slamming Forces on Truss Structures in Shallow Water," WaveSlam (HyIV-FZK-05), Technical Report, Norwegian University of Science and Technology, Trondheim and University of Stavanger, Stavanger.

[12] Von Karman, T., 1929, "The impact of seaplane floats during landing," Technical Note 321, NACA, Washington.

[13] Wagner, H., 1932, "Über stoß- und gleitvorgänge an der oberfläche von flüssigkeiten. ZAMM," Journal of Applied Mathematics and Mechanics, Vol. 12(4), pp. 193–215.

[14] Tanimoto, K., Takahashi, S., Kaneko, T., and Shiota, K., 1986, "Impulsive breaking wave forces on an inclined pile exerted by random wave," Proceedings of the 20th International Conference on Coastal Engineering, Taipei, Taiwan, Vol. 3, pp. 2288 – 2302.

[15] Basco, D.R., and Niedzwiedzki, J.M., 1989, “Breaking wave force distributions and design criteria for slender piles,” Proceedings of Offshore Technology Conference, Houston, Texas, United States, pp. 425 – 431.

[16] American Bureau of Shipping (ABS), 2011, “Design standards for offshore wind farms”, Houston, Texas, United States.

[17] Hildebrandt, A., 2013, “Hydrodynamics of breaking waves on offshore wind turbine structures,” PhD thesis, Gottfried Wilhelm Leibniz Universität Hannover, Hannover, Germany.

[18] Aashamar, M., 2012, “Wave slamming forces on truss support structures for wind turbines,” Master thesis, Norwegian University of Science and Technology (NTNU), Department of Civil and Transport Engineering, Trondheim, Norway.

[19] Choi, S.J, 2014, “Breaking wave impact forces on an offshore structure,” PhD thesis (UiS No.231), , University of Stavanger, Department of Mechanical and Structural Engineering and Material Science, Stavanger, Norway.

[20] Ros, X., 2011, “Impact forces from plunging breaking waves on a vertical pile,” Master thesis, Technical University of Catalonia, Barcelona, Spain, carried out at the Department of Civil and Transport Engineering, NTNU, Trondheim, Norway.

[21] Jose, J., Podrażka, O., Obhrai, C., Gudmestad, O. T., and Cieślikiewicz, W., 2015, “Experimental analysis of slamming loads for truss structures within the framework of WaveSlam project,” Hydralab IV, Technical Report, University of Stavanger, University of Gdańsk. Retrieved from: http://www.hydralab.eu/project_publications.asp.

[22] Huang, N.E., Zheng, S., and Long, S.R., 1999, “A new view of nonlinear water waves: The Hilbert Spectrum,” Annual Review of Fluid Mechanics, Vol. 31, pp. 417-457.

[23] Määttänen, M., 1979, “Laboratory tests for dynamic ice structure interaction,” Engineering Structures, Vol. 3 (2), pp. 111-116.

[24] Tørum, A., 2013, “Analysis of force response data from tests on a model of truss structure subjected to plunging breaking waves,” Technical Report, Norwegian University of Science and Technology, Trondheim, Norway.

[25] Chella, M. A., Bihs, H., and Myrhaug, D., 2015, “Characteristics and Profile Asymmetry Properties of Waves Breaking over an Impermeable Submerged Reef,” Coastal Engineering, Vol. 100, pp. 26-36.

[26] Stansberg, C.T., 2008, “A wave impact parameter,” Proceedings of 27th International Conference on Offshore Mechanics and Arctic Engineering, Estoril, Portugal, pp. 301-308.

[27] Peng, Z., 2014, “Wave slamming impact on offshore wind turbine foundations,” Proceedings of 34th International Conference on Coastal Engineering, Seoul, Korea, Vol. 34, pp. 43-50.

[28] Soares, C. G., Cherneva, Z., and Antao, E. M., 2004, “Steepness and Asymmetry of the Largest Waves in Storm Sea States,” Ocean Engineering, Vol. 31, pp. 1147-1167.

[29] Goda, Y., 2010, “Reanalysis of regular and random breaking wave statistics,” Coastal Engineering, Vol. 52(1), pp. 71-106.

[30] Lee, K.H., 2006, “A study on time domain analysis of nonlinear dynamic interaction amount waves, currents and bed materials,” PhD thesis, Nagoya University, Department of Civil Engineering, Japan.

[31] Hirt, C.W., and Nichols, B.D., 1981, “Volume of fluid method for the dynamics of free boundaries,” Journal of Computational Physics, Vol. 39(1), pp. 201- 225.

[32] Hirt, C.W., Sicilian, J.M., 1985, “A porosity technique for the definition of obstacles in rectangular cell meshes,” Proceedings of 4th International Conference on Numerical Ship Hydrodynamics, Washington, United States, pp. 1-10.

[33] Smagorinsky, J., 1963, “General circulation experiments with the primitive equations,” Monthly Weather Review, Vol. 91(3), pp. 99-164.

[34] Hinatsu, M., 1992, “Numerical simulation of unsteady viscous nonlinear waves using moving grid systems fitted on a free surface,” Journal of the Kansai Society of Naval Architects, Japan, 217, pp. 1-11.

[35] Amsden, A.A., and Harlow, F.H., 1970, “A simplified MAC technique for incompressible fluid flow calculation, Journal of Computational Physics, Vol. 6, pp. 322-325.

[36] Allied Engineering, 2011. “User’s Manual for Advanced Parallel AMG Version 1.3,” Tokyo, Japan.

[37] Irschik, K., Sparboom, U., and Oumeraci, H., 2004, “Breaking wave loads on a slender pile in shallow water,” Proceedings of 29th International Conference on Coastal Engineering, Lisbon, Portugal, pp. 568-580.

[38] Choi, S.J., Lee, K.H., and Gudmestad, O.T., 2015, “The effect of dynamic amplification due to a structure’s vibration on breaking wave impact,” Ocean Engineering, Vol. 96, pp. 8-20.

[39] Hu, C., and Kashiwagi, M., 2004, “A CIP-based method for numerical simulations of violent free-surface flows,” Journal of Marine Science and Technology, Vol. 9, pp. 143-157.

Appended Papers

Paper I Jose, J., Podrażka, O., Obhrai, C., Gudmestad, O.T., and Cieślikiewicz, W., 2016, "Methods for Analysing Wave Slamming Loads on Truss Structures used in Offshore Wind Applications based on Experimental Data," International Journal of Offshore and Polar Engineering, Vol. 26(2), pp. 100-108.
DOI: dx.doi.org/10.17736/ijope.2016.mkr05

Paper II Jose, J., Podrażka, O., Gudmestad, O.T., and Cieślikiewicz, W., 2017, "Characteristics of the Wave Slamming Forces on Jacket Structures under Plunging Breaking Waves based on Experimental Data," In the Proceedings of ASME 36th International Conference on Ocean, Offshore and Arctic Engineering (OMAE2017), Trondheim, Norway, June 25-June 30.
DOI:10.1115/OMAE2017-61789

Paper III Jose, J., Podrażka, O., Gudmestad, O.T., and Cieślikiewicz, W., 2017, "Detailed Study on Breaking Wave Interactions with a Jacket Structure based on Experimental Investigations," Journal of Offshore Mechanics and Arctic Engineering, Vol. 140(2), pp. 021301.1-021301.14.
DOI: dx.doi.org/10.1115/1.4037829

Paper IV Jose, J., Choi, S.J., Giljarhus, K.E.T., and Gudmestad, O. T., 2017, "A Comparison of Numerical Simulations of

Breaking Wave Forces on a Monopile Structure using Two Different Numerical Models based on Finite Difference and Finite Volume Methods," Ocean Engineering, Vol. 137, 78-88.
DOI: doi.org/10.1016/j.oceaneng.2017.03.045

Paper V Jose, J., Choi, S.J., and Gudmestad, O.T., 2017, "Sensitivity Study on a 3D Numerical Model for Estimating Breaking Wave Forces on a Jacket Structure," In the Proceedings of 27th International Ocean and Polar Engineering Conference (ISOPE2017), San Francisco, California, June 25- June 30.
ISBN: 978-1-880653-97-5

Paper VI Jose, J., Choi, S.J., Lee, K.H., and Gudmestad, O.T., 2016, "Breaking Wave Forces on an Offshore Wind Turbine Foundation (Jacket Type) in the Shallow Water," In the Proceedings of 26th International Ocean and Polar Engineering Conference, Rhodes, Greece, June 26-July 2.
ISBN: 978-1-880653-88-3

Paper VII Jose, J., and Choi, S.J., 2017, "Estimation of Slamming Coefficients on Local Members of Offshore Wind Turbine Foundation (Jacket Type) under Plunging Breaker," International Journal of Naval Architecture and Ocean Engineering, Vol. 9(6), pp. 624-640.
DOI: dx.doi.org/10.1016/j.ijnaoe.2017.03.006

Paper 4

Jose, J., Choi, S.J., Giljarhus, K.E.T., and Gudmestad, O. T., 2017, "A Comparison of Numerical Simulations of Breaking Wave Forces on a Monopile Structure using Two Different Numerical Models based on Finite Difference and Finite Volume Methods," *Ocean Engineering*, Vol. 137, pp. 78-88.
DOI: doi.org/10.1016/j.oceaneng.2017.03.045

Ocean Engineering 137 (2017) 78–88

Contents lists available at ScienceDirect

Ocean Engineering

journal homepage: www.elsevier.com/locate/oceaneng

A comparison of numerical simulations of breaking wave forces on a monopile structure using two different numerical models based on finite difference and finite volume methods

Jithin Jose[a,*], Sung-Jin Choi[b], Knut Erik Teigen Giljarhus[c], Ove Tobias Gudmestad[a]

[a] Department of Mechanical and Structural Engineering and Materials Science, University of Stavanger, Norway
[b] Loads Copenhagen, DNV GL, Copenhagen, Denmark
[c] Lloyd's Register, Stavanger, Norway

ARTICLE INFO

Keywords:
Finite volume method
Finite difference method
Wave breaking
Secondary loads
Monopile
Volume of fluid method

ABSTRACT

The nonlinear forces from breaking waves are a major concern in the design of offshore structures. Due to the complexity of the wave-breaking phenomenon, understanding the interaction of breaking waves with a structure is always a challenging task. The use of numerical models can be a useful tool for studying such a phenomenon. At present, many numerical models are available, using either a Finite Difference Method (FDM) or a Finite Volume Method (FVM), for solving the governing equations. In wave breaking studies, different researchers have come up with reasonable results, using both models. However, there have been few attempts to compare the relative strengths and weaknesses of the two methods. In the present paper a comparison of both methods applied to breaking wave studies is performed. Two different 3D Navier-Stokes solvers, 2PM3D (FDM) and OpenFOAM (FVM), are used to simulate the breaking wave forces on a monopile structure. Two different scenarios are considered for generating non-breaking and breaking waves, and the results are compared with theoretical results and available experimental measurements. For both numerical models, the breaking wave interactions with the monopile were in good agreement with the experimental measurements.

1. Introduction

In real sea, offshore structures are subjected to nonlinear wave interactions, such as wave breaking and green water impact. These nonlinear wave interactions sometimes result in damage to offshore structures. Therefore, understanding these phenomena is very important for the design of offshore structures. The forces from breaking waves have been a major concern for offshore structures installed in shallow waters, and these breaking wave impact forces sometimes govern the overall design of such structures. The physical realization of breaking wave interactions with the structure is a challenging task, due to the complexity of the wave-breaking phenomenon and the time-dependent shape of the breaking wave (Hull and Müller, 2002). Most previous studies on breaking waves focused on experimental measurements (Goda et al., 1966; Wienke and Oumeraci, 2005), and were limited to simple structures and specific experimental conditions.

The solution to these challenges could be the use of a well-validated numerical model, which can simulate breaking waves. The increase in computational capabilities and advanced numerical codes makes numerical modelling a powerful tool to predict the wave-breaking forces on structures. Moreover, these numerical models can estimate the wave forces by means of direct pressure integration over the structure, without using any empirical relations. However, the accuracy and efficiency of the numerical model depends on the numerical methods used.

Numerical models based on solving Navier Stokes equations are widely used to simulate breaking waves. There are two main classical methods for obtaining the solution to these differential equations, namely, the Finite Difference Method (FDM) and the Finite Volume Method (FVM). The former is based on the application of the Taylor series expansion to approximate the governing differential equations (Sherwin and Peiro, 2005). It uses a rectangular grid of lines to represent the discretization of the differential equations. In the Finite Volume Method, the integral form of the differential equation is considered. The governing quantities are conserved over a finite volume. Within both the FDM and the FVM, there are many options for the discretization of the various terms in the governing equation, which also contributes to the accuracy of both methods.

Hur and Mizutani (2003) used a Navier-Stokes solver, based on the Finite Difference Method, to study the wave forces on an asymmetric

* Corresponding author.
E-mail address: jithin.jose@uis.no (J. Jose).

http://dx.doi.org/10.1016/j.oceaneng.2017.03.045
Received 7 November 2016; Received in revised form 22 March 2017; Accepted 24 March 2017
Available online 30 March 2017

structure installed over a submerged breakwater. The model combines the Volume of Fluid (VOF) method (Hirt and Nichols, 1981) and the porous body model to simulate nonlinear wave deformation. The Large Eddy Simulation (LES) model was used to calculate the turbulence in the flow. Lee et al. (2011) studied the wave interactions around two vertical cylinders, using a 3D Navier-Stokes solver based on the FDM. The VOF method was used to account for free surface tracking. The computed results showed a good agreement with the experimental measurements. Hu and Kashiwagi (2004) developed a FDM with a Constrained Interpolation Profile (CIP) algorithm to study violent wave interactions with the structure. The free surface is distinguished by a density function, which is solved using the CIP method. Park et al. (2003) developed a finite difference viscous Navier-Stokes solver to study the nonlinear wave forces and run-up, around a conical gravity-based structure. The nonlinear free surface was treated by the marker-density function technique. The numerical model gave a reliable estimate of the maximum wave loading and run-up including a series of higher harmonic components. Choi (2014) used a 3D numerical model based on the FDM to simulate the breaking wave interactions on a vertical cylinder pile. To resolve the air-water interface, the VOF method was utilized.

On the other hand, Christensen et al. (2005) used a numerical model, based on solving 3D Navier- Stokes equations using the Finite Volume Method, to study the extreme wave forces and wave run-up on a cylindrical pile during wave breaking. The free surface is resolved with a VOF technique. Mo et al. (2007) developed a 3D numerical model, based on the Navier-Stokes equations, to study the wave interactions on a vertical pile. The model used the FVM to solve the governing equations, and the results were compared with the experimental measurements from the Large Wave Flume in Hannover. The VOF method was employed to track the nonlinear free surface. Chella et al. (2016) simulated wave breaking over a sloping seabed, using a numerical model, based on Reynolds averaged Navier-Stokes equations coupled with the level set method. The simulation results showed reasonable agreement with the experimental measurements by Ting and Kirby (1996). Jacobsen et al. (2012) developed a wave generation toolbox, waves2Foam, integrated with the open-source library, OpenFOAM, which is based on the FVM. The applicability of the toolbox to generate and absorb waves was demonstrated by comparing the results with benchmark test cases. Paulsen (2013) coupled the OpenFOAM with a potential flow solver to study the wave interactions with a vertical cylinder. The coupled FVM model results showed good agreement with the experimental measurements.

Apart from the above-mentioned Eulerian approaches, there is another well-known method, based on the Lagrangian scheme, in which the fluid is treated as particles and the path of each individual particle is tracked. Gotoh and Sakai (1999) used a moving particle semi-implicit (MPS) method to simulate breaking waves in the numerical wave tank. The method avoids the use of any free surface tracking method, such as VOF, to obtain the fluid surface. Shao (2006) used a numerical model, based on the smoothed particle hydrodynamic method coupled with a k-ε turbulence model, to simulate spilling and plunging waves. The mesh-free numerical results showed very good agreement with the experimental measurements. In comparison with the Eulerian approach, the Lagrangian approach required more computational time (Gotoh and Sakai, 1999), as each particle in the flow is tracked and the particle number needs to be very large to ensure the stability of the flow. However, this approach is not within the scope of the present paper.

There are many available numerical models, which use either FDM or FVM for solving the Navier-Stokes equations. In the wave breaking studies, different researchers have obtained reasonable results, using either model. According to the authors' knowledge, however, there has been no attempt to compare the relative strengths and weaknesses of the two models. There is an ongoing debate on the adequacy of both models in the study of highly nonlinear physical phenomena like wave breaking. The present paper performs a comparison of the two methods, using two different 3D Navier-Stokes solvers, the 2PM3D solver (Lee, 2006), which is based on the FDM, and OpenFOAM with waves2Foam toolbox, which is based on the FVM. The 2PM3D model uses a rectangular grid system to discretize the governing equations in the computational domain. In this model, in order to account for the geometry in the fluid domain, the cut cell method is used. However, in OpenFOAM, an unstructured mesh with body fitted grid method is used to model the geometries in the fluid domain. In the present study, two different scenarios are considered for simulating breaking and non-breaking waves in the numerical wave tank. The numerical models are used to simulate the breaking wave forces on a monopile structure. The simulation results are compared with available theoretical results and experimental measurements from the hydraulic model tests previously undertaken by Irschik et al. (2004). Secondary loads are observed on the cylinder when the wave flows across the structure. The capability of both numerical models to simulate the secondary load cycle on the cylinder structure is also analysed.

2. Model description

2.1. Experimental set-up

The experiment was carried out at the Large Wave Flume in Hannover, Germany (Irschik et al., 2004; Choi et al., 2015). The wave flume is 300 m long, 5 m wide and 7 m high. The slope at the bottom of the channel is 1/10. A cylindrical structure of 0.7 m diameter and 5 m length was erected at the edge of the slope. The pile was supported at the top and bottom by a transverse frame. During the experiments, there were two strain gauges integrated to the top and bottom of the monopile structure to measure the forces acting on the structure. The total breaking wave forces were calculated as the sum of the forces measured by these top and bottom transducers. The monopile structure was tested for a number of incident wave conditions for different orientations (vertical and inclined) of the pile. The waves were generated by a piston-type wave generator. Wave gauges and Acoustic Doppler Velocimeters (ADV) were distributed along the channel in order to track the wave surface elevation and water particle velocities, respectively. More details of the experimental set-up are given in Irschik et al. (2004).

2.2. Numerical model

In the present study, two different numerical models were used to simulate breaking waves in the computational domain. The numerical model 2PM3D, based on the FDM, was previously validated by Lee et al. (2011) and Choi et al. (2015). The OpenFOAM model with waves2Foam toolbox uses the FVM for solving the governing equations. Although the governing equations for both numerical models are the same, the method for solving the equations and treating the geometries in the computational domain differ. The numerical description of each model is provided in the following sections.

2.2.1. 2PM3D model

In order to study the breaking wave interactions with the structure, a numerical wave tank method developed by Lee (2006) was used. It comprises an internal wave source, an artificial damping zone to prevent the wave reflections at the lateral boundaries and a surface tracking function to treat the free surface. Assuming the two fluids are viscous, immiscible and incompressible, the fluid flow is governed by the continuity equation and the modified Navier-Stokes equation.

$$\frac{\partial(mv_j)}{\partial x_j} = q^* \tag{1}$$

$$m\frac{\partial v_i}{\partial t} + mv_j\frac{\partial v_i}{\partial x_j} = \frac{-m}{\tilde{\rho}}\frac{\partial p}{\partial x_i} + \frac{\partial}{\partial x_j}(2\tilde{\nu}D_{ij} - \tau_{ij}) - Q_i - \beta_{ij}v_j + f_i \quad (2)$$

where t is time; $v_i = [u, v, w]^T$ is the velocity vector; p is pressure; $x_i = [x, y, z]^T$ is the position vector; m is the ratio of the fractional area open to the flow; f_i is the arbitrary body forces due to the effects of gravity and surface tension. The surface tension is treated using a continuum surface force (CSF) model; $D_{ij} = (\partial v_i/\partial x_j + \partial v_j/\partial x_i)/2$ is the strain rate tensor; the Smagorinsky SGS model (Smagorinsky, 1963) was used to estimate small-scale turbulence during the wave breaking in the surf zone. τ_{ij} is the turbulent stress based on the Smagorinsky SGS (sub-grid scale) model; β_{ij} is the dissipation factor matrix; $q^* = q(y, z, t)/\Delta x_s$ is the wave generation source, where $q(y, z, t)$ is the source density assigned only at the source position ($x = x_s$) and Δx_s is the mesh width at the source position. In order to prevent abrupt oscillation at the start of wave generation, flux density q is increased gradually using an exponential function; $\tilde{\rho}$ and $\tilde{\nu}$ are the density and the kinematic viscosity averaged over the computational grid, respectively, and Q_i is the wave source vector.

In order to track the free surface, the VOF method developed by Hirt and Nichols (1981) was used. In this method, the interface between air and water is modelled according to a VOF function, F. The VOF function calculates the volume of water in each cell over time, instead of directly tracking the free surface. The value of the VOF function varies between zero and unity, depending upon the air and water proportion in each cell. The advection of the VOF function is obtained by solving the conservation of fluid mass in each cell as follows:

$$\frac{\partial(mF)}{\partial t} + \frac{\partial(mv_jF)}{\partial x_j} = Fq^* \quad (3)$$

If the fluids are assumed to be incompressible and immiscible, the density and kinematic viscosity can be calculated using the VOF function F,

$$\hat{\rho} = F\,\rho_w + (1 - F)\rho_a \quad (4)$$

$$\hat{\nu} = F\nu_w + (1 - F)\nu_a \quad (5)$$

where ρ_w and ρ_a are the density of water and air, respectively; ν_w and ν_a are the kinematic molecular viscosity of water and air, respectively.

The numerical model uses a Cartesian grid system to discretize the governing equations. In order to incorporate obstacles (e.g., the monopile structure and bottom slope) in the numerical domain, the cut cell method was used. This method is similar to the fraction area/volume obstacle representation (FAVOR) method, developed by Hirt and Sicilian (1985). The shape of the structure was made up of cut cells, whose details were stored in the input data file. The information stored in the input data file included the following four parameters in each cell: the ratio of fractional volume open to flow, m_v; the ratio of fractional area open to flow in each direction, m_x, m_y, and m_z; the area of the wetted surface of the structure; and the unit normal vectors to the obstacle surfaces. The governing equations were formulated in terms of the computed four parameters to block portions of each cell containing the obstacle. The FDM was used to solve the governing equations and the VOF advection equations. That means, 2PM3D solves the differential equations in the form of difference terms, in which a local Taylor series expansion of the terms was carried out. The solution of the governing equations was evaluated at a point in space, which depended on the values at the surrounding points. However, the order of the solution depended on the numerical schemes used in the model.

2PM3D uses a staggered variables system, in which the parameters such as pressure, wave source and the VOF function, are obtained at the cell centre and the velocities are obtained at the cell face centres. The continuity equation is discretised using a second order central difference scheme. The numerical solution for the momentum equations can be split into two different phases: an advection phase and a non-advection phase. For the discretization of the advection phase, an M-type CIP (i.e., a modified CIP) method, and for the non-advection phase, a second order central difference method, were used. The time-derivative terms use a forward difference method. The simplified maker and cell (SMAC) method (Amsden and Harlow, 1970) was incorporated for the velocity and pressure correction. In order to solve the Poisson pressure equation, an algebraic multi-grid (AP-AMG) solver, developed by Allied Engineering Corporation (2011), was used.

In respect of the boundary conditions, the dynamic boundary condition was automatically satisfied due to the two-phase flow model (i.e., the water and the air phase were modelled as a fluid), while the kinematic boundary condition was achieved by tracking the VOF function. An impermeable (normal velocities) and a non-slip condition (tangential velocities) were imposed to treat the bottom boundary condition and obstacle boundary condition. In order to prevent the reflected waves in the computational domain, there were numerical dissipation zones, which were added to the inlet and outlet open boundaries. The dissipation method is similar to that proposed by Hinatsu (1992), in which the dissipation zones are gradually coarsened towards the open boundary. More details of the numerical model are given in Lee (2006).

2.2.2. OpenFOAM model - waves2Foam

OpenFOAM is an open source CFD software package, consisting of C++ library applications, which contains solvers and utilities. Waves2Foam is an additional solver added to the OpenFOAM library to handle flow related problems. It is a modification of the available solver, interFoam, in the OpenFOAM library. In addition, it constitutes a new toolbox for wave generation and absorption, capable of generating linear and nonlinear waves in the computation domain. When the two fluids are incompressible, viscous and immiscible, the fluid flow is governed by the Navier-Stokes equations (Eq. (6)), along with the continuity equation (Eq. (7)),

$$\rho\frac{\partial}{\partial t}(u_i) + \rho\frac{\partial}{\partial x_j}(u_iu_j) = -\frac{\partial p^*}{\partial x_i} - \rho g_i + \frac{\partial}{\partial x_i}(\mu\frac{\partial u_i}{\partial x_i} - \tau_{ij}) + f_i \quad (6)$$

$$\frac{\partial u_i}{\partial x_i} = 0 \quad (7)$$

where u is the velocity field in the Cartesian coordinate system, given by u = (u, v, w), p^* is the dynamic pressure, ρ is the density, g is the acceleration due to gravity and μ is the dynamic viscosity. The density ρ varies, depending on the air/water content in each cell. f_i is the surface tension force; $f_i = \sigma_T\kappa_\gamma\Delta F$, in which σ_T is the surface tension coefficient, and κ_γ is the surface curvature. The surface tension force is evaluated using a CSF model (Brackbill et al., 1992), which represents the surface tension effects as a continuous volumetric force, acting at the interface. As the fluids obey the Newtonian law of viscosity, the stress tensor τ is given by,

$$\tau = \frac{\mu_t}{\rho}\left[\frac{\partial u_j}{\partial x_i} + \frac{\partial u_i}{\partial x_j}\right] \quad (8)$$

μ_t is the dynamic eddy viscosity.

The surface tracking was done by using the VOF method similar to that used in 2PM3D. The scalar value of VOF function F was associated with each cell in the computation domain and followed the transport equation of the form (Jacobsen et al., 2012),

$$\frac{\partial F}{\partial t} + \nabla.\,[\mathrm{u}F] + \nabla.\,[\mathrm{u}_rF(1 - F)] = 0 \quad (9)$$

In order to prevent the numerical smearing of the interface, an additional compression term (last term on the left side of Eq. (9)) was added to Eq. (9). The compression term was applied to a thin interface region due to the multiplication with the factor $F(1 - F)$. The solution outside the interface region was not affected. The value u_r in the

compression term is the relative velocity, which was calculated, based on the maximum velocity at the interface. The air-water interface was calculated at each time step using the VOF method. The other fluid properties, such as density and kinematic viscosity, were represented using the VOF function similar to the 2PM3D model.

In the present project, the wave was generated using the waves2Foam toolbox, which contains the mathematical formulation for all well-known wave theories. The theoretical wave profile based on the wave theory was imposed on the inlet patch to generate the actual waves in the computational domain. In the waves2Foam toolbox, relaxation zones were defined for the inlet and outlet boundaries. The former was to avoid any internal waves in the wave generation zone that could interfere with the generated waves, while the latter was to avoid the effect of the reflected waves. A couple of relaxation techniques are presented in the waves2Foam toolbox; however, for the present study the relaxation technique used was an extension to the method used by Mayer et al. (1998). Based on this explicit relaxation scheme, before solving the momentum equation, the following changes were made in the calculation of u and F:

$$\mathrm{u} = (1 - s)\mathrm{u}_{target} + s\mathrm{u}_{computed} \tag{10}$$

$$F = (1 - s)F_{target} + sF_{computed} \tag{11}$$

where $s \in [0, 1]$ is a weighting function, calculated based on an exponential weight function.

To represent the computational domain, OpenFOAM uses an unstructured mesh, giving the user the freedom to use a body fitted mesh to model complicated geometries in the domain. The governing equations were discretized using the Finite Volume Method, in which the equations were integrated over the control volume and time. The boundary condition requirements in OpenFOAM are similar to those in the 2PM3D model. In the present OpenFOAM model, the k-ω SST model (Menter, 1994) was used for simulating the turbulence.

OpenFOAM uses a collocated variable system, in which all the parameters are stored in the same position. In the present model, for the discretization of the continuity equation and for the advection term in the momentum equation, a second order limited central difference scheme was used. For the non-advection and the time-derivative terms, a central difference scheme was used. With regard to the discretization of the VOF function, the MUSCL scheme (van Leer, 1979) was employed for the advection term and the interface compression scheme for the interface correction term. The PIMPLE algorithm with three corrector steps was implemented for the pressure-velocity coupling. A preconditioned bi-conjugate gradient (PBiCG) linear solver was utilized to solve for the velocity and a generalized geometric-algebraic multi-grid (GAMG) solver for pressure calculations.

2.3. Application of numerical models

In the present study, in order to validate the numerical simulation results, measurements from the experiment previously undertaken by Irschik et al. (2004) were used. The numerical wave tank, similar to the experimental set-up, was modelled in both numerical models. Fig. 1 shows the schematic arrangement of the numerical wave tank. The total length of the numerical wave tank was 54 m, without considering the inlet and outlet relaxation zones. The location of the numerical wave gauges (WG) and numerical velocity gauge (VG) are shown in Table 1.

Table 1
Measuring positions.

	X (m)	Y (m)	Z (m)
WG1	32.00	0.60	–
WG2	37.65	0.60	–
VG1	37.65	4.40	2.60

The modelling techniques differ in each numerical model. 2PM3D uses a separate application called Geometry 3D for pre-processing the geometry. This application calculates the fractional volume open to flow and the fractional area open to flow in x, y and z directions, as well as the unit normal vectors for each cell in the computational domain. Fig. 2a shows the vertical cylinder and bottom geometry developed by Geometry 3D. In Fig. 2b, the edge of the cell cut by the obstacle (cylinder) and the edge intersection on the cell face are shown. The parameters obtained for that particular cell are also shown.

Numerical dissipation zones were added to the inlet and outlet open boundaries, which were of length 2 L, where L is the wavelength, in order to prevent waves from being reflected in the computational domain. The inlet dissipation zone prevents waves from being reflected near the inlet boundary where the wave was generated, whereas the outlet dissipation zone prevents waves from being reflected from the outlet boundary. The internal wave generator, located at the end of the inlet dissipation zone, generated regular waves in the computational domain.

OpenFOAM uses an unstructured mesh, and the governing equations are solved using the Finite Volume Method. The modelling in OpenFOAM is quite flexible; the user can import models from different compatible CAD software and use them directly for simulations. In the present model, stereolithography (STL) files for the cylinder and bottom slope obtained from AutoCAD (Fig. 3a) were used, along with the *snappyHexMesh* utility, to install those obstacles in the computational domain (Fig. 3b).

2.4. Comparison of 2PM3D and OpenFOAM

A comparison of the two models used in the present study is shown in Table 2. The technique for considering the geometry in the computational domain differs in each model. This influences the number of cells used in each model. 2PM3D employs a cut cell method to represent the geometry, whereas body fitted mesh is used in OpenFOAM. The number of cells used in the numerical models directly

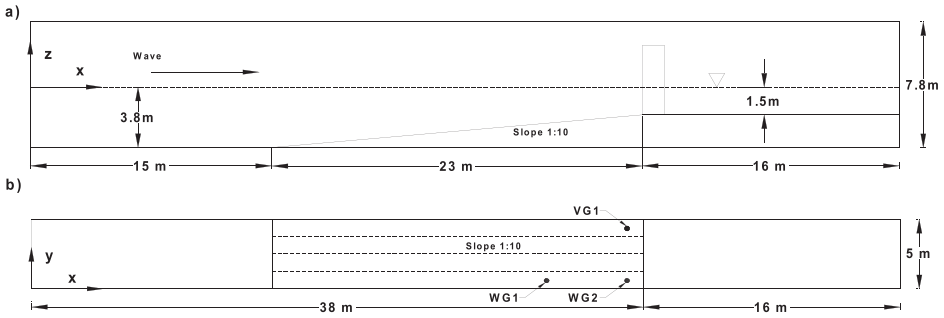

Fig. 1. Schematic representation of numerical wave tank: a) Cross section, b) Plan view.

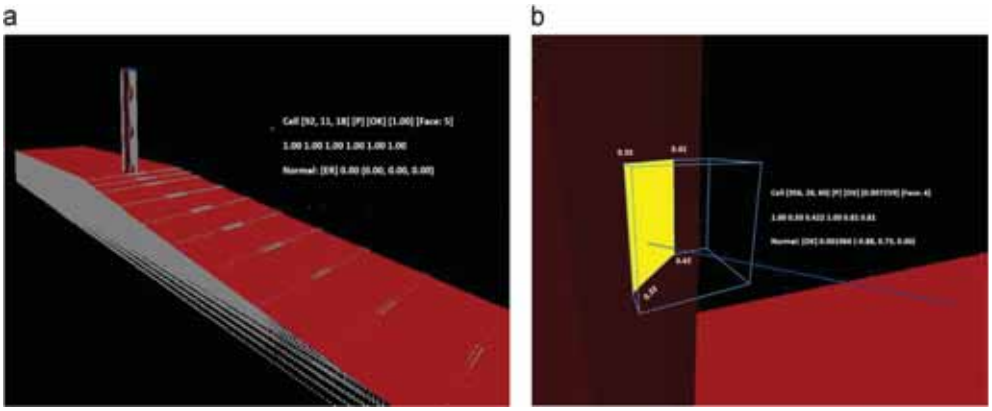

Fig. 2. a) Vertical cylinder and bottom slope in Geometry 3D application, and b) the cut-cell and the parameters calculated for the particular cell on the cylinder.

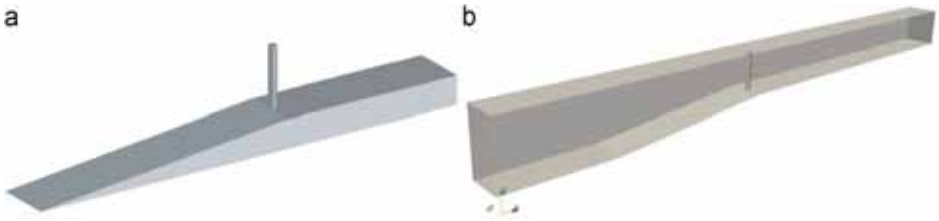

Fig. 3. a) STL files for the bottom geometry and cylinder, and b) Computational domain with bottom slope and vertical cylinder.

Table 2
Comparison of 2PM3D and OpenFOAM.

Description	2PM3D	OpenFOAM-waves2Foam
Spatial Discretisation	Finite Difference Method	Finite Volume Method
Mesh	Structured Mesh	Unstructured Mesh
Modelling Method	Cut Cell Method	Body Fitted Mesh
Pressure Velocity Coupling	Simplified Marker Cell (SMAC)	PIMPLE
Turbulence Model	Large Eddy Simulation (LES)	SST k-ω
Surface Tracking Method	VOF Method	VOF Method
Relaxation Method	Artificial Damping Method	Explicit Method

Table 3
Incident wave condition.

Case	Wave Height (m)	Wave Period (s)
1	1.3	4.0
2	1.4	4.0

affects the computation time. In the present study, the number of cells used in the 2PM3D numerical wave tank was 2.62 million; for waves2Foam, the number was 2.26 million. To perform the simulation

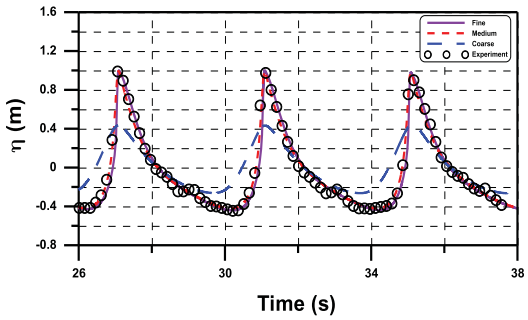

Fig. 4. Comparison with the experimental results of free surface elevation using fine, medium and coarse mesh in OpenFOAM.

with 2PM3D, a normal workstation computer with 12 cores was employed, while, a cluster with 18 cores was used for the OpenFOAM simulation. The total computational time required for the 2PM3D model to simulate 40 s of time was 116 h, whereas for OpenFOAM it was only 40 h.

To track the free surface, both models used the VOF method. However, the advection of the VOF function differed slightly in the two models. In waves2Foam, an interface correction term was used, along with the VOF advection equation, to prevent the numerical smearing of the air water interface. However, such a correction term was not used in 2PM3D. For the relaxation zones, in 2PM3D, an artificial damping

Table 4
Grid sizes (in the vicinity of the cylinder).

Model	Coarse Grid	Medium Grid	Fine Grid
OpenFOAM	0.50 m×0.50 m×0.50 m	0.10 m×0.10 m×0.10 m	0.05 m×0.05 m×0.05 m
2PM3D	0.08 m×0.10 m×0.10 m	0.06 m×0.05 m×0.08 m	0.05 m×0.04 m×0.05 m

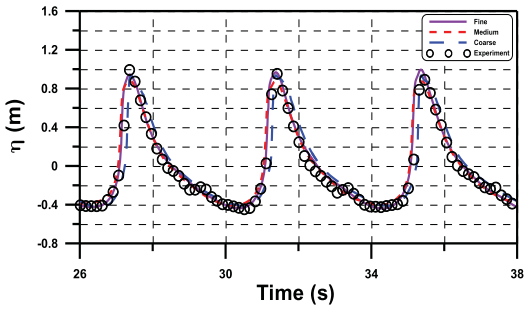

Fig. 5. Comparison with the experimental results of free surface elevation using fine, medium and coarse mesh in 2PM3D.

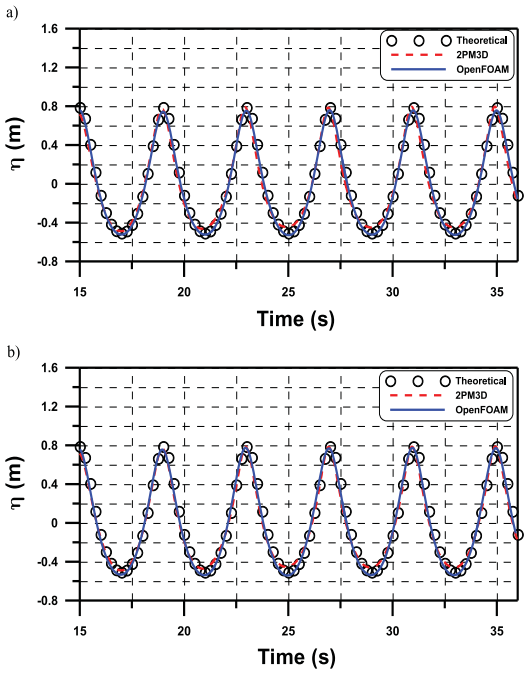

Fig. 6. Comparison of wave surface elevation, obtained by the numerical model, with the theoretical waves, for case 1. a) Wave surface elevation at WG1 (32 m), and b) wave surface elevation at WG2 (37.65 m).

effect was created at the inlet and outlet to prevent waves from being reflected in the domain. The inlet dissipation zone was located behind the wave generator to ensure accurate wave generation. However, in the OpenFOAM model, an explicit relaxation technique available in waves2Foam was used, in which the instantaneous wave properties in the relaxation zone were corrected to match with the required values. Unlike 2PM3D, the inlet relaxation zone was located in front of the wave generator in OpenFOAM.

3. Results

In the present paper, in order to make a comparison between the FVM and FDM models, two different scenarios were considered. The wave conditions chosen for the present simulation are shown in Table 3.

In the first scenario, the numerical wave tank without any geometry or bottom slope was validated by simulating various relevant wave conditions (shown in Table 3) and the results were compared with the

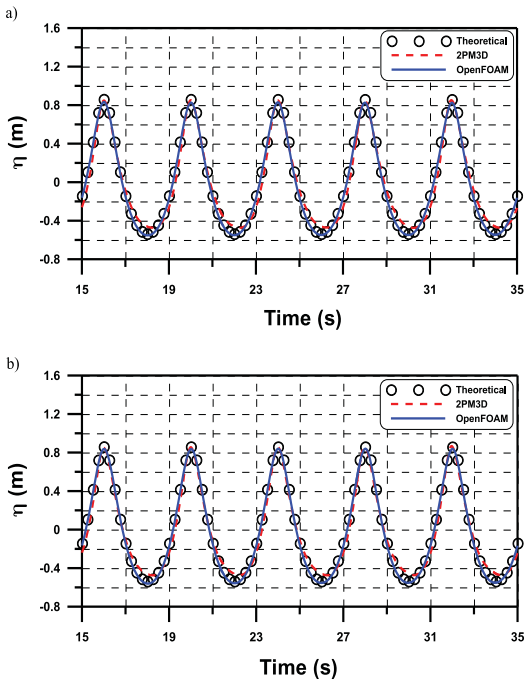

Fig. 7. Comparison of wave surface elevation, obtained by the numerical model, with the theoretical waves, for case 2. a) Wave surface elevation at WG1 (32 m), and b) wave surface elevation at WG2 (37.65 m).

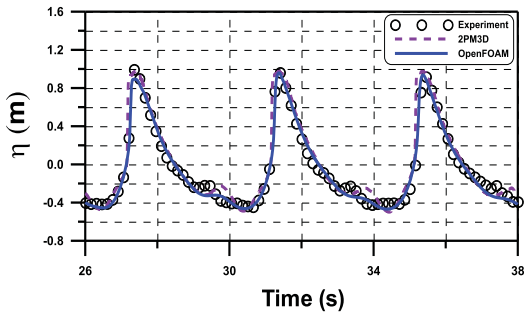

Fig. 8. Comparison between numerical models and experimental results of wave surface elevation measured at WG2 (37.65 m), for wave case 1.

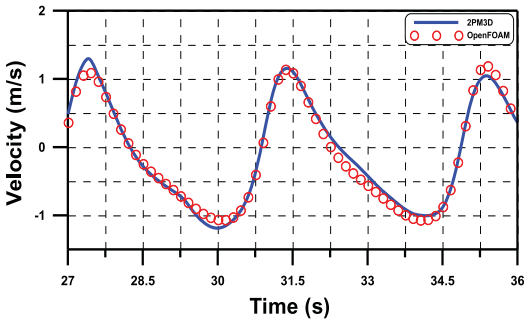

Fig. 9. Comparison of horizontal water particle velocity measured at VG1 by the numerical models, for wave case 1.

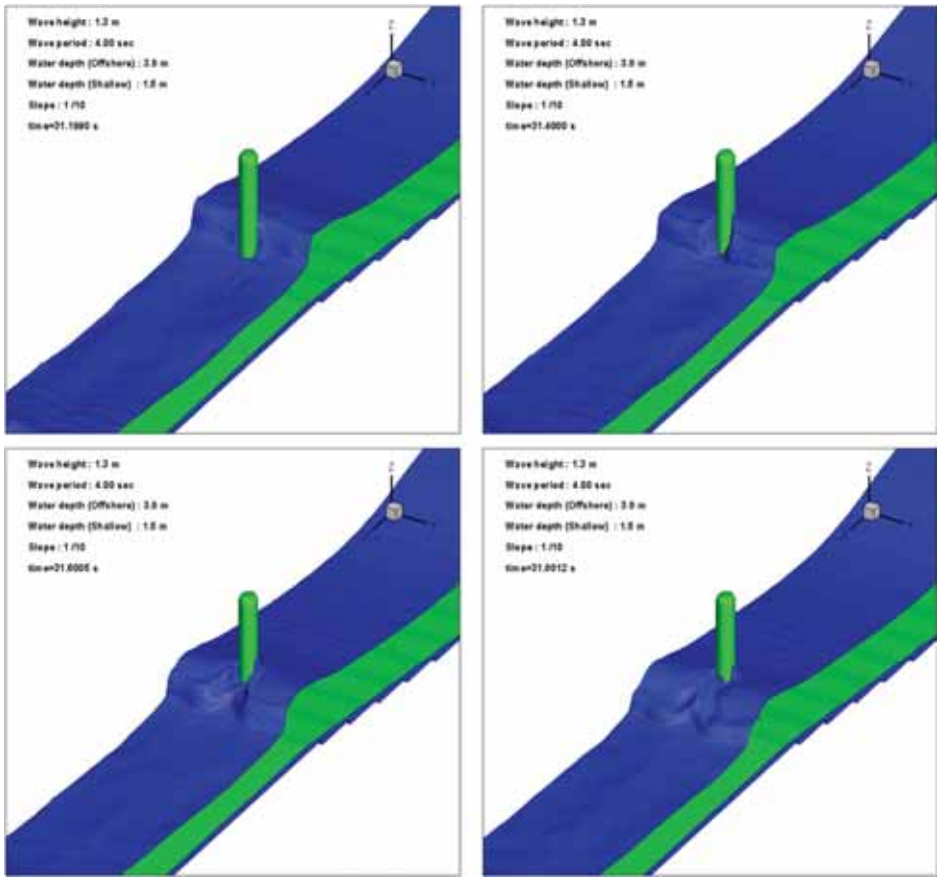

Fig. 10. Spatiotemporal plots from 2PM3D simulations for wave case 1– time steps 31.19 s, 31.40 s, 31.60 s and 31.80 s.

theoretical waves. The second scenario considered the numerical wave tank with the bottom slope and the cylindrical pile; both the wave surface elevation and the wave forces on the cylindrical pile were compared with the experimental measurements. To summarize, the scenarios studied in the present project were;.

- Scenario 1: 3D numerical wave tank without the bottom slope and cylinder.
- Scenario 2: 3D numerical wave tank with the bottom slope and cylinder.

3.1. Mesh sensitivity study

As the solution method differs for the two models, it is important to study the mesh sensitivity on the solutions. In the present study, the mesh sensitivity was studied with respect to the wave surface elevation calculated at WG2, the wave gauge located 37.65 m from the wave generator; see Fig. 1. The minimum grid size in x, y and z directions for both models were varied, and the surface elevations were compared. Table 4 shows the grid details for both the models.

Fig. 4 shows the comparison of wave surface elevations calculated at wave gauge WG2 in OpenFOAM, for the different mesh configurations given in Table 4. The results show similar agreements with the experimental measurements for the medium mesh and fine mesh size. Hence, for the present simulations in OpenFOAM, the medium mesh was used in order to save computational time. However, for the wave test case with the cylinder in the domain, the mesh size near the cylinder was further refined, using the *snappyhexMesh*.

Fig. 5 presents the comparison of wave surface elevations for different grid sizes in the 2PM3D case is shown in Fig. 5. The mesh size in the 2PM3D model should be chosen wisely in order to ensure structural integrity, as a coarse mesh could sometimes result in losing the exact shape of the structure. This is considered as one of the limitations of the cut cell method. In the present simulations, with respect to the fine grid size, results were found to match the experimental measurements more closely. Hence, a fine grid size was chosen for the simulations in 2PM3D. When calculating local pressure forces on the structure, the size of the mesh significantly affects the accuracy of the solution. However, it was only within the scope of the present study to calculate the total force on the cylinder; the mesh size would not had a significant impact on the solution.

3.2. Scenario 1- without bottom slope and geometry

This scenario considered the numerical wave tank (NWT) without bottom slope or geometry. In order to validate the wave generation and the ability of the models to transport the wave without excessive dissipation, the simulated wave surface elevation results were compared with the theoretical waves. The different wave cases considered in this study are shown in Table 3. As the Ursell value for the present simulations was below 40, both the stream function and Stokes 5th Order wave theory satisfied the generated waves. However, for the theoretical wave comparison, stream function results were used, as both wave theories produced exactly the same wave. In the absence of

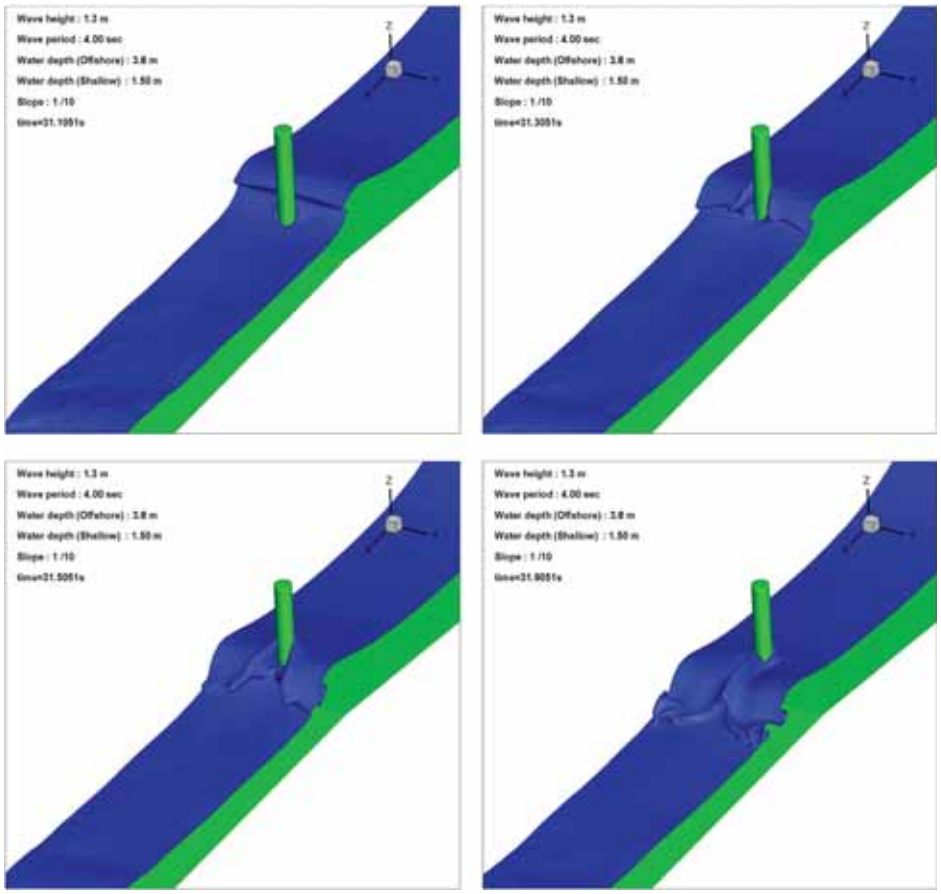

Fig. 11. Spatiotemporal plots from waves2Foam simulations for wave case 1– time steps 31.10 s, 31.30 s, 31.50 s and 31.90 s.

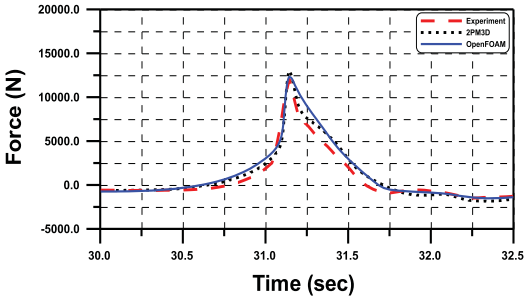

Fig. 12. Comparison of total breaking wave force obtained by the numerical models with the filtered experimental measurement, for wave case 1.

any bottom slope in the numerical wave tank, there would not be any wave breaking. Hence, it was expected that the same wave would travel along the entire length of the NWT. The wave surface elevations were compared at two different wave gauge positions, WG1 and WG2, located at 32 m and 37.65 m from the wave generator, respectively, to ensure that the same wave was generated along the NWT. Figs. 6 and 7 show the comparison of the free surface elevation calculated by the two numerical models for the two wave cases. Good overall agreement on the wave surface elevations was observed in both numerical models with the theoretical waves. In some detail, using 2PM3D, the wave trough was overestimated at wave gauges WG1 and WG2 for both wave cases, compared to the theoretical waves. The overestimation of the wave trough was around 9%. For wave case 1, the wave elevation calculated at WG1 by OpenFOAM was underestimated by 5% near the crest, compared to the theoretical waves.

3.3. Scenario 2- with bottom slope and cylindrical pile

In this scenario, the numerical wave tank was organized to be similar to the experimental set-up. The cylindrical pile was modelled near the edge of the slope. The wave surface elevation obtained by the numerical wave gauge at 37.65 m was compared with the experimental measurements. The wave surface elevation obtained by the numerical models for wave case 1 is shown in Fig. 8. The agreement with the experimental results was very good. The ripples near the trough of the wave surface elevation in both numerical models depicted the effect of wave structure interaction, as observed in the experimental measurements. However, the occurrence of the ripples was slightly delayed in both numerical models, compared with the experimental measurements. The magnitude of the fluctuations calculated by 2PM3D was found to be closer to the experimental results than when using OpenFOAM. Fig. 9 shows the comparison of the horizontal water particle velocities calculated by both the numerical models at VG1. There is good agreement in the velocities calculated by both of the numerical models. However, the experimental measurements from the velocity gauges were noisy and hence not included in the comparison. Figs. 10 and 11 show the spatiotemporal variations of wave surface

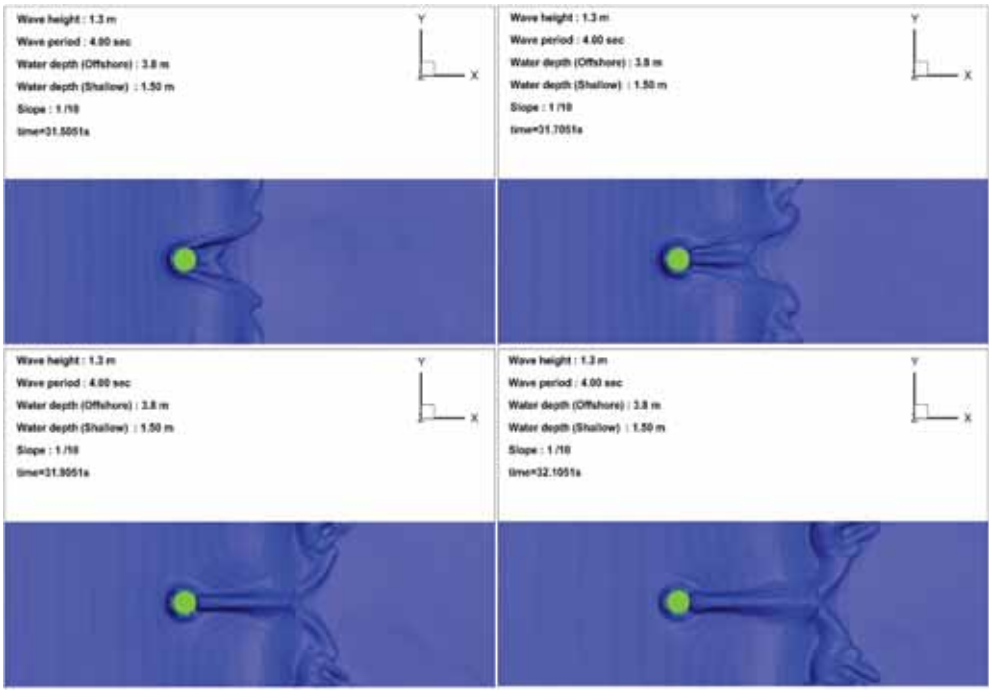

Fig. 13. The effect of secondary load cycle when wave breaks on the structure (waves2Foam), for wave case 1.

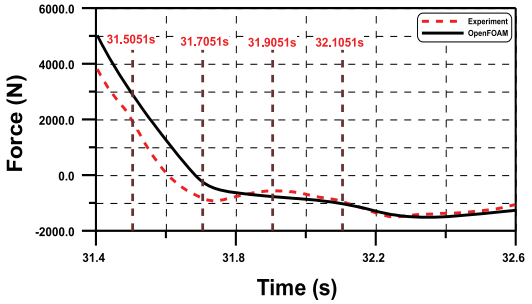

Fig. 14. Secondary wave force on the cylinder based on OpenFOAM simulations, for wave case 1. The time steps in Fig. 13 are marked on the graph.

elevations in both numerical models for different time steps. The overall wave breaking process in both numerical models was found to be similar.

A comparison of the total forces on the monopile is provided in Fig. 12. The total force on the monopile is the sum of the Morison force (quasi-static) and the breaking wave force. In the numerical models, the total forces on the structure were obtained by integrating the local pressure on the wetted surface areas of the structure in time. The numerical model results showed slightly higher (7%) peak forces, compared to the experimental measurements. This was expected, due to the use, in the present simulations, of the incompressible flow model. In the experimental measurements, when the wave broke on the structure, there were many air bubbles in the breaker, which reduced the effective density of the water in the wave breaker. This in turn reduced the wave force acting on the structure in the experimental measurements. However, in the present numerical models, those effects could be simulated due to the incompressible assumption. There was no measurement on entrained air bubbles in the wave breaker during the experiments. Based on the comparison of the total forces calculated by the numerical models and experimental measurements, the impact of the entrained air bubbles on the total force was less significant. According to many previous studies (Jacobsen et al., 2012), turbulence modelling was found to be important in simulating wave breaking in the numerical model. The use of two different turbulence models in 2PM3D and OpenFOAM could also have contributed to slight differences in the numerical results. As shown in Figs. 10 and 11, in the visualization of breaking waves, there was a slight variation in the breaking wave front simulated by the numerical models. However, the impact of this variation was not evident in the total wave force on the structure. The rise time in the total force time series simulated by both models showed good agreement (see Fig. 12). The peak force calculated by the two numerical models was almost the same, although the 2PM3D results were slightly higher (5%) compared to OpenFoam results. In 2PM3D, the force time series calculated during the fall time were closer to the experimental results initially and somewhat, later, overestimated compared to the experiment result. However, in OpenFOAM, force during the fall time is over estimated after the peak force. Overall, the force time series were calculated by both numerical models were similar.

3.4. Secondary load cycle

It was observed from the simulations that, as the wave passed the cylinder, the blockage of the flow by the cylinder resulted in the downstream gap at the back of the cylinder being filled by the diffracted waves. In Figs. 13 and 15, a hump of water piled up at the back of the cylinder demonstrates this phenomenon. The diffracted wave would be collected at the back of the cylinder, creating a local pressure. This pressure would act in the opposite direction to that of the flow and exert a negative force on the back of the cylinder. This negative force on the cylinder is a secondary load. In the present simulations, the secondary load occurred at a later stage in the wave breaking process. Secondary load cycles have previously been observed and discussed by several researchers (Chaplin et al., 1997;

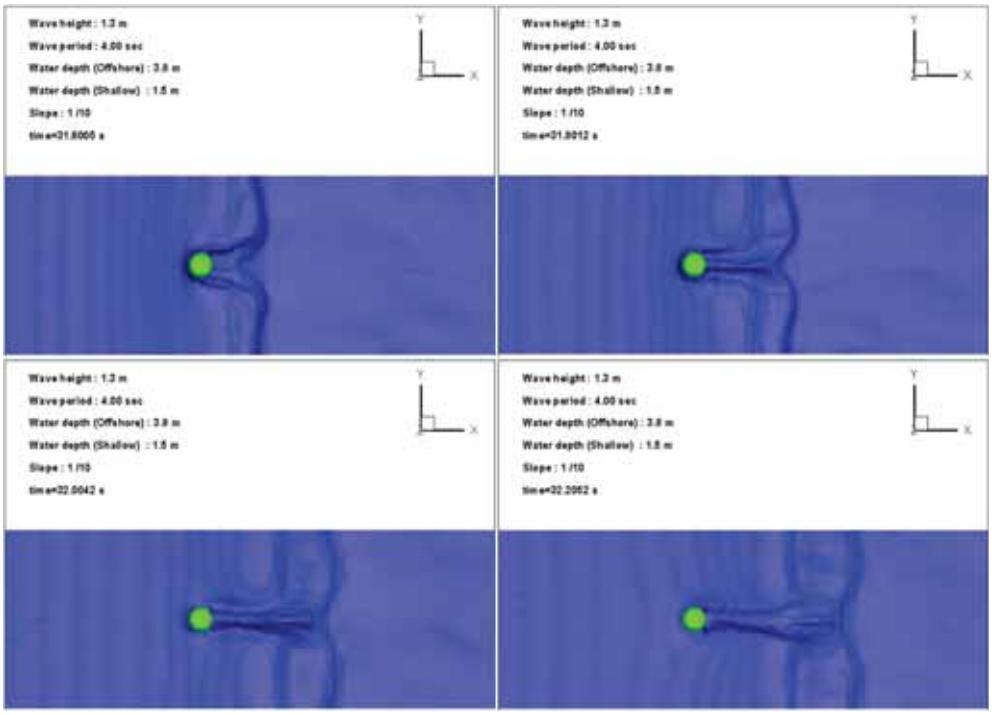

Fig. 15. The effect of secondary load cycle when wave breaks on the structure (2PM3D), for wave case 1.

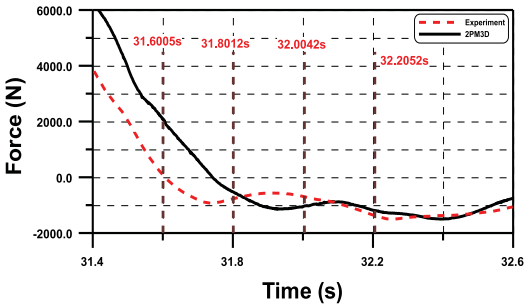

Fig. 16. Secondary wave force on the cylinder based on 2PM3D simulations, for wave case 1. The time steps in Fig. 15 are marked on the graph.

Grue, 2002; Grue and Huseby, 2002; Rainey, 2007). Many factors affect the secondary load acting on the structure; these need to be explored further. As in the simulations, the secondary load cycle was experienced after the initiation of wave breaking; the turbulence would also contribute to an accurate estimation of the secondary forces acting on the structure. In the total wave force time series (Figs. 14 and 16), the secondary loading effect was observed between a time range of 31.7–32.4 s. In both numerical models, the secondary load occurred slightly later than in the experimental results. The delay was very similar for both models. As the present numerical models were based on incompressible flow, the entrained air bubbles in the wave breaker were not considered in the simulations. The absence of entrained air bubbles in the breaker reduces the energy dissipation by 20–25% (Hoque, 2002). This can contribute to the delay in the secondary load cycle in the numerical models. However, the secondary forces calculated by OpenFOAM looked more spread in time, compared to the 2PM3D results. This difference could be due to the different turbulence models used in the two numerical models.

4. Conclusion

In the present study, two different numerical models, 2PM3D, based on the Finite Difference Method, and OpenFOAM with waves2Foam toolbox, based on the Finite Volume Method, were used to simulate breaking wave forces on a monopile structure in a numerical wave tank. The validation of both numerical models was carried out by simulating a number of non-breaking and breaking waves in the numerical wave tank and comparing the results with theoretical waves and experimental measurements. The simulated results from both numerical models showed good agreement with the experimental and theoretical results. The numerical models calculated the wave nonlinearities well, compared with the experimental measurements. The peak total breaking wave forces on the monopile calculated by both numerical models were found to have been overestimated (7%), compared to the experimental measurements. This could be due to the incompressible flow models used in the present simulations, which did not account for the presence of air bubbles in the breaking wave. In addition, for the present simulations, the finite difference model was observed to use a higher number of cells than its finite volume model counterpart.

The numerical models also calculated the secondary load effects on the structure during the wave breaking. In both numerical models, the secondary load effect was slightly delayed, compared to the experimental results. This discrepancy could be due to the present simulations' use of the incompressible flow model, which reduced the energy dissipation after the wave breaking, resulting in these discrepancies in the secondary loads. The estimation of the secondary load cycles by numerical simulation demands further study.

Based on the comparison, it can be concluded that both numerical models can be suitable for breaking wave studies. The wave structure interactions were, in our opinion, simulated well by both numerical models.

Acknowledgements

This research was supported by NORCOWE (Project No: PR-10077) and the University of Stavanger, Norway. The AP-AMG solver for solving the Poisson Pressure Equation in the 2PM3D model was provided by Chihiro Iwamura, Allied Engineering Corporation, Japan.

References

Allied Engineering, 2011. User's Manual for Advanced Parallel AMG Version 1.3, Tokyo.
Amsden, A.A., Harlow, F.H., 1970. A simplified MAC technique for incompressible fluid flow calculation. J. Comput. Phys. 6, 322–325.
Brackbill, J.U., Kothe, D.B., Zemach, C., 1992. A continuum method for modeling surface tension. J. Comput. Phys. 100 (2), 335–354.
Chaplin, J.R., Rainey, R.C.T., Yemm, R.W., 1997. Ringing of a vertical cylinder in waves. J. Fluid Mech. 350, 119–147.
Chella, A.M., Bihs, H., Myrhaug, D., Muskulus, M., 2016. Breaking solitary waves and breaking wave forces on a vertically mounted slender cylinder over an impermeable sloping seabed. J. Ocean Eng. Mar. Energy, 1–19.
Choi, S.J., 2014. Breaking Wave Impact Forces on an Offshore Structure, PhD thesis (UiS No.231). University of Stavanger, Norway, at the Department of Mechanical and Structural Engineering and Material Science.
Choi, S.J., Lee, K.H., Gudmestad, O.T., 2015. The effect of dynamic amplification due to a structure's vibration on breaking wave impact. Ocean Eng. 96, 8–20.
Christensen, E.D., Bredmose, H., Hansen, E.A., 2005. Extreme Wave Forces and Run-up on Offshore Wind Turbine Foundations. Copenhagen Offshore Wind, Copenhagen(http://citeseerx.ist.psu.edu/viewdoc/download?doi=10.1.1.619.2573 & rep=rep1 & type=pdf).
Goda, Y., Haranaka, S., Kitahata, M., 1966. Study of impulsive breaking wave forces on piles. Rep. Port. Harb. Res. Inst. 5 (6), 1–30, (Concept was also presented in English language in Watanabe, A., Horikawa, K.,)(1974). (Breaking wave forces on large diameter cell, Proceedings of 14th International Conference on Coastal Engineering, 1741–1760).
Gotoh, H., Sakai, T., 1999. Lagrangian simulation of breaking waves using particle method. Coast. Eng. J. 41 (3–4), 303–326.
Grue, J., 2002. On four highly nonlinear phenomena in wave theory and marine hydrodynamics. Appl. Ocean Res. 24 (5), 261–274.
Grue, J., Huseby, M., 2002. Higher-harmonic wave forces and ringing of vertical cylinders. Appl. Ocean Res. 24 (4), 203–214.
Hinatsu, M., 1992. Numerical simulation of unsteady viscous nonlinear waves using moving grid systems fitted on a free surface. J. Kansa. Soc. Nav. Archit. Jpn. 217, 1–11.
Hirt, C.W., Nichols, B.D., 1981. Volume of fluid method for the dynamics of free boundaries. J. Comput. Phys. 39 (1), 201–225.
Hirt, C.W., Sicilian, J.M., 1985. A porosity technique for the definition of obstacles in rectangular cell meshes, Proceedings of the 4th International Conference on Numerical Ship Hydrodynamics, pp. 1–10.
Hoque, A., 2002. Air Bubble Entrainment by Breaking Waves and Associated Energy Dissipation, (PhD thesis). Toyohashi University of Technology, Japan, at the Department of Architecture and Civil Engineering.
Hu, C., Kashiwagi, M., 2004. A CIP-based method for numerical simulations of violent free-surface flows. J. Mar. Sci. Technol. 9, 143–157.
Hull, P., Müller, G., 2002. An investigation of breaker heights, shapes and pressures. Ocean Eng. 29 (1), 59–79.
Hur, D.S., Mizutani, N., 2003. Numerical estimation of the wave forces acting on a three dimensional body on submerged breakwater. Coast. Eng. 47, 329–345.
Irschik, K., Sparboom, U., Oumeraci, H., 2004. Breaking wave loads on a slender pile in shallow water. In: Proceedings of 29th International Conference on Coastal Engineering, pp. 568–580.
Jacobsen, N.G., Fuhrman, D.R., Fredsøe, J., 2012. A wave generation toolbox for the open-source CFD library: OpenFOAM. Int. J. Numer. Methods Fluids 70 (9), 1073–1088.
Lee, K.H., 2006. A Study on Time Domain Analysis of Nonlinear Dynamic Interaction Amount Waves, Currents and Bed Materials, (PhD thesis). Nagoya University, Japan, at the Department of Civil Engineering.
Lee, K.H., Park, J.H., Baek, D.J., Cho, S., Kim, D.S., 2011. Discussion on optimal shape for wave power converter using oscillating water column. J. Korean Soc. Coast. Ocean Eng. 23 (5), 345–357.
Mayer, S., Garapon, A., Sørensen, L.S., 1998. A fractional step method for unsteady free-surface flow with applications to non-linear wave dynamics. Int. J. Numer. Methods Fluids 28 (2), 293–315.
Menter, F.R., 1994. Two-equation eddy-viscosity turbulence models for engineering applications. Am. Inst. Aeronaut. Astronaut. J. 32 (8), 1598–1605.
Mo, W., Irschik, K., Oumeraci, H., Liu, P.L.F., 2007. A 3D numerical model for computing non-breaking wave forces on slender piles. J. Eng. Math. 58, 19–30.
Park, J.C., Kim, M.H., Miyata, H., Chun, H.H., 2003. Fully nonlinear numerical wave tank (NWT) simulations and wave run-up prediction around 3-D structures. Ocean Eng. 30, 1969–1996.
Paulsen, B.T., 2013. Efficient Computations of Wave Loads on Offshore Structures, (PhD thesis). Technical University of Denmark, at the Department of Mechanical Engineering.
Rainey, R.C.T., 2007. Weak or strong nonlinearity: the vital issue. J. Eng. Math., 1–27.
Shao, S.D., 2006. Simulation of breaking wave by SPH method coupled with K-epsilon model. J. Hydraul. Res. 44 (3), 338–349.
Sherwin, S.J., Peiro, J., 2005. Finite Difference, Finite Element and Finite Volume Methods for Partial Differential Equations, Handbook of Materials Modeling. Springer, 1–30.
Smagorinsky, J., 1963. General circulation experiments with the primitive equations. Mon. Weather Rev. 91 (3), 99–164.
Ting, F.C.K., Kirby, J.T., 1996. Dynamics of surf-zone turbulence in a spilling breaker. Coast. Eng. 27, 131–160.
van Leer, B., 1979. Towards the ultimate conservative difference scheme. V. A second-order sequel to Godunov's method. J. Comput. Phys. 32, 101–136.
Wienke, J., Oumeraci, H., 2005. Breaking wave impact force on vertical and inclined slender pile-theoretical and large-scale model investigations. Coast. Eng. 52 (5), 435–462.

Paper 7

Jose, J., and Choi, S.J., 2017, “Estimation of Slamming Coefficients on Local Members of Offshore Wind Turbine Foundation (Jacket Type) under Plunging Breaker,” *International Journal of Naval Architecture and Ocean Engineering*, Vol. 9(6), pp. 624-640.
DOI: dx.doi.org/10.1016/j.ijnaoe.2017.03.006

Available online at www.sciencedirect.com

ScienceDirect

Publishing Services by Elsevier

International Journal of Naval Architecture and Ocean Engineering 9 (2017) 624–640
http://www.journals.elsevier.com/international-journal-of-naval-architecture-and-ocean-engineering/

Estimation of slamming coefficients on local members of offshore wind turbine foundation (jacket type) under plunging breaker

Jithin Jose [a,*], Sung-Jin Choi [b]

[a] Department of Mechanical and Structural Engineering and Materials Science, University of Stavanger, Norway
[b] Loads Copenhagen, DNV GL, Copenhagen, Denmark

Received 16 September 2016; revised 7 February 2017; accepted 9 March 2017
Available online 6 April 2017

Abstract

In this paper, the slamming coefficients on local members of a jacket structure under plunging breaker are studied based on numerical simulations. A 3D numerical model is used to investigate breaking wave forces on the local members of the jacket structure. A wide range of breaking wave conditions is considered in order to get generalized slamming coefficients on the jacket structure. In order to make quantitative comparison between CFD model and experimental data, Empirical Mode Decomposition (EMD) is employed for obtaining net breaking wave forces from the measured response, and the filtered results are compared with the computed results in order to confirm the accuracy of the numerical model. Based on the validated results, the slamming coefficients on the local members (front and back vertical members, front and back inclined members, and side inclined members) are estimated. The distribution of the slamming coefficients on local members is also discussed.

Keywords: Navier Stokes; Numerical simulation; Wave breaking; Slamming coefficient; Jacket

1. Introduction

Due to the increased energy demand and thrive for clean energy, offshore wind energy has become popular these days. A large number of offshore wind turbines are been supported by fixed type substructures (e.g., monopile, gravity foundations, tripod, or jacket type). Among these, the monopile structures are generally used because of simplicity in the design and installation. However, the increase in the turbine capacity and feasibility of fixed type Offshore Wind Turbine (OWT) in deeper water depths made the industry to focus more on rigid type of substructures, such as jacket type structures.

Most of the existing offshore wind turbine substructures are installed in relatively shallow water in order to reduce the cost of fabrication, maintenance and grid connectivity. However, in case where the substructures are installed in shallow waters where wave breaking occurs (e.g., Thornton bank wind farm near Belgian coast), the breaking waves would give rise to serious damages to the substructure. Since the wave-breaking phenomenon is extremely complicated and involve strong non-linear effect, the breaking wave forces would be one of the major concerns in the design of these OWT substructures.

Till date, a semi-empirical formula has been used to calculate the breaking wave forces on monopile structures (Goda et al., 1966). The slamming coefficient used in the semi-empirical formula should be determined in advance, based on the previous researches. Many researches have been done in past to estimate the slamming coefficients (Goda et al., 1966; Sawaragi and Nochino, 1984; Wienke and Oumeraci, 2005) valid for monopile structures. However, it is revealed that there is a major uncertainty in the value of slamming

* Corresponding author.
E-mail address: jithin.jose@uis.no (J. Jose).
Peer review under responsibility of Society of Naval Architects of Korea.

http://dx.doi.org/10.1016/j.ijnaoe.2017.03.006

coefficients, which is to be used for the calculation of breaking wave forces on monopile structures using the semi-empirical formula. For example, the slamming coefficients estimated by different researchers showed a considerable degree of scatter (from 3.14 to 6.28). The design guidelines (IEC 61400-3 (2009), ISO 21650 (2007), GL (2005), ABS (2010), DNV-RP-C205 (2010), API RP 2A-WSD (2007) and ISO 19902 (2007)), also shows no exact agreement on the slamming coefficient to be used for the design of such structures. The strong nonlinear wave–structure interactions during the wave breaking and difficulties in the accurate measurement of the breaking waves would make the exact physical representation of breaking waves a challenging task.

In the case of jacket type structures, there have been not many attempts in the past to estimate the breaking wave forces on the structures. In comparison with monopile, the jacket type structures are complex due to more members, joints and different member orientations. Hence, it is important to investigate the slamming coefficients on each local members (e.g., front and back vertical members, front and back inclined piles and lateral inclined member) of the jacket structure in the wave breaking zone. Moreover, the distribution of the slamming coefficients on the local members is important in the design of OWT substructure (e.g., base shear and bending moments). Nevertheless, in the design guidelines (and previous researches), there is limited information on the design of jacket structures against breaking waves.

The WaveSlam project (Arntsen and Gudmestad, 2014; Arntsen et al., 2013) was carried out in 2013, with the aim to investigate the wave forces from plunging breaking waves on a jacket structure in shallow waters. In the experiment, the jacket structure was tested for number of wave breaking cases and the response of the structure was measured. Jose et al. (2016b) performed initial studies on the experimental measurement data and proposed methods to obtain actual breaking wave forces on jacket members from the measured responses. However, the experimental studies have some limitation in terms of the instrumentation to measure the variation of local wave forces along the jacket members.

The development of a Navier Stokes solver to study the breaking wave forces have been an active field of research in recent past (Mo et al., 2013; Lee, 2006; Lee et al., 2011; Christensen et al., 2005; Alagan Chella et al., 2016; Choi et al., 2015). Mo et al. (2007) developed a Navier–Stokes solver to compute the wave–structure interaction on vertical slender pile. Christensen et al. (2005) studied the nonlinear run-up and the breaking wave forces on a cylindrical pile under spilling and plunging breakers using Navier Stokes solver. Kamath et al., 2016 studied breaking wave interactions on a vertical cylinder with respect to different wave breaking positions. They used open source CFD model REEF3D to simulate the breaking wave forces on the vertical cylinder. Choi (2014) and Choi et al. (2015) used a 3D numerical model based on finite difference method to calculate the breaking wave forces on monopile structures. The breaking wave forces on monopile structure at various orientations were simulated in those studies. The numerical results showed good agreement with the experimental measurements. However, most of these studies were limited to monopile structures. As there were limited experimental results available for jacket structures, there have been not many attempts to develop a numerical model to predict the breaking wave forces on the jacket structures.

Recently, Jose et al. (2016a) validated a 3D numerical model with the WaveSlam experimental data for the jacket structures. Based on the numerical simulations, slamming coefficients were estimated for the front and back vertical members of the jacket structure. The maximum slamming coefficient for the vertical members was found to be slightly smaller than the value suggested by Goda et al. (1966). A triangular distribution of wave slamming coefficients on the vertical members was obtained in contrast to the rectangular distribution proposed by Goda et al. (1966) and Wienke and Oumeraci (2005). However, in the research, the simulations were performed for a limited number of wave cases and final values of slamming coefficient could not be ascertained.

The objective of the present study is to estimate the slamming coefficients for the local members of a jacket structure. The present paper is an extension to Jose et al., 2016a. A wide range of breaking wave conditions (from short wave (4.6 s) to long wave (5.55 s)) are considered in order to get generalized slamming coefficients on local members of the jacket structure. In order to make quantitative comparison between experimental and CFD results, empirical mode decomposition (Huang et al., 1999; Choi et al., 2015) is used to filter out the dynamic amplification component in the measured response force time series data and the filtered results are compared with the computed results in order to confirm the accuracy of the numerical model. Based on the validated numerical results, the slamming coefficients on the local members (front and back vertical members, front and back inclined members, and side inclined members) are estimated. The distribution of slamming coefficients on the local members is studied. Moreover, the slamming coefficients obtained from the present study are compared with the values presented in previous studies by other researchers.

2. Model description

2.1. Experimental setup

The WaveSlam experiment was carried out in 2013 at the Large Wave Channel, Hannover, with the aim to study the breaking wave forces on a jacket structure. The truss structure of 1:8 scale was tested for large number of wave breaking conditions (Jose et al., 2016b). The experimental setup is shown in Fig. 1.

The large wave flume in Hannover is of 300 m long, 5 m wide and 7 m depth. The slope of the bottom of the tank is 1:10. The diameters of all the jacket members are 0.14 m. The jacket structure was located at a distance of approximately 200 m from the wave generator. The truss structure was equipped with total and local force transducers to measure the wave forces on the structure. There were wave gauges

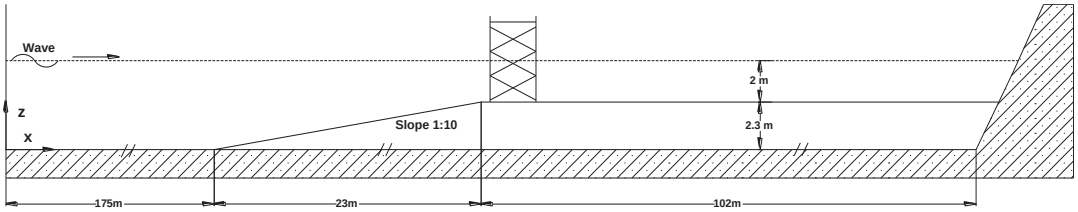

Fig. 1. Experimental set-up on the large wave flume FZK (Arntsen et al., 2013).

distributed along the wave channel to track the wave transformation during the wave breaking. The water particle velocities during the breaking wave were measured using Acoustic Doppler Velocity meter (ADVs) installed in line with the front leg of the truss structure. Fig. 2 shows the instrumented jacket structure in the wave tank.

2.2. Numerical model

2.2.1. Governing equations

When a fluid is modelled as a viscous and incompressible fluid with constant density, the fluid motion can be described by the continuity equation (Eq. (1)) and the modified Navier–Stokes equation (Eq. (2)). The free surface is governed by the Volume of Fluid (VOF) function (F) in Eq. (3) (Choi, 2014).

$$\frac{\partial(mv_j)}{\partial x_j} = q^* \tag{1}$$

$$m\frac{\partial v_i}{\partial t} + mv_j\frac{\partial v_i}{\partial x_j} = \frac{-m}{\tilde{\rho}}\frac{\partial p}{\partial x_i} + \frac{\partial}{\partial x_j}\left(2\tilde{\nu}D_{ij} - \tau_{ij}\right) - Q_i - \beta_{ij}v_j + f_i \tag{2}$$

$$\frac{\partial(mF)}{\partial t} + \frac{\partial\left(mv_jF\right)}{\partial x_j} = Fq^* \tag{3}$$

where, t is the time; $v_i = [u, v, w]^T$ is the velocity vector; p is pressure; $x_i = [x, y, z]^T$ is the position vector; is the ratio of the fractional area open to the flow; m is the arbitrary body forces due to the effects of gravity and surface tension; $D_{ij} = (\partial v_i/\partial x_j + \partial v_j/\partial x_i)/2$ is the strain rate tensor; τ_{ij} is the turbulent stress based on the Smagorinsky SGS (sub-grid scale) model; $\beta_{ij} = \beta\delta_{i3}\delta_{j3}$ is the dissipation factor matrix, in which β is the dissipation factor that equals 0, except in the added dissipation zone; $q^* = q(y, z; t)/\Delta x_s$ is the wave generation source, where $q(y, z; t)$ is the source density assigned only at the source position $(x = x_s)$ and Δx_s is the mesh width at the source position; $\tilde{\rho}$ and $\tilde{\nu}$ are the density and the kinematic viscosity averaged over the computational grid, respectively; F is the VOF function and Q_i is the wave source vector.

An application based on cut cell method is used to install the complex geometries (e.g., Jacket structure and bottom slope) in the computational domain. For the discretization of the continuity equation, the central difference scheme is used. In the discretization of Navier Stokes equations, the forward difference scheme for time derivative terms, the hybrid scheme (the combination of central difference scheme and upwind difference scheme) for advection terms and the central difference scheme for non-advection terms are employed. The Simplified Maker and Cell (SMAC) method (Amsden and Harlow, 1970) is incorporated for the velocity and pressure correction. In order to solve the Poisson pressure equation, an algebraic multi grid (AP-AMG) solver developed by Allied Engineering Corporation (2011) is used.

In the numerical model, the small-scale turbulence generated during the wave breaking in the surf zone is modelled using a Smagorinsky SGS (Sub-Grid Scale) model, while the large-scale turbulence is simulated by solving the governing equations.

Fig. 2. Instrumented jacket structure in the wave tank. Total force transducers are marked by red circles.

As for the boundary conditions, the dynamic boundary condition is automatically satisfied due to the use of a two-phase flow model (i.e., the water and the air phase are modelled as a fluid), while, the kinematic boundary condition is satisfied by tracking the VOF function (Hirt and Nichols, 1981). An impermeable (normal velocities) and a non-slip condition (tangential velocities) are imposed to treat bottom boundary condition and obstacle boundary condition. More details on the numerical model are given in Choi et al. (2015).

2.3. EMD method

The EMD method was developed by Huang et al. (1999), to decompose the given signal in the time domain. It decomposes the signal into number of intrinsic mode functions and a residue. Choi et al. (2015) used the EMD method to filter out the dynamic amplification in the measured response force time series data. Jose et al. (2015) verified the applicability of the EMD method for the total measured forces on the jacket structures. In the present study, the EMD will decompose the measured total response force into an IMF, which will represent the amplified force component due to the structure's vibration and a residue, which is the net breaking wave force.

The various steps in EMD algorithm are:

1) Obtain the upper and lower envelop for the measured force by connecting local maxima and minima, respectively.
2) The extracted local extremes are connected to obtain the upper and lower envelope.
3) The mean of the upper envelope and the lower envelope is obtained, which is the residue and is subtracted from the measured signal to obtain the IMF.
4) The residue represents the net breaking wave force and the IMF represents the amplified component of the force due to the structure's vibration.

2.4. Calculation of slamming coefficients

Fig. 3 shows the locations of the local force transducers on the jacket structure in the CFD model. The local force transducers are distributed along the local members in the global coordinate system. In the numerical model, each local force transducer is described by defining a local region is space around the member. The numerical model identified the wet surface areas in the defined local region and integrated the pressure on these wet surfaces to calculate the local forces. There are 14 local force transducers on each of the bracing members (B1–B6) and 38 force transducers on the front and back vertical members (V1 and V2). The local force transducers on the vertical members are of the size of grid cells (z direction) covering the circumference of the member. The force transducers on the inclined members are formed similar to the vertical force transducers, except that there is a clearance of grid cell between the adjacent transducers. The local wave forces on the jacket members are obtained by direct integration of the pressure distribution along the circumference of the members.

Goda et al. (1966) and Wienke and Oumeraci (2005) proposed a semi-empirical formula (Eq. (4)) to calculate the breaking wave forces on the cylindrical pile.

$$F_s = \frac{1}{2}\rho_w C_s D C_b^2 \lambda \eta_b \tag{4}$$

where, F_s is the total breaking wave force,C_s is the slamming coefficient; C_b is the breaking wave celerity, λ is the curling factor; η_b is the breaking wave height; ρ_w is the water density; D is the diameter of the cylinder.

Eq. (4) is proved to be a good approximation for calculating the breaking wave forces on the cylindrical pile except the uncertainty in the slamming coefficient to the used. Moreover,

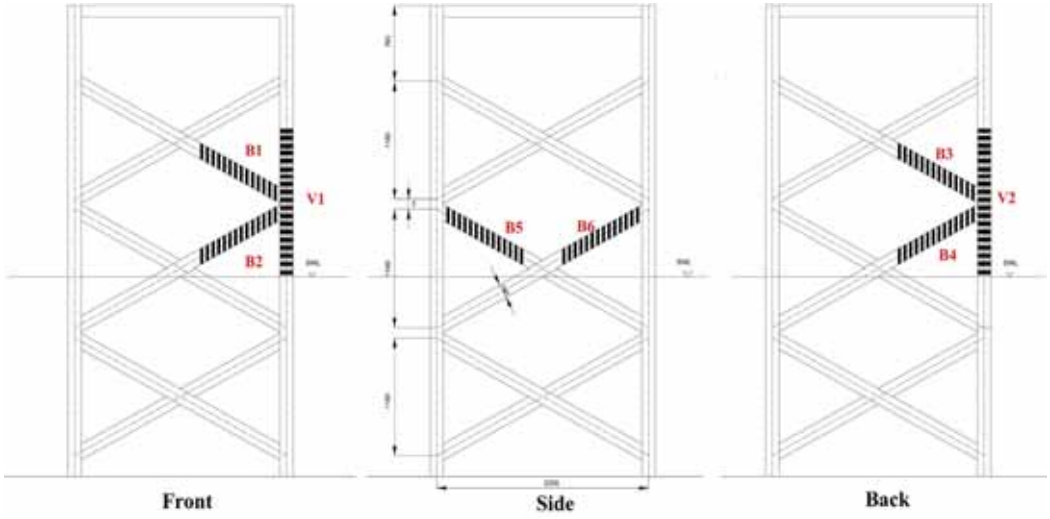

Fig. 3. Locations of the local force transducers on the Jacket structure in the CFD model.

Table 1
Incident wave conditions.

Case	Type	Wave height (m)	Wave period (s)	Water depth (m)
a1	Non-breaking	0.75	4.00	4.3
b1	Breaking	1.50	5.55	4.3
b2		1.60		
b3		1.70		
c1	Breaking	1.50	5.20	4.3
c2		1.60		
c3		1.70		
d1	Breaking	1.50	4.90	4.3
d2		1.60		
d3		1.70		
e1	Breaking	1.50	4.60	4.3
e2		1.60		
e3		1.70		

according to Tanimoto et al. (1986) and Wienke and Oumeraci (2005), Eq. (4) can also be used for inclined piles by changing some parameters. As the maximum slamming force is expected at the time of the impact (t = 0), the slamming coefficients are estimated for the maximum forces calculated by the local force transducers. The projected area is same as the projected area of the local force transducers. The breaking wave celerity is taken directly from the numerical model.

By using Eq. (4), the slamming coefficients for the local force transducers are estimated as,

$$C_s = \frac{2f_l}{\rho_w C_b^2 A_P} \tag{5}$$

A_P is the projected area of the local force transducer; f_l is the maximum slamming force computed by the local force transducers. The projected area A_P, is different for vertical and inclined members of the jacket structure.

2.5. Application of 3D numerical model

A numerical wave tank (NWT) similar to WaveSlam experimental setup is developed. The NWT has a length of 50.0 m, a width of 5.0 m, and a height of 7.0 m. The jacket structure and bottom geometry are modelled in the NWT by considering the x−z plane of symmetry. Only half of the structures is modelled in order to reduce the computational time. The total forces on the structure are calculated by multiplying the forces acting on the half of the structure with a factor 2. The water depths at the wave generator and at the plateau are 4.3 m and 2.0 m, respectively. The jacket structure is located near the edge of the slope. The slope of the bottom is considered to be 1/10.

In order to suppress the internal waves and reflected waves in the NWT, numerical dissipation zones are provided on the left and right side of the computational domain. The length of the dissipation zone is twice the wavelength. The internal wave generator is located on the left side of the computational domain to generate the regular wave train, using a stream function wave theory. Total 13 incident wave conditions are used for making breaking waves in front of, in the middle of, and in the rear of the structure (see Table 1). The free surface elevation and water particle velocities are calculated by the numerical gauges (wave gauges (WG1−WG6) and velocity gauges (VG1 and VG2)) distributed in NWT similar to the experimental setup (see Fig. 4). In the CFD model, the total breaking wave forces on the jacket structure are obtained by integrating the pressures on the structure. The local breaking wave forces are obtained from the force transducers distributed on the circumference of the members (see Fig. 3) along the length of the member (front, side and back vertical and inclined members). The time increment is automatically adjusted at each time step in order to obtain maximum efficiency. The model is run for 10 wave periods.

3. Results and discussion

In the WaveSlam experiment (Jose et al., 2016b), the jacket structure was tested for number of non-breaking and breaking wave cases. Among them, most of the critical wave cases are simulated in the NWT to get slamming coefficients on local

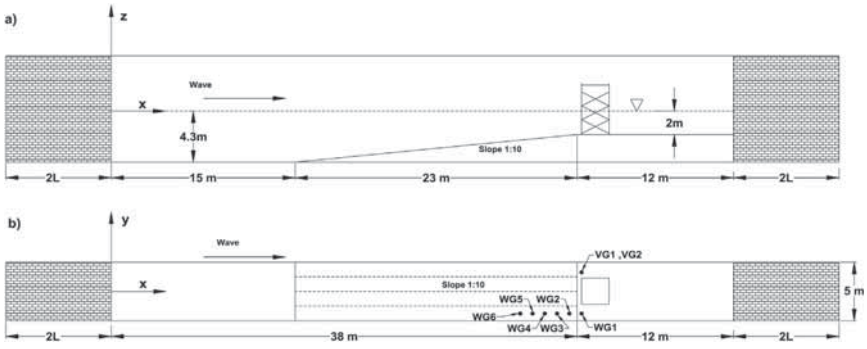

Fig. 4. Schematic representation of Numerical Wave tank (Jose et al., 2016a). a) Cross section, b) Plane view.

Table 2
Grid configurations.

G1	G2
0.04 m × 0.03 m × 0.03 m	0.03 m × 0.03 m × 0.03 m

members of the jacket structure. Table 1 shows 13 incident wave conditions (one non-breaking case and 12 breaking cases) considered in the present research. Each of these test cases is studied in detail in terms of breaking wave shapes, wave breaking points, total breaking wave forces on the jacket structure and breaking wave forces on the local members of the jacket structure. Moreover, the variation in the slamming coefficients along the length of the local members is discussed.

A grid sensitivity study is carried out on the numerical model before performing the simulations. The simulations were performed for two different grid configurations as shown in Table 2. Fig. 5 shows the wave surface elevation and total wave forces on the structure for the two different grid configurations, G1 and G2. The grid configuration G1 is comparatively coarser than G2. It is observed that the there is no significant difference in the results for both grid configurations. However, in the present simulations a finer grid (G2) is used to calculate the wave forces on the structure. In the NWT, the grid size varied from a minimum of 0.03 × 0.03 × 0.04 m near the jacket structure to a maximum of 0.3 × 0.2 × 0.4 m far from the structure.

3.1. Wave surface elevation

As the wave breaking is very sensitive to the wave height, it is important to accurately simulate the exact wave height in the numerical model. The free surface elevation calculated by the numerical model is validated against the experimental data for all the wave cases presented in Table 1. As all the wave gauges used in the experiment were resistance type wave gauges, we cannot expect a reliable measurement after the breaking point due to the curling of the wave and entrained air bubbles in the wave breaker. Hence, in all test cases the comparison of free surface elevation between the CFD results and the measured results are performed for the wave gauges, which are just before the wave breaking.

Fig. 6 shows the comparison of free surface elevation for the non-breaking wave case at the wave gauges WG1 and WG2. In the case of the non-breaking wave (see Fig. 6), the numerical calculations shows exact agreement with the experimental measurements. The nonlinearity in the wave is not much predominant in this case.

Figs. 7 and 8 show the comparison between the calculated and the measured free surface elevation at WG4, WG5, and WG6, for cases b3 and d2. Overall, the calculated results agree reasonable well with the experimental measurements for all the simulated cases. Especially, for case d2, the peaks at both the wave crest and trough are reproduced very well in the numerical results. However, for case b3, the calculated results

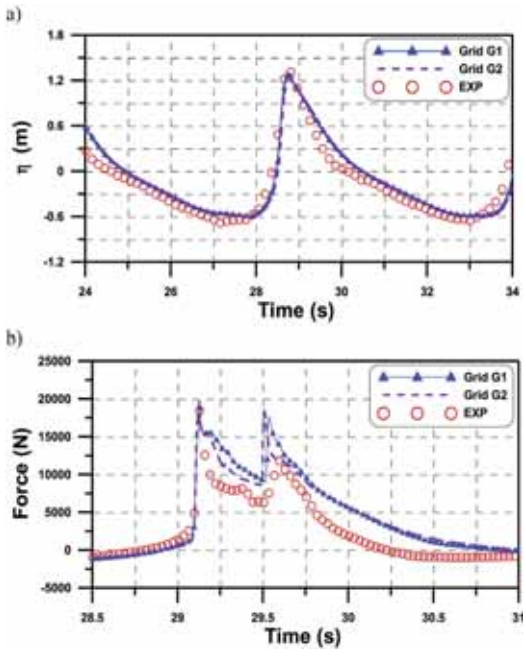

Fig. 5. Comparison of the wave surface elevations and total force on the structure using two different grid configurations for the wave case b3. a) Wave surface elevation at wave gauge WG4 using grid configuration G1 and G2. b) Total force on the jacket structure using grid configurations G1 and G2.

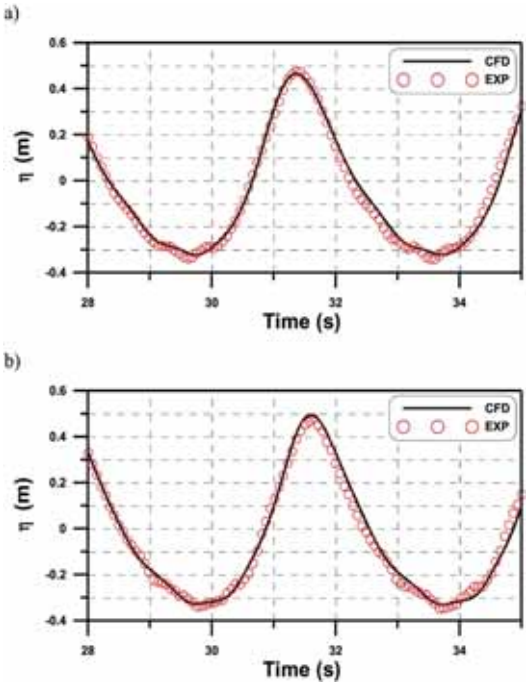

Fig. 6. Comparison of the free surface elevations between the CFD results and experimental results for case a1 (Jose et al., 2016a). (a) Wave gauge WG2 and (b) Wave gauge WG1.

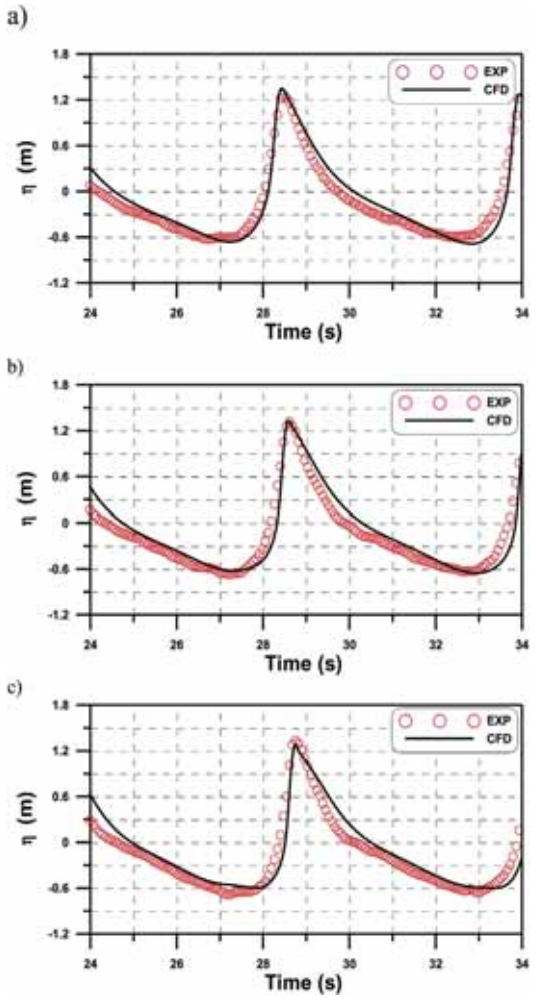

Fig. 7. Comparison of the free surface elevations between the CFD and experimental results for case b3. (a) Wave gauge WG6; (b) Wave gauge WG5 and (c) Wave gauge WG4.

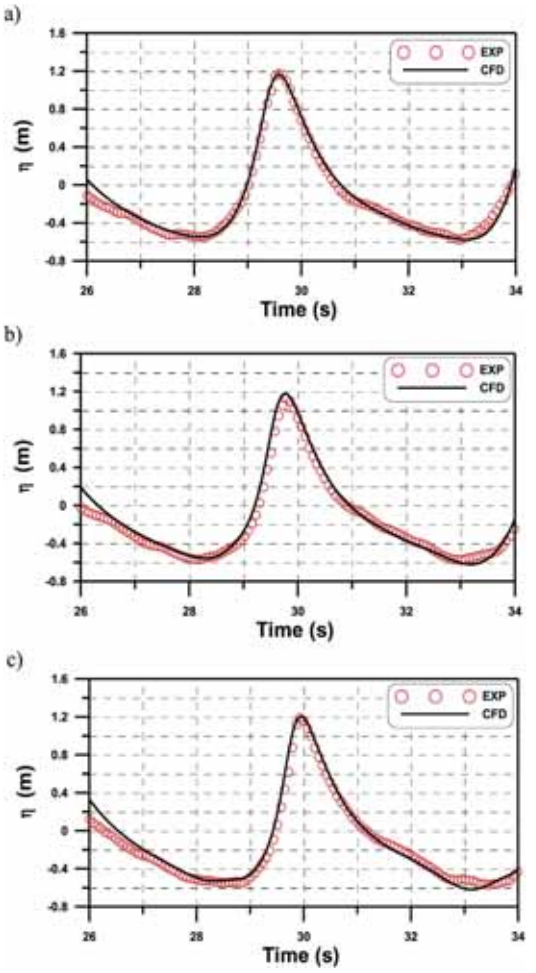

Fig. 8. Comparison of the free surface elevations between the CFD and experimental results for case d2.(a) Wave gauge WG5; (b) Wave gauge WG4 and (c) Wave gauge WG3.

on the fall-time are slightly overestimated compared with the measured results. Meanwhile, it should be noted that even though the results for other cases are not presented in the paper, the calculated results also show a reasonable agreement with the measured data. The snapshots of the spatiotemporal variations of the instantaneous water level for case b3 are shown in Fig. 9.

3.2. Water particle velocities

In the experiment, three Acoustic Doppler Velocity (ADV) meters were used to measure the water particle velocities. However, the ADV meter near the SWL didn't accurately register measurements due to air pockets in the wave breaker. Moreover, some noises are observed in the measurements for strong breaking wave cases.

Figs. 10 and 11 show the comparison of water particle velocities between the measured data and CFD results, for cases b3 and d2, respectively. The velocities calculated by the Navier–Stokes solver agree reasonably well with the measured velocities. There is a good agreement in peak velocities with the experimental and numerical results. The slight discrepancies observed would be due to the disturbances in the measuring equipment due to the high turbulence during the wave breaking. Moreover, the experimental measurements look noisy compared to numerical results.

3.3. Total breaking wave forces

In the experiment, the total breaking wave forces on the jacket structure were measured using four total force transducers integrated with the jacket structure. The measured force

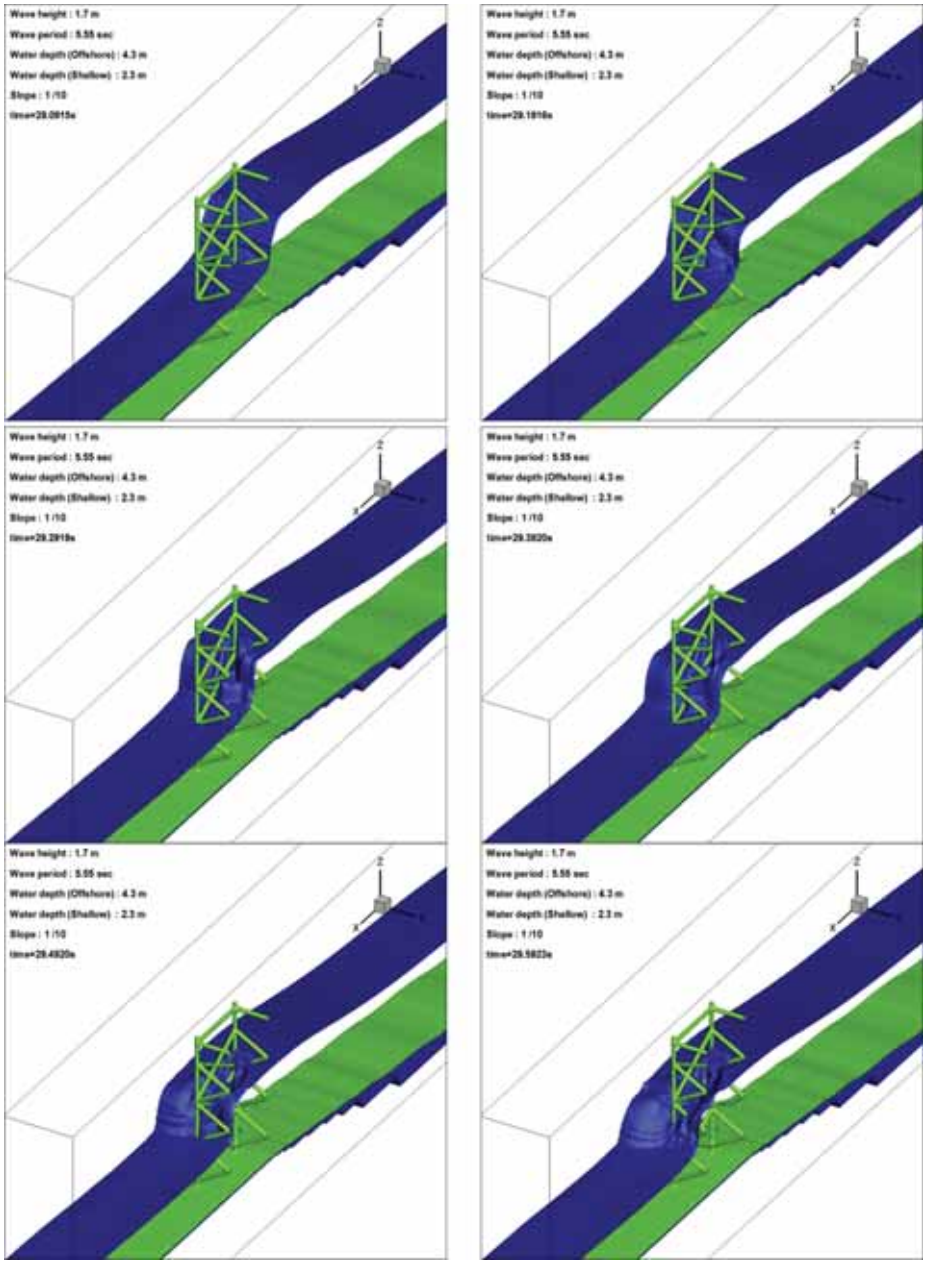

Fig. 9. Snapshots of the spatiotemporal variations of instantaneous water level for case b3 (time = 29.0915 s, 29.1916 s, 29.2919 s, 29.3920 s, 29.4920 s and 29.5923 s).

responses contain the quasi-static forces, the net breaking wave forces and the amplified force component due to structure's vibration. On the other hand, in the numerical model, the jacket structure is modelled as completely rigid structure which cannot induce dynamic amplification due to the structure's vibration. Therefore, in order to make quantitative comparison between the CFD results and experimental data, the amplified forces component due to structure's vibration in the measured force responses should be removed with the help of the EMD method as explained by Jose et al. (2016a), and then the filtered results are compared with the CFD results.

Fig. 12 shows the total wave forces on the structure for the non-breaking case a1. There is no dynamic amplification in the measured response forces, hence a direct comparison of the

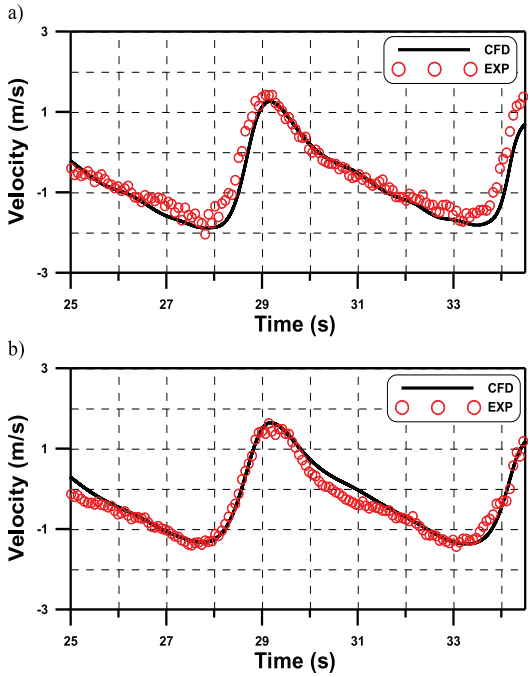

Fig. 10. Comparison of the water particle velocities between the CFD and experimental results for case b3. (a) Velocity gauge VG1 and (b) Velocity gauge VG2.

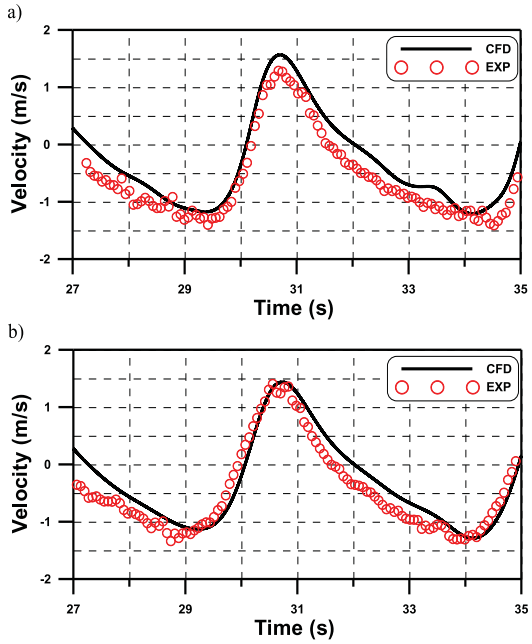

Fig. 11. Comparison of the water particle velocities between the CFD and experimental results for case d2. (a) Velocity gauge VG1 and (b) Velocity gauge VG2.

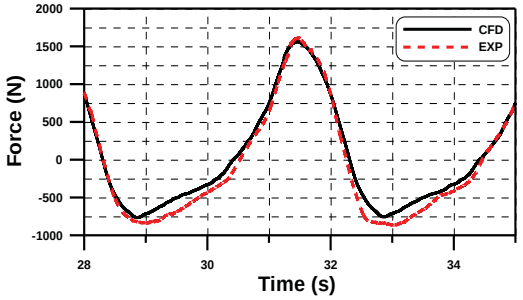

Fig. 12. Comparison of total wave force on the structure between the CFD and experimental results for non-breaking case a1.

measured total force and the numerical calculation is done. The total force is similar to the quasi-static Morison force. The CFD results show very good agreement with the experimental results. Figs. 13–16 show the comparison of filtered breaking wave forces (EXP) and breaking wave forces computed by the CFD model for difference wave cases. For the breaking waves, in the total force time series there are two different peaks, which represent the wave impacts on front and back side of the jacket structure. Based on the initial observation of the total force time series, it is observed that for higher periods and wave heights, the forces on the jacket structure are high. In all the wave cases with wave height 1.5 m, the wave breaking occurs beyond the front of the jacket structure. The higher second peak in the total force time series is observed for these wave cases (b1, c1, d1 and e1). For the other wave cases, in most of the time the wave breaks ahead of the structure. However, the total forces depend on many other parameters such as wave breaking position, wave height, wave period, etc.

In the total force comparison, the first peak in the CFD model shows very good agreement with the experimental data, however, the second peak is slightly overestimated. As explained by Jose et al. (2016a), there are many reasons attribute to this difference in the force. Firstly, in the experimental measurements, when the wave breaks on the structure there are lot of entrained air bubbles in the wave breaker. The presence of these air bubbles in the wave breaker reduces the effective density of the water hitting the structure and hence reduces the forces on the structure. Similar observations are made by several researchers based on experimental and numerical studies (Choi et al., 2015; Hu and Kashiwagi, 2004; Obhrai et al., 2004; Tang and Wai, 2016; Hoque, 2002). However, in the present numerical model, these kinds of effects cannot be simulated due to the use of incompressible flow model. The absence of entrained air bubbles in the wave breaker (in incompressible model) reduces the energy dissipation by 20–25% (Hoque, 2002). This reduced energy dissipation would cause larger energy in wave breaker even after the wave breaking is initiated. Secondly, the unsymmetrical wave breaking on the jacket structure will introduce difference in the experimental measurements. It was observed in the experimental measurements that the wave is not hitting the structure symmetrical always, i.e., the breaking wave front is not exactly

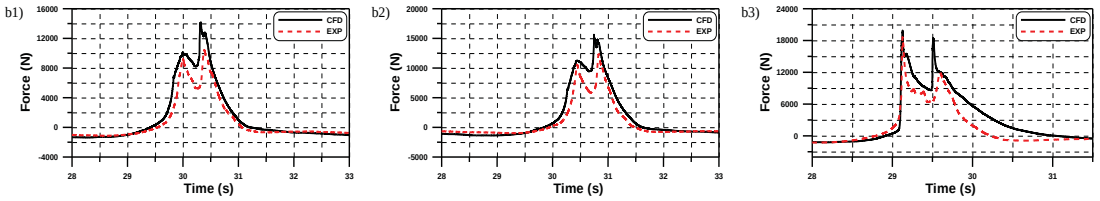

Fig. 13. Comparison of total wave force on the structure between the CFD and experimental results for breaking cases b1–b3.

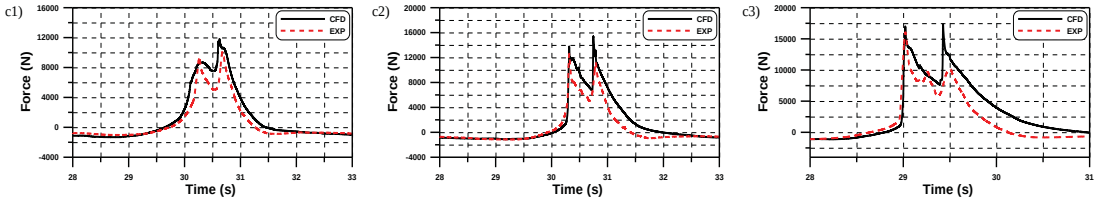

Fig. 14. Comparison of total wave force on the structure between the CFD and experimental results for breaking cases c1, c2 (Jose et al., 2016a) and c3.

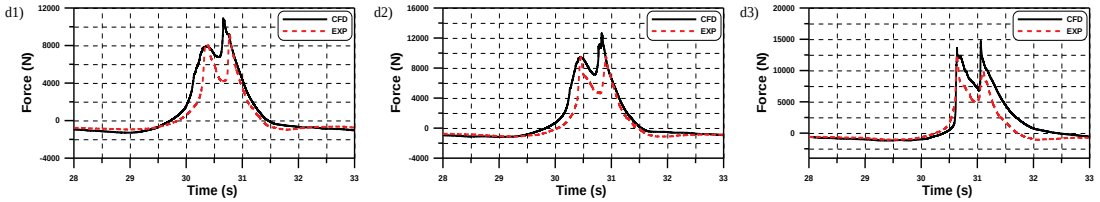

Fig. 15. Comparison of total wave force on the structure between the CFD and experimental results for breaking cases d1–d3.

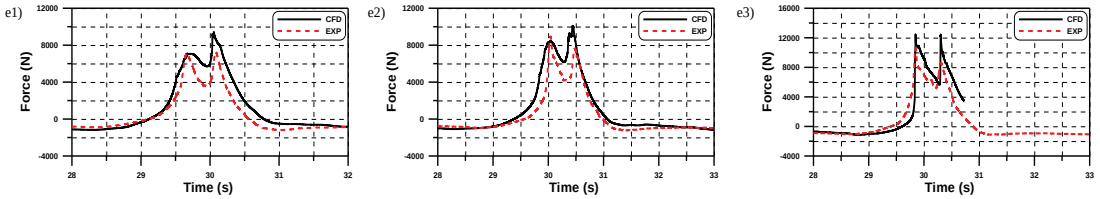

Fig. 16. Comparison of total wave force on the structure between the CFD and experimental results for breaking cases e1–e3.

parallel to the jacket structure always. Even though the degree of asymmetry is in terms of milliseconds, it has a larger impact on the total forces on the structure. These kinds of unsymmetrical wave impact cannot be simulated by the present CFD model. Thirdly, in the CFD model, the jacket structure is modelled taking into account x-axis symmetry. The total forces on the jacket structure are calculated by multiplying the forces on half structure with a factor of 2. However, in the experimental measurements it was observed that the wave interactions on the left and right side of the structure is slightly different. Finally, in the present numerical model the wave breaking is slightly slower compared to the experimental measurements in terms of energy dissipation. The absence of entrained air bubbles in the breaker would result shift in the wave breaking position (Hoque, 2002). Despite the discrepancies, the overall results show a reasonable agreement with experimental data. Therefore, it is concluded that the proposed numerical model can be used to predict the slamming coefficients on local members of a jacket structure.

4. Calculation of slamming coefficients

Based on the validated numerical results, the slamming coefficients for the members B1 (front upper inclined member), B2 (front lower inclined member), B3 (back upper inclined member), B4 (back lower inclined member), B5 (side-downward member), B6 (side-upward member), V1 (front vertical member) and V2 (back vertical member) of the jacket structure are obtained. The slamming coefficients on the members are calculated as discussed in the section 2.4.

Figs. 17–24 show the variation of maximum slamming coefficients along the length of the members for different wave conditions shown in Table 1. It is evident that the distribution of slamming forces on the structure depends greatly on the breaking wave conditions. For example, if the wave breaks too far from the structure, broken waves will reach the structure and the breaking wave forces will be less and more spread. One the other hand, if the wave breaks in front of the structure, very high breaking wave forces will act on the structure. As in the present cases the water depth is fixed, the wave height and wave period decides the intensity of wave breaking forces on the structural members. Hence, a detailed comparison of slamming coefficients for different combinations of wave height and period are carried out in this section.

4.1. Vertical member V1

Fig. 17 shows the variation in the slamming coefficients on the front-vertical member of the jacket structure V1. A triangular distribution of slamming coefficient is observed for all the cases, unlike the distribution presented by Goda et al. (1966) and Wienke and Oumeraci (2005). Looking at Fig. 17a, for the wave height 1.5 m case, the slamming coefficient variation looks similar for different wave periods. Since the wave breaks in between the structure (weakly breaking case at the front vertical member), the slamming coefficients obtained are found to be similar to drag coefficient. For 1.6 m case (Fig. 17b), the wave breaking points are shifted more to the front vertical member. Hence, the wave breaking is stronger than the 1.5 m case. The maximum slamming coefficient for the 1.6 m case is obtained for the wave period 5.2 s (Fig. 17b) due to the breaking of wave near the front members of the jacket structure. In the case of wave height 1.7 m (Fig. 17c), the wave breaking point is in front of the structure causing larger wave forces to act on the front member. The distribution of slamming coefficients along the vertical member becomes steeper as the wave periods decrease (from 5.55 s to 4.6 s). Especially, for case e3 (H = 1.7 m and T = 4.6 s), because of the high wave steepness the breaking wave forces on the front-vertical member become less spread and result in higher slamming coefficient compared to the other cases. The maximum slamming coefficient obtained for the vertical member V1 is 2.96.

4.2. Vertical member V2

Fig. 18 shows the variation in the slamming coefficient on the back-vertical member of the jacket structure, V2. A triangular distribution of slamming coefficient is observed for all the cases. For the cases with wave height 1.5 m (Fig. 18a), since the waves break beyond the front of the structure, the higher wave forces are observed at the back vertical member. The slamming coefficients increase as the wave period decrease from 5.55 s to 4.9 s due to the shifting of the wave breaking position from the back side of the structure to the front of the back members. Maximum slamming coefficient for the vertical member V2 is observed for the wave period 4.9 s. For wave height 1.6 m case (Fig. 18b), the slamming coefficients are still high at the back vertical member. The positions of maximum slamming coefficients are slightly lower than the positions for the wave height 1.5 m case due to the shifted wave breaking point. Meanwhile, for 1.7 m cases (Fig. 18c), broken wave reaches the back members and hence the distribution of slamming force is more spread and less impulsive. The maximum slamming coefficient obtained for the vertical member V2 is 2.63.

4.3. Bracing member B2

Fig. 19 shows the variation in the slamming coefficients on the front-lower bracing of the jacket structure, B2. The distribution of slamming coefficient is found to be more uniform (like rectangular type) along the bracing member. The results imply that the breaking wave impacts the member like a vertical wall of water. In some details, for the wave case b3

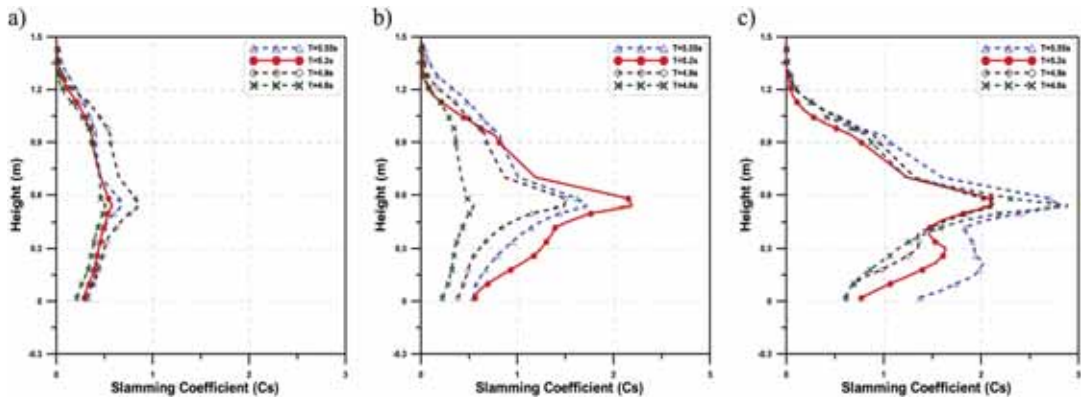

Fig. 17. Comparison of maximum slamming coefficient along the length of the vertical member V1 of the jacket structure for a) H = 1.5 m (b1, c1, d1 and e1), b) H = 1.6 m (b2, c2, d2 and e2), c) H = 1.7 m (b3, c3, d3 and e3).

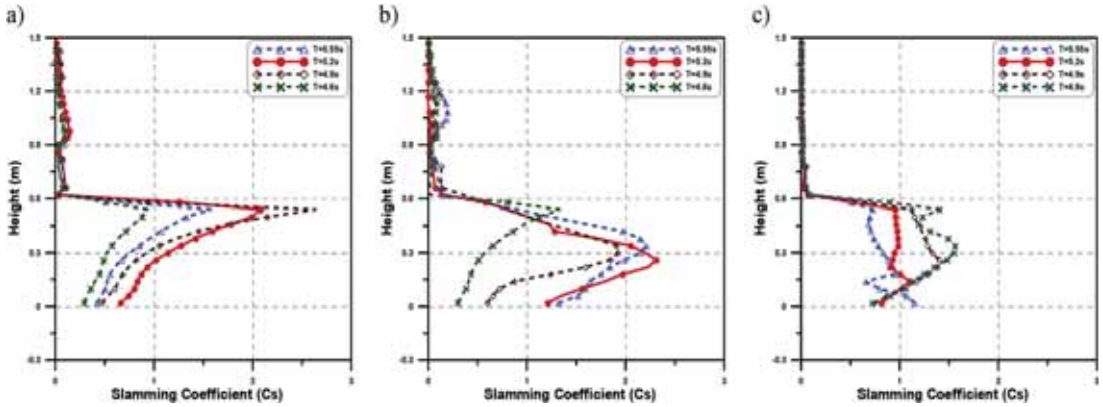

Fig. 18. Comparison of maximum slamming coefficient along the length of the vertical member V2 of the jacket structure for a) H = 1.5 m (b1, c1, d1 and e1), b) H = 1.6 m (b2, c2, d2 and e2), c) H = 1.7 m (b3, c3, d3 and e3).

(H = 1.7 m, T = 5.55 s), the variation in the slamming coefficient on the member is fluctuating compared with other cases. This can be attributed to the violent breaking of the wave on the structure member. Looking at Fig. 19a, the slamming coefficients for various wave cases look similar. In all these cases the breaking of the wave is beyond the front members of the jacket structure. On the other hand, Fig. 19b, due to the shifting of the wave breaking position toward the front of the jacket structure with the decrease in the wave period, higher slamming coefficients are obtained for c2 (H = 1.6 m, T = 5.2 s). The maximum slamming coefficient for the bracing member B2 is obtained for wave case e3 (H = 1.7 m, T = 5.55 s) and the value is 7.87. This value is slightly higher than the slamming coefficient suggested by Wienke and Oumeraci (2005). However, this higher value of slamming coefficient is obtained very local to the bracing member. When we compare the distribution of slamming coefficient on the upper bracing member (B1) and lower bracing member (B2), the slamming coefficient is triangular type for the upper member and nearly rectangular type for the lower member. This is agrees with the physical representation of the breaking wave that the upper part of the breaker is curled and lower part is more like a vertical wall of water. This also indicates that the distribution of slamming forces on the member depends directly on the shape of the wave front hitting the structure.

4.4. Bracing member B4

Fig. 20 shows the variation in the slamming coefficient on the back-lower bracing of the jacket structure, B4. In contrast with the front lower bracing member B2, the distribution of slamming coefficient is more triangular. When the wave reaches the back members, the 'wall of water' impact effect is absent due to the overturning of the wave after breaking. Hence a triangular distribution of slamming coefficient is observed, especially for wave height 1.7 m (Fig. 20c). In the case of wave height 1.5 m cases (Fig. 20a), the wave breaking

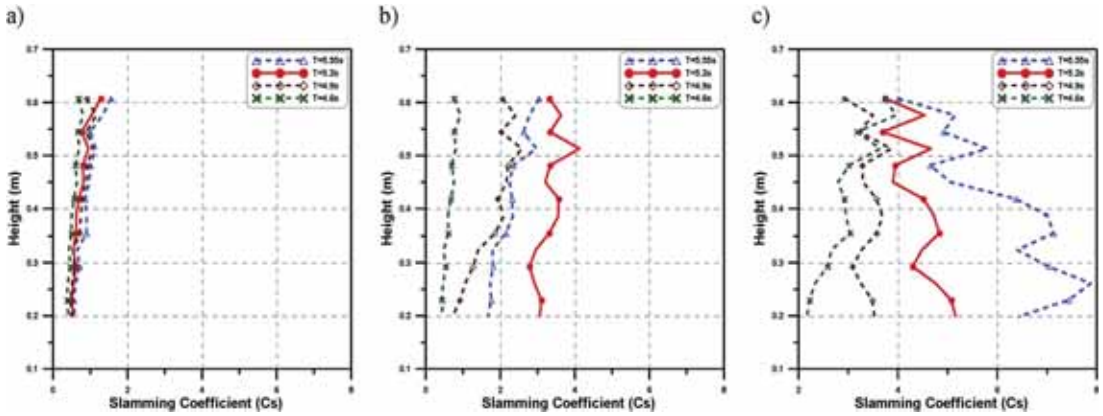

Fig. 19. Comparison of maximum slamming coefficient along the length of the bracing member B2 of the jacket structure for a) H = 1.5 m (b1, c1, d1 and e1), b) H = 1.6 m (b2, c2, d2 and e2), c) H = 1.7 m (b3, c3, d3 and e3).

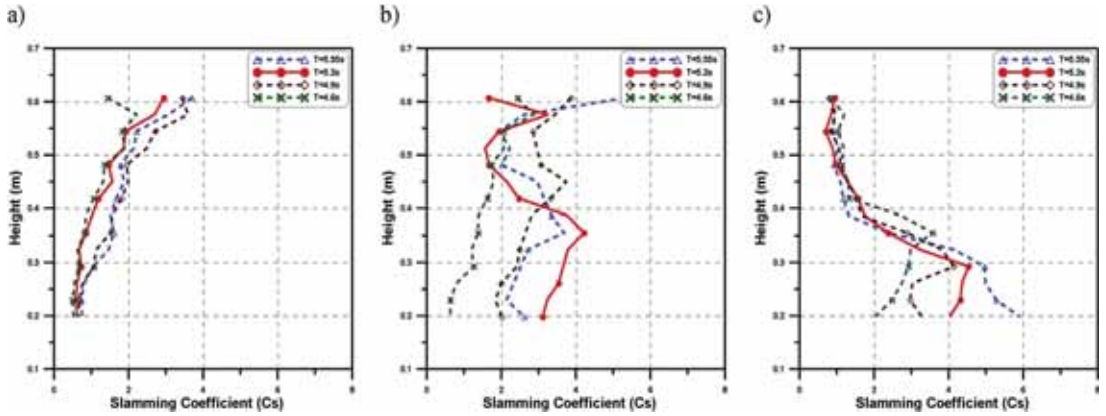

Fig. 20. Comparison of maximum slamming coefficient along the length of the bracing member B4 of the jacket structure for a) H = 1.5 m (b1, c1, d1 and e1), b) H = 1.6 m (b2, c2, d2 and e2), c) H = 1.7 m (b3, c3, d3 and e3).

take place near the back of the jacket structure. Hence a uniform distribution of slamming coefficient is observed for the back bracing members. The maximum slamming coefficient obtained for the bracing member B4 is 5.90.

4.5. Bracing member B1

Fig. 21 shows the variation of maximum slamming coefficients along the length of the front upper bracing member, B1. The maximum slamming coefficients are observed at the bottom elevation of the member. A linear variation in the slamming coefficient is observed for various wave cases. Looking at Fig. 21a, for the wave height 1.5 m the slamming coefficient looks very small due to the weakly breaking wave near the front members. However the for 1.6 m (Fig. 21b) and 1.7 m (Fig. 21c), the wave breaking is more on to the front members, hence higher the slamming coefficients. The maximum slamming coefficient is observed for the wave case b3 (H = 1.7 m, T = 5.55 s), where the wave breaks just ahead of the structure. The maximum slamming coefficient calculated was 2.4.

4.6. Bracing member B3

Fig. 22 shows the variation in the slamming coefficient on the back-upper bracing of the jacket structure, B3. Unlike the results for the front upper bracing B1, the variation of slamming coefficient along the bracing member follows different pattern depending on the wave breaking conditions. Looking at Fig. 22c, for the wave height 1.7 m cases, the slamming coefficient for the back upper bracing member is small compared to 1.5 m (Fig. 22a) and 1.6 m (Fig. 22b) wave cases. This is due to the less intense wave reaching the upper bracing members for 1.7 m case. However, for 1.6 m and 1.5 m cases, a triangular distribution of slamming coefficient is observed for shorter wave periods, due to the breaking of the waves on the back members. The maximum slamming coefficient obtained for the bracing member B3 is 3.06.

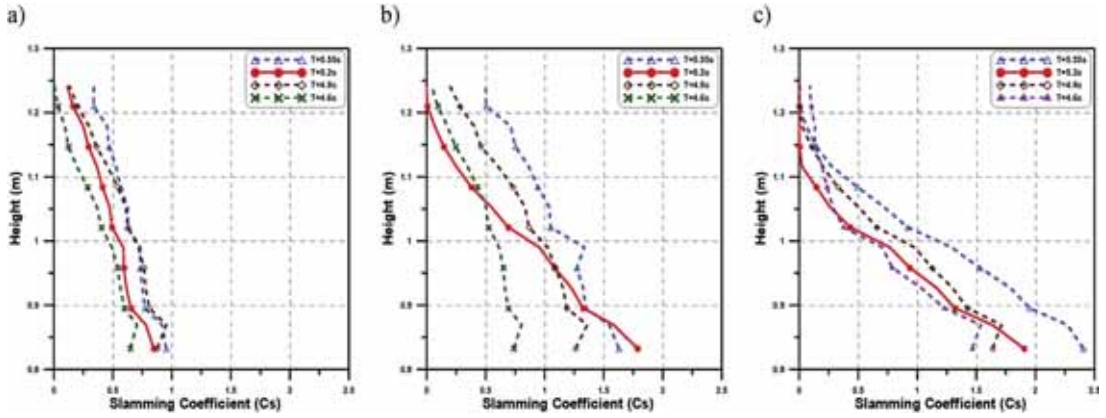

Fig. 21. Comparison of maximum slamming coefficient along the length of the bracing member B1 of the jacket structure for a) H = 1.5 m (b1, c1, d1 and e1), b) H = 1.6 m (b2, c2, d2 and e2), c) H = 1.7 m (b3, c3, d3 and e3).

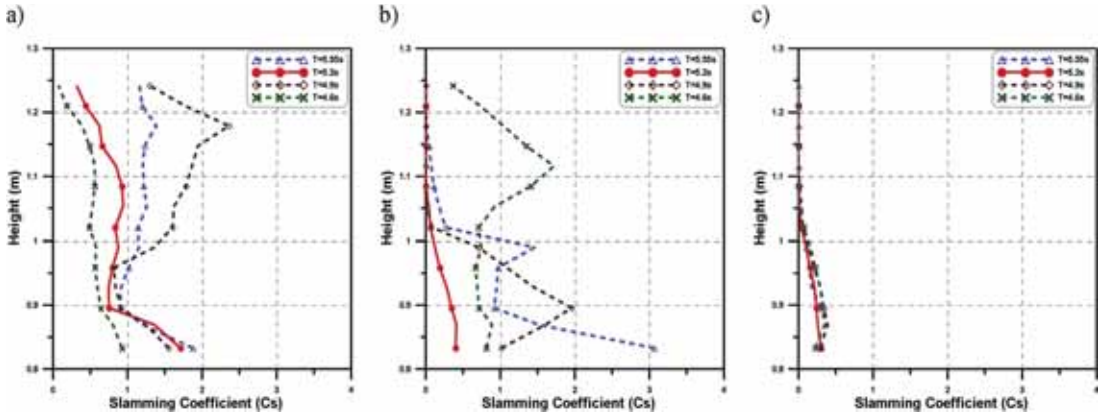

Fig. 22. Comparison of maximum slamming coefficient along the length of the bracing member B3 of the jacket structure for a) H = 1.5 m (b1, c1, d1 and e1), b) H = 1.6 m (b2, c2, d2 and e2), c) H = 1.7 m (b3, c3, d3 and e3).

4.7. Bracing member B5

Fig. 23 shows the variation in the slamming coefficient for the side-downward bracing of the jacket structure B5. Based on the video recordings from the experiment and simulations, it was evident that the slamming forces on the side members are shaded by the front vertical members. However, due to the encounter of the waves which are generated at the left and right sides of the front vertical member, high wave forces are observed in the middle of the member B5. This effect diminishes with the distance from the front member, which results on larger forces near the middle length of the bracing member as shown in Fig. 23a and b. For 1.7 m (Fig. 23c), due to the strong plunging breaker, the encounter of the waves are not predominant and hence the forces increases almost linearly with the distance from the front vertical member. The maximum slamming coefficient obtained for the bracing member B5 is 1.00, which is similar to the drag coefficient. It is expected that the slamming forces on these members will become critical if the wave impacts the structure in oblique direction.

4.8. Bracing member B6

Fig. 24 shows the variation in the slamming coefficient for the side-upward bracing (B6) of the jacket structure. For the wave height 1.7 m case (Fig. 24c), the broken wave is reaching the member and the computed forces are small. However, for 1.5 m (Fig. 24a) cases, the force is larger as the wave is breaking near the back members. The shading effect of the front vertical member V1 is not obvious in this case as the member is far from the vertical member. The maximum slamming is observed near the upper elevation of the bracing member. The maximum slamming coefficient obtained for the bracing member B5 is 1.45.

4.9. Discussion on slamming coefficients

In earlier studies on monopile structures (Wienke and Oumeraci, 2005), the slamming coefficients were determined only for cases where the wave breaks in front of structure. However, compared to monopile, a jacket structure is more

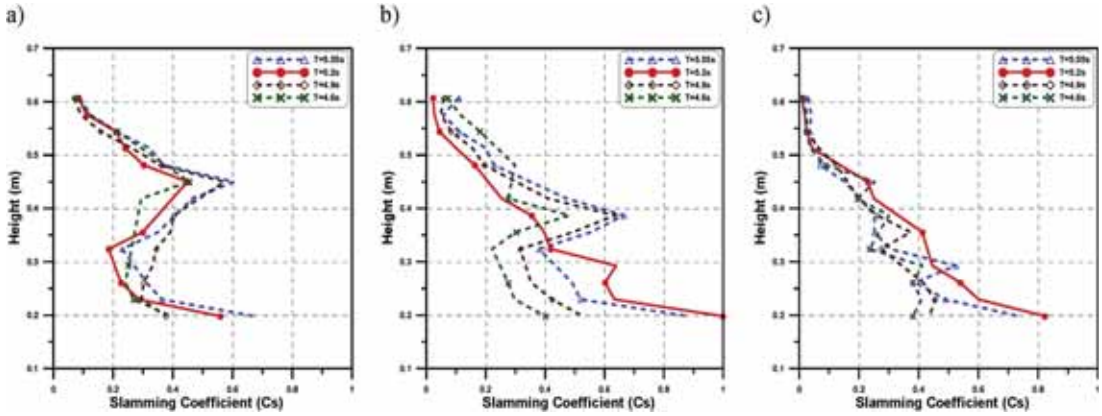

Fig. 23. Comparison of maximum slamming coefficient along the length of the bracing member B5 of the jacket structure for a) H = 1.5 m (b1, c1, d1 and e1), b) H = 1.6 m (b2, c2, d2 and e2), c) H = 1.7 m (b3, c3, d3 and e3).

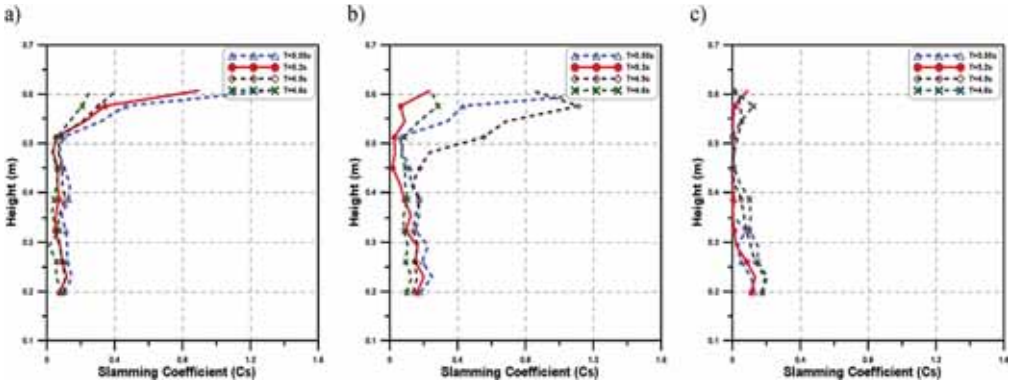

Fig. 24. Comparison of maximum slamming coefficient along the length of the bracing member B6 of the jacket structure for a) H = 1.5 m (b1, c1, d1 and e1), b) H = 1.6 m (b2, c2, d2 and e2), c) H = 1.7 m (b3, c3, d3 and e3).

complex having more structural members. It is therefore important to investigate the effect of wave breaking positions relative to the structure on the local member forces. A number of breaking wave cases are simulated in present study and conclusions are drawn.

It is found that the wave breaks at different positions relative to the jacket structure depending upon the wave height and the wave period. The strong breaking waves are represented by the cases where wave breaks in front of the structure. These cases are simulated by a wave height of 1.7 m and 1.6 m and the maximum slamming coefficients are estimated on the front members of the jacket structure. It is also observed that the wave breaking position shifts slightly ahead of the structure as the wave period decreases. This reduces the slamming forces on the structure members and a range of slamming coefficients is expected for the jacket members depending on the wave breaking positions. For the front upper bracing member, a maximum slamming coefficient is found in the range 0.80–2.40 for the cases where wave breaks in front of the structure. The smaller values of slamming coefficients are estimated for the shorter waves due to early breaking of the wave. For the back upper bracing members, the slamming coefficients are found to be smaller than the drag coefficients due to broken waves reaching the members. However, for the same wave breaking positions, the slamming coefficients are found to be higher for the lower bracing members. The coefficients are in range of 0.93–7.87 and 2.86 to 5.90 for front and back lower bracing members respectively. A similar trend is observed for front vertical members where the slamming coefficients are in range of 0.55–2.96. For back vertical members, the coefficients are close to the drag coefficients. It is observed that as the distance from the members of the structure and the breaking point increases, the slamming coefficient decreases. Also, the forces on the back members are lower than the front members in all these cases.

For weakly breaking waves, the wave breaking position further shift beyond the front of the structure. These cases are represented by a wave height of 1.5 m and some of the cases with 1.6 m wave height, in the present simulations. Among these cases, the 1.6 m cases are found more critical resulting in higher slamming force on the jacket members. However, the slamming coefficients are found to be lower than the cases where the wave breaks in front of the structure. The maximum wave breaking forces are observed for the back members due to wave breaking beyond the front of the jacket structure. For the back lower bracing, the maximum slamming coefficient is found to be in the range of 2.22–5.33. The lower values correspond to the cases where the wave breaks far from the back member. The slamming coefficient for the front lower and back upper bracing members is in range of 0.81–3.03 and 0.92 to 3.06 respectively. In addition, smaller values of the slamming coefficient are observed for the front upper bracings. The range of slamming coefficients for the back vertical members is 0.93–2.63 and for the front vertical member is 0.51–1.72. Table 3 summarized the values of maximum slamming coefficients calculated for different members of jacket structure in the wave impact zone.

Table 3
Summary of maximum slamming coefficients for different wave cases (maximum slamming coefficient for each member is shown).

Wave case	Slamming coefficient, C_s								Breaking position
	B1	B2	B3	B4	B5	B6	V1	V2	
b1	0.95	1.55	1.88	3.70	0.67	1.32	0.68	1.57	Behind the back leg
b2	1.63	3.03	3.06	5.33	0.88	1.45	1.72	2.21	Middle of the structure
b3	2.40	7.87	0.39	5.90	0.74	0.13	2.81	1.15	In front of front leg
c1	0.85	1.29	1.71	2.96	0.56	0.90	0.58	2.08	At the back leg
c2	1.79	4.12	0.41	4.22	1.00	0.24	2.19	2.31	In front of front leg
c3	1.90	5.17	0.30	4.53	0.82	0.13	2.09	1.10	In front of front leg
d1	0.95	1.16	2.36	3.59	0.57	0.41	0.86	2.63	In front of back leg
d2	1.36	2.58	1.96	3.87	0.64	1.11	1.50	1.92	In front of front leg
d3	1.71	3.87	0.39	4.13	0.45	0.19	2.15	1.40	In front of front leg
e1	0.70	0.81	0.92	2.22	0.45	0.26	0.51	0.93	Middle of the structure
e2	0.80	0.93	1.72	2.86	0.48	0.28	0.55	1.33	In front of front leg
e3	1.24	3.96	1.24	3.57	0.41	0.21	2.94	1.56	In front of front leg

5. Conclusions

A comprehensive study on breaking wave interaction on a jacket structure is performed by simulating wide range of breaking wave conditions in the NWT. The wave surface elevation, water particle velocities and the breaking wave forces on the jacket structure are computed by the 3D numerical model and the computed results show a good agreement with the experimental measurements. However, slight discrepancies are observed due to the use of incompressible flow model used in the present simulations.

The local breaking wave forces on the members of the jacket structure were calculated by the force transducers distributed along the jacket members. The maximum forces calculated by each of these local force transduces were used to estimate the corresponding local maximum slamming coefficients. Further, the distribution of maximum slamming coefficients along the length of the jacket members is obtained. The distribution of slamming forces on the local members in impact area are triangular shape, unlike the research by Goda et al. (1966) and Wienke and Oumeraci (2005) (In their research, breaking wave forces are evenly distributed along the impact area). This discrepancy can cause different response characteristics of entire (or local) structure. Therefore, the use of accurate distribution is of great importance in the design of OWT substructure.

In the present study a wide range of wave breaking cases are taken into account, from weakly breaking to strongly breaking wave cases. The maximum slamming coefficients are estimated for the front members of the jacket structure, when the wave breaks in front of the structure. Based on the present simulations, the maximum slamming coefficient for the bracing members of the jacket structure in the wave impact zone is estimated as 7.87, which is similar to the value suggested by Wienke and Oumeraci (2005). On the other hand, in the case of vertical member, maximum slamming coefficient is obtained to be 2.96, which is slightly smaller than the values suggested by Goda et al. (1966). However, in the design of OWT substructures, it is not advised to use the maximum value of slamming coefficient along the entire member. A triangular distribution of force should be adopted in the calculation of slamming forces on the members.

The limitations of the present study are also identified. One of the limitations is the use of numerical model based on incompressible flow. As a result, the presence of entrained air bubbles in the breaker is not considered in the present simulations. It is reported that the absence of entrained air bubbles in the simulation have some influence on the wave breaking position and the forces on the structure (Hoque, 2002). Further studies are needed to verify the proposed slamming coefficients for the jacket structure and also to investigate the effect of air bubbles on these values.

Acknowledgements

This research was supported by NORCOWE (Project No: PR-10077) and University of Stavanger. The authors would like to thank Professor. Ove Tobias Gudmestad (UiS) for his critical review of the paper and comments. The AP-AMG solver for solving the Poisson Pressure Equation was provided by Chihiro Iwamura, Allied Engineering Corporation, Japan.

References

Alagan Chella, M., Bihs, H., Myrhaug, D., Muskulus, M., 2016. Breaking solitary waves and breaking wave forces on a vertically mounted slender cylinder over an impermeable sloping seabed. J. Ocean Eng. Mar. Energy 1–19.

Allied Engineering, 2011. User's Manual for Advanced Parallel AMG Version 1.3. Tokyo.

Amsden, A.A., Harlow, F.H., 1970. A simplified MAC technique for incompressible fluid flow calculation. J. Comput. Phys. 6, 322–325.

Arntsen, Ø.A., Gudmestad, O.T., 2014. Wave slamming forces on truss structures in shallow water. In: Proceedings of the HYDRALAB IV Joint User Meeting. HYDRALAB, Lisbon.

Arntsen, Ø.A., Obhrai, C., Gudmestad, O.T., 2013. "Data Storage Report: Wave Slamming Forces on Truss Structure in Shallow Water," WaveSlam (HyIV-FZK-05), Technical Report. Norwegian University of Science and Technology and University of Stavanger.

Choi, S.J., Lee, K.H., Gudmestad, O.T., 2015. The effect of dynamic amplification due to a structure's vibration on breaking wave impact. Ocean Eng. 96, 8–20.

Choi, S.J., 2014. Breaking Wave Impact Forces on an Offshore Structure (PhD thesis (UiS No. 231)). University of Stavanger, Norway, at the Department of Mechanical and Structural Engineering and Material Science.

Christensen, E.D., Bredmose, H., Hansen, E.A., 2005. Extreme Wave Forces and Run-up on Offshore Wind Turbine Foundations. Copenhagen Offshore Wind, Copenhagen.

Goda, Y., Haranaka, S., Kitahata, M., 1966. Study of Impulsive Breaking Wave Forces on Piles. In: Report of Port and Harbour Research Institute, vol. 5(6), pp. 1–30. Concept also in English language in Watanabe, A., Horikawa, K., (1974). Breaking wave forces on large diameter cell. Proc. 14th Intern. Conf. on Coastal Eng, 1741–1760.

Hirt, C.W., Nichols, B.D., 1981. Volume of fluid method for the dynamics of free boundaries. J. Comput. Phys. 39 (1), 201–225.

Hoque, A., 2002. Air Bubble Entrainment by Breaking Waves and Associated Energy Dissipation (PhD thesis). Toyohashi University Of Technology, Japan, at the Department of Architecture and Civil Engineering.

Huang, N.E., Zheng, S., Long, S.R., 1999. A new view of nonlinear water waves: the Hilbert Spectrum. Annu. Rev. Fluid Mech. 31, 417–457.

Hu, C., Kashiwagi, M., 2004. A CIP-based method for numerical simulations of violent free-surface flows. J. Mar. Sci. Technol. 9, 143–157.

Jose, J., Podrażka, O., Obhrai, C., Gudmestad, O.T., 2015. Experimental Analysis of Slamming Loads for the Truss Structures within the Framework of WaveSlam Project, Hydralab IV (http://www.hydralab.eu/project_publications.asp), Technical Report. University of Stavanger and University of Gdansk.

Jose, J., Choi, S.J., Lee, K.H., Gudmestad, O.T., 2016a. Breaking wave forces on an offshore wind turbine foundation (jacket type) in the shallow water. In: Proceedings of 26th International Ocean and Polar Engineering Conference, Rhodes, Greece, pp. 164–172.

Jose, J., Podrażka, O., Obhrai, C., Gudmestad, O.T., Cieślikiewicz, W., 2016b. Methods for analysing wave slamming loads on truss structures used in offshore wind applications based on experimental data. J. Offshore Polar Eng. 26 (2), 100–108.

Kamath, A., Chella, M.A., Bihs, H., Arntsen, Ø.A., 2016. Breaking wave interaction with a vertical cylinder and the effect of breaker location. Ocean Eng. 128, 105–115.

Lee, K.H., 2006. A Study on Time Domain Analysis of Nonlinear Dynamic Interaction Amount Waves, Currents and Bed Materials (PhD thesis). Nagoya University, Japan, at the Department of Civil Engineering.

Lee, K.H., Park, J.H., Baek, D.J., Cho, S., Kim, D.S., 2011. Discussion on optimal shape for wave power converter using oscillating water column. J. Korean Soc. Coast. Ocean Eng. 23 (5), 345–357.

Mo, W., Irschik, K., Oumeraci, H., Liu, P.L.F., 2007. A 3D numerical model for computing non-breaking wave forces on slender piles. J. Eng. Math. 58, 19–30.

Mo, W., Jensen, A., Liu, P.L.F., 2013. Plunging solitary wave and its interaction with a slender cylinder on a sloping beach. Ocean Eng. 74, 48–60.

Obhrai, C., Bullock, G., Wolters, G., Muller, G., Peregrine, H., Bredmose, H., Grune, J., 2004. Violent wave impacts on vertical and inclined walls: large scale model tests. In: Proceedings of the 29th International Conference on Coastal Engineering, vol. 1(4), pp. 4075–4086.

Sawaragi, T., Nochino, M., 1984. Impact forces of nearly breaking waves on a vertical circular cylinder. Coast. Eng. Jpn. 27, 249–263.

Tanimoto, K., Takahashi, S., Kaneko, T., Shiota, K., 1986. Impulsive breaking wave forces on an inclined pile exerted by random waves. In: Proceedings of 20th International Conference on Ocean Engineering, pp. 2288–2302.

Tang, L., Wai, O.W.H., 2016. Numerical study of air entrainment and bubble plume dynamics under breaking waves. In: Proceedings of 26th International Ocean and Polar Engineering Conference, Rhodes, Greece, pp. 669–672.

Wienke, J., Oumeraci, H., 2005. Breaking wave impact force on vertical and inclined slender pile-theoretical and large-scale model investigations. Coast. Eng. 52 (5), 435–462.